*DOT/FAA/AR-xx/xx

Air Traffic Organization
NextGen & Operations Planning
Office of Research and
Technology Development
Washington, DC 20591

Volume IV – UAS Airborne Collision Severity Evaluation – Engine Ingestion

August 2017

Final Report

This document is available to the U.S. public through the National Technical Information Services (NTIS), Springfield, Virginia 22161.

This document is also available from the Federal Aviation Administration William J. Hughes Technical Center at actlibrary.tc.faa.gov.

U.S. Department of Transportation
Federal Aviation Administration

Technical Report Documentation Page

1. Report No.	2. Government Accession No.	3. Recipient's Catalog No.
DOT/FAA/AR-xx/xx		

4. Title and Subtitle

Volume IV – UAS Airborne Collision Severity Evaluation – Engine Ingestion

5. Report Date

August 2017

6. Performing Organization Code

7. Author(s)

Kiran D'Souza, Troy Lyons, Thomas Lacy, Kalyan Raj Kota

8. Performing Organization Report No.

9. Performing Organization Name and Address

The Ohio State University
Gas Turbine Laboratory
2300 West Case Road
Columbus, OH 43235

Mississippi State University
Department of Aerospace Engineering
PO Box A
Mississippi State, MS 39762

10. Work Unit No. (TRAIS)

11. Contract or Grant No.

12. Sponsoring Agency Name and Address

U.S. Department of Transportation
Federal Aviation Administration
Office of Aviation Research
Washington, DC 20591

13. Type of Report and Period Covered

14. Sponsoring Agency Code

15. Supplementary Notes

16. Abstract

Unmanned aerial vehicles (UAVs) are becoming more abundant, and the risk of a UAV-airplane collision is growing with their popularity. Airplane collisions with birds and ice have been researched for several decades, however those impacts are not representative of an airplane with a UAV. UAVs contain materials which are harder and denser than birds. Here simulations of a UAV ingestion into a jet engine are studied with the commercially available software LS-DYNA. Parametric study models of fan stages of mid-sized business jets housed in a containment tank were used for the ingestion simulations. Collaborating research groups created the two finite element UAV models that were used in this study. The collaborating research groups simulated and compared their finite element models of key UAV components against experimental crash tests to ensure UAV component model accuracy. This computational research shows that UAVs are capable of causing severe damage to jet engines, and lays the foundation for further computational and experimental studies of ingestion events.

17. Key Words	18. Distribution Statement
Crashworthiness, Engine Ingestion, UAS, Ohio State University, OSU	This document is available to the U.S. public through the National Technical Information Service (NTIS), Springfield, Virginia 22161. This document is also available from the Federal Aviation Administration William J. Hughes Technical Center at actlibrary.tc.faa.gov.

19. Security Classif. (of this report)	20. Security Classif. (of this page)	21. No. of Pages	22. Price
Unclassified	Unclassified		

ACKNOWLEDGEMENTS

The authors would like to acknowledge the FAA's Center of Excellence for Unmanned Aircraft Systems, ASSURE for funding this work.

The authors would also like to acknowledge Dr. Mike Dunn and Dr. Jim Gregory from The Ohio State University for their administrative efforts and guidance during the course of this project. We also acknowledge the help of Erica Johnson, Chris Keener, Eric Kurstak, and Mitchell Doerzbacher, students at The Ohio State University who helped in the modeling effort. We would also like to acknowledge the input and guidance of Bob Morris and Steve Conner from Pratt & Whitney.

The authors also acknowledge the collaborations with Dr. Gerardo Olivares, Luis Gomez, and Jaime Espinosa de los Monteros from the National Institute of Aviation Research at Wichita State University who created the quadcopter model, and consulted on and ran some of the engine ingestion test cases; Dr. Doug Cairns from Montana State University for his support, guidance, and assistance during the project; Tom Aldag from the National Institute for Aviation Research at Wichita State University for his support and administrative efforts; and Colonel Stephen Luxion (retired) and Marty Rogers from Mississippi State University for his administrative efforts.

The authors would also like to acknowledge the Ohio Super Computer Center[1], which provided additional computing resources used to run the simulations presented in this work.

Finally, we would like to particularly thank Paul Rumberger, Daniel Cordasco, William Oehlschlager, Bill Emmerling, Sabrina Saunders-Hodge, Amela Zanacic, Benjamin Bradley, and Chris Swider, from the FAA for their comments, suggestions, and guidance over the course of this project.

TABLE OF CONTENTS

LIST OF FIGURES

LIST OF ACRONYMS

ASSURE	Alliance for System Safety of UAS through Research Excellence
AWG	LS-DYNA Aerospace Working Group
CAD	Computer-Aided Design
CFR	Code of Federal Regulations
FAA	Federal Aviation Administration
FBO	Fan Blade Out
FE	Finite Element
NACA	National Advisory Committee for Aeronautics
NIAR	National Institute for Aviation Research
OSU	The Ohio State University
RPM	Revolutions per minute
UAS	Unmanned Aerial System
UAV	Unmanned Aerial Vehicle

EXECUTIVE SUMMARY

The use of unmanned aerial vehicles (UAVs) has increased dramatically in recent years. The effect of a UAV ingestion into an aircraft engine is of great concern to the public and government officials at all levels. Currently, there are regulations and engine tests for bird and ice ingestions to ensure a plane can survive impacts with these objects. These tests and regulations cannot be directly transferred from birds and ice to UAVs since the materials that compose a UAV are very different to the composition of birds. This research proposes to evaluate the severity of small UAV (under 55 pounds) collisions with propulsion systems. Understanding the effects of a UAV-engine collision is critical for establishing regulations surrounding UAVs, and would provide critical information to better prepare the flight crew if this collision were to take place.

The results presented in this work focus on the initial effort of analyzing the ingestion of two different types of UAVs (a small quadcopter and a fixed wing) into generic engine models for a mid-sized business jet. The engine model geometries for two 40 inch diameter fans were developed in consultation with industry to be reasonable approximations of solid titanium fan blades on the thin side and thick side for the chosen engine size, but were not meant to represent any particular engines in service. The materials used for each of the engine components are reflective of some of the materials currently used in engines and were selected with industry input. Current in service jet engines differ greatly in geometry and material composition, so no single engine model could be developed to be representative of all the engines of this approximate size currently in service. The focus of this study is to understand the effect of certain parameters on the damage to the engine and it is not to determine the damage to any specific design.

The initial simulations presented in this work are focused on identifying the critical variables in an ingestion of a UAV. It was found that the damage from the fixed wing ingestion is larger than that of the quadcopter ingestion due to its heavier and larger core components, particularly the motor and the camera. A trend observed from both the quadcopter and the fixed wing ingestions is that the damage increases significantly as the ingestion moves from the center (nosecone), to the inner blade and then to the outer blade. As expected, the takeoff scenario is the worst case since the fan has the highest rotational speed in this case. Other factors that have a major impact on the damage level include the thickness of the blade and the orientation of the UAV during the impact. None of the ingestion simulations from this preliminary work resulted in a loss of containment.

Additional ingestion studies should be carried out to explore the effects of more parameters on the ingestion. Moreover, additional material models for composite fan stages are also needed. There is ongoing research into these composite material models and incorporating them into an engine ingestion simulation is another path for future work. Additional fan stage models of commercial jet engines is another area to be investigated. Engines for commercial jets vary greatly in size but are generally larger than the mid-size business jet engine studied in this work. Finally, a key part of future work is to conduct full scale ingestion experiments of UAVs into fan stages running at operational speed. These experiments are critical in verifying the computational models that are being developed. Rotating engine experiments are particularly important for several reasons. First, the fan blades will stiffen when rotating at their operational speed. Second, the actual geometry of the blades will change due to the centripetal acceleration. Third, the relative velocity of the fan and the UAV comes from both the speed of the plane moving forward as well as the speed of the rotating fan blades. If the UAV hits the blade close to the tip, the relative velocity can be sonic, which is much greater than the plane speed in landing and take-off conditions.

1. INTRODUCTION

The intent of this document is to describe a computational research program designed to determine the behavior of mid-sized business class engine fan stages, which are reasonable approximations of solid titanium fan blades on the thin side and thick side for these engines, operating under conditions such as take-off, approach, and flight below 10,000 ft. when impacted by an unmanned aerial vehicle (UAV), report on the initial computational results, and discuss future work. The intent of this work is to understand how different parameters influence the expected level of damage to the engine models, and therefore, the engine models will be referred to as parametric study models hereafter. While much is known about soft body impacts (usually birds) on the propulsion systems from bird ingestion tests and from inflight occurrences, the same cannot be said for hard body impacts such as UAVs. The goal of this research program is to develop an accurate computational simulation of a small UAV (under 55 pounds) impacting a fan stage operating at conditions reflective of take-off, approach, and flight below 10,000 ft. The computational work is closely aligned with future experiments that can be conducted at The Ohio State University (OSU) Gas Turbine Laboratory in later phases of the proposed project. The computational method is developed and used on generic fan stage models housed within a generic containment tank that are impacted by UAV models developed at the National Institute for Aviation Research (NIAR) at Wichita State University and Mississippi State University. The computational tool is planned to be used with the same fan stage that is obtained for future experiments for verification of the method.

1.1 MOTIVATION

The use of UAVs has increased dramatically in recent years. UAVs have been used by the military for years and recently there has been a strong interest in their commercial and recreational applications. As the number of UAVs sold continues to increase, proper integration of UAVs into the airspace is a major safety concern due to the potential for a UAV-airplane collision. Hobbyist UAV users are the highest safety concern, as they may be unaware or unconcerned with government rules and restrictions when they fly their UAVs. The UAVs of hobbyists are relatively small and more likely to be ingested by an engine in a collision event. Currently, there are regulations and engine tests for bird and ice ingestions to ensure a plane can survive impacts with these objects. These tests and regulations cannot be directly transferred from birds and ice to UAVs since the materials that compose a UAV are very different to the composition of birds. Some of the UAV components, including the motor, camera, and battery, can be far more dense and stiff than birds (which are typically modeled as a fluid since they are over 70% water) and ice. Understanding the effects of a UAV-engine collision is critical for establishing regulations surrounding UAVs, and would provide critical information to better prepare the flight crew if this collision were to take place.

1.2 SCOPE OF THE WORK

In this work, parametric study models of a mid-sized business engine's fan stage, nosecone, and containment ring were developed and integrated for use in ingestion simulations. The models were created using previous FAA projects as points of reference, and then modified based upon industry input. The test cases considered in this preliminary study covered several parameters at three flight conditions representing take-off, approach, and flight below 10,000 ft., where it is most likely an ingestion event would take place. The simulations of the UAV ingestion into the jet engines were carried out with the commercially available finite-element software LS-DYNA. The software is well equipped to model highly nonlinear dynamic events with explicit time integration, which is necessary for high-velocity impact events. Additionally, the software includes an implicit solver that is used to find the pre-stressed loads from the centripetal acceleration of the spinning fan stage. The material models used in these impact events need to be sophisticated so that they can accurately capture material failure. In this work, the material models used for the fan blades, fan disk and nosecone have been developed from extensive experimental testing, and take 3D stress, strain rate, temperature, and element size into account. This is necessary over traditional piecewise-linear material models because high velocity collisions (such as fan blades with a UAV) will have large strain rates and heating due to plastic deformation that will have insufficient time to dissipate, which will cause the local temperature in deformed elements to rise significantly. Also, the material model used for the fan is able to predict multiple types of failure modes. Accurate modeling of the UAVs used for the ingestion simulation is also critical. Two UAVs were chosen for this work: a common quadcopter UAV, the DJI Phantom 3, popular among hobbyists; and a common fixed wing UAV, the Precision Hawk. Mississippi State and NIAR created models of the UAVs and compared simulations of crash tests of key UAV components against aluminum plates with the corresponding experiments, and then tuned the models to match the experiments. UAV model details can be found in the reports on the quadcopter[2] and the fixed wing[3]. The simulations show that the initial conditions of the UAV ingestion greatly affect the level of damage to an engine, and lay the foundation for further parameterized studies and experimental UAV-engine impact events.

2. UAS PROJECTILE DEFINITIONS

Two UAVs were modeled for their ingestion into an engine: a quadcopter and a fixed wing.

2.1 QUADCOPTER

The quadcopter chosen for the engine ingestion is the DJI Phantom 3 - weighing 2.68 lbs. This quadcopter's abundance and ease of use make it one of the most likely types of UAVs to impact an airplane[4]. The quadcopter finite element (FE) model shown in Figure 1 and used in this impact study was made by a collaborating group at NIAR at Wichita State University. This group reverse engineered the DJI Phantom 3 to be used in computational impact studies.

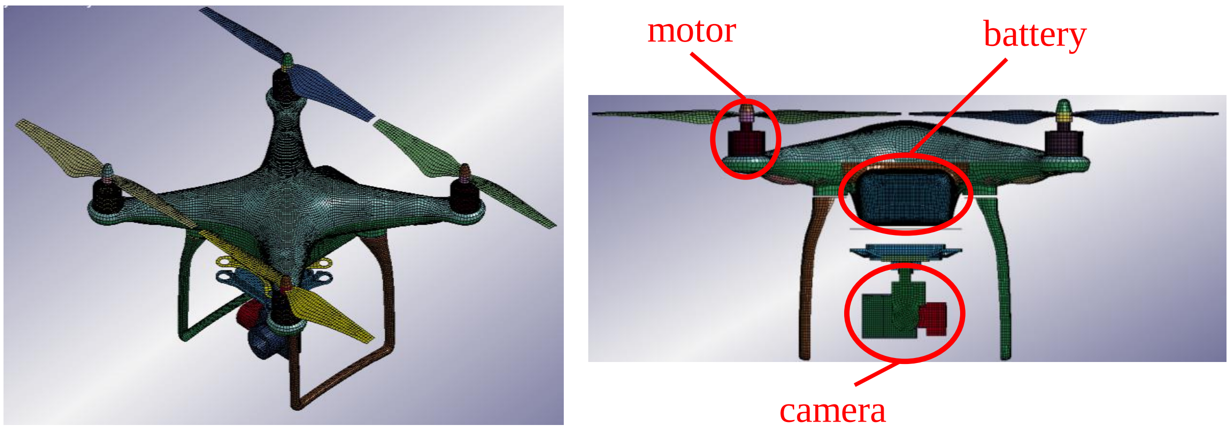

(a) Oblique view (b) Front view

Figure 1: Quadcopter FE model

The quadcopter model obtained from NIAR was scanned to extract the geometry for the quadcopter model. The material models used were developed from experiments to produce material failure under a variety of conditions. The three major components (motor, battery, and camera) are identified in Figure 1(b). These components were shot at aluminum plates of varying thickness. These experimental impacts were compared to LS-DYNA simulated impacts. The LS-DYNA models of these components were adjusted to match the damage to both the plate and the quadcopter components in the experiment. The FE models of these components are shown in Figure 2. Additional details on the construction of the quadcopter model can be found in the companion report[2].

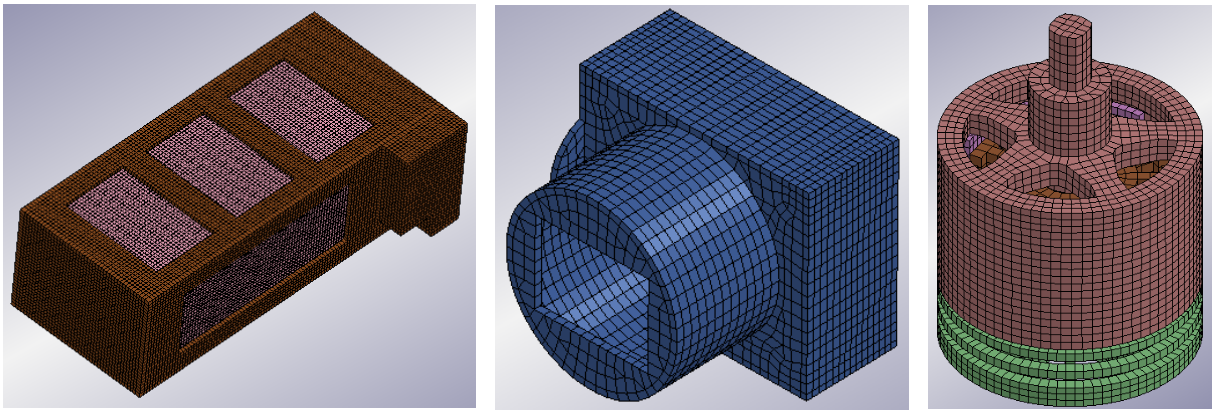

(a) Battery (b) Camera (c) Motor

Figure 2: Critical components of the quadcopter

2.2 FIXED WING

The fixed wing chosen for the engine ingestion is the Precision Hawk Lancaster Hawkeye Mark III - weighing 4.0 lbs. The fixed wing UAV impact scenarios are distinct from those of rotorcraft-based UASs (e.g., differences in geometries, relative velocities, mass distribution, and total mass), and therefore separate fixed wing ingestion scenarios were studied in addition to quadcopter ingestions. The fixed wing FE model used in this study was made by a collaborating group at Mississippi State University and is shown in Figure 3. This group reverse engineered the Precision Hawk to be used in computational impact studies. Due to the size of the fixed wing with respect to the business class engine, a model of the Precision Hawk without the wings was used in the ingestion simulations.

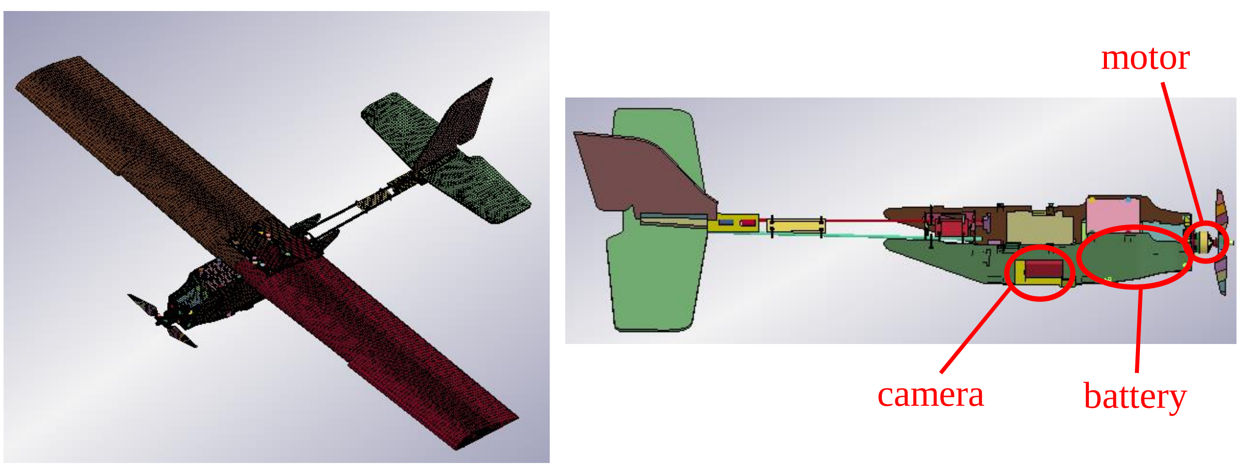

(a) Full Precision Hawk model (b) Wings removed from Precision Hawk

Figure 3: Fixed wing models

The UAV model obtained from Mississippi State University was scanned to extract the geometry for the UAV model. The material models used were developed from experiments to capture material failure under a variety of conditions. The motor and battery were shot at aluminum plates of varying thickness. These experimental impacts were compared to LS-DYNA simulated impacts. The LS-DYNA models of the components were adjusted to match the damage to both the plate and the UAV component in the experiment. The critical components of the fixed wing are identified in Figure 3(b), and the FE models of the key components are shown in Figure 4. Additional details on the construction of the UAV model can be found in a companion report[3].

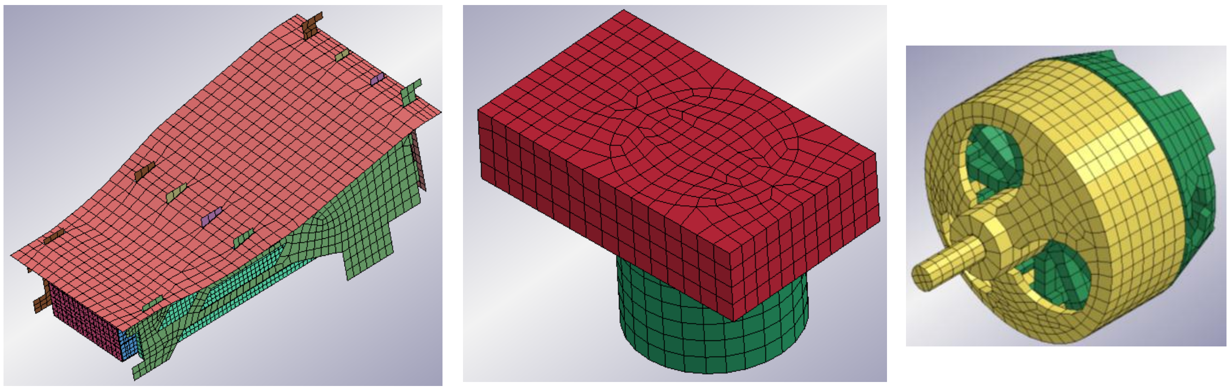

(a) Battery (b) Camera (c) Motor

Figure 4: Critical components of the fixed wing

3. JET ENGINE DEFINITION

Several key pieces of a jet engine were created or derived from previous FAA reports and used for the engine ingestion analysis. The modeled components in this generic engine include the nosecone, shaft, fan disk, fan blades, nacelle, and containment ring. The assembled engine model is shown in Figure 5 (the Kevlar® wraps of the fan containment case are shown in yellow). The shaft, fan disk, fan blades, and nacelle were derived from a pre-existing jet engine model used to study a fan blade out event (FBO)[5]. This FBO model is publically available[6] on the LS-DYNA Aerospace Working Group (AWG) website. The fan is 40 inches in diameter, which represents a mid-size business jet engine. A pre-existing modern containment ring was also included in the engine that was developed from a previous FAA project focused on multilayer composite fabric containment systems for gas turbines[7] and it is also publically available on the AWG website[8]. A generic biconic nosecone was developed for the engine as well.

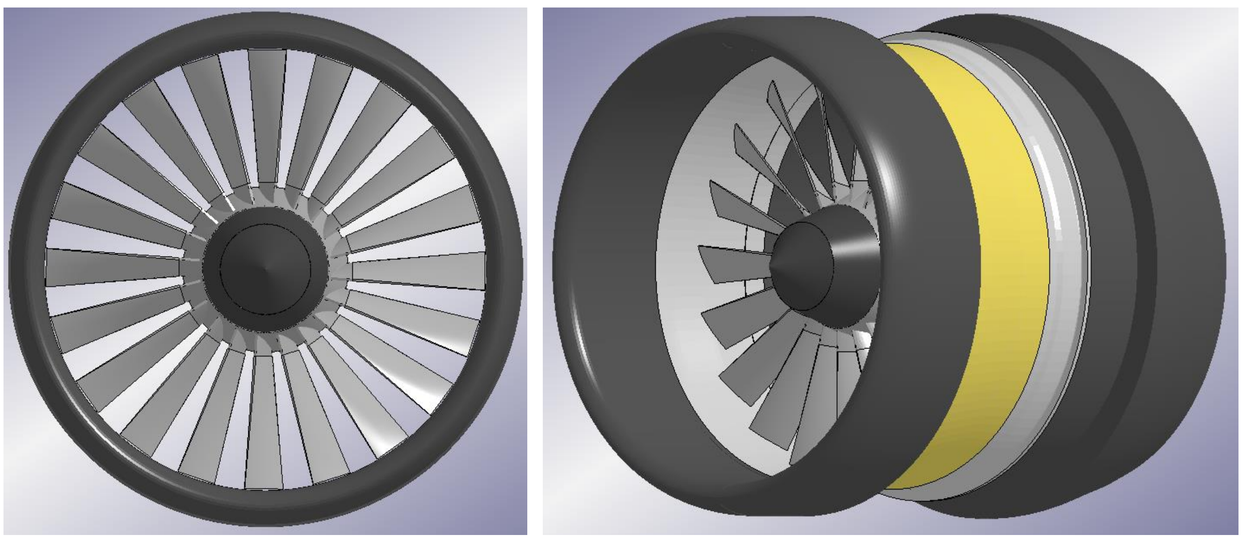

(a) Front view (b) Oblique view

Figure 5: Assembled generic mid-sized business jet engine model

3.1 JUSTIFICATION

The primary goal of this study is to investigate how several parameters in a UAV ingestion (i.e., flight conditions, location of impact) affect a typical mid-size business jet engine's fan blades, fan containment system, and nosecone. The goal of the model is to capture geometric and material characteristics consistent with modern mid-size business jet engines and the model is not intended to represent a specific engine in service.

The size of the engine was chosen to be the same as previous FAA studies focused on analyzing fan containment models[7] and fan blade out studies[5] used for a generic mid-size business jets. Representative engines in this class size are given in Table 1.

Table 1: Mid-size business jet engines and their fan diameter

Engine	**Business Jets**	**Fan Diameter**	**Company**
PW306B	Dornier 328JET	44.8"	Pratt & Whitney Canada
TFE731	Learjets, Gulfstream G100	39"	Garrett/Honeywell
AE3007	Cessna Citation X, Embraer ERJ 145 family	38.5"	Rolls Royce
CFE738	Dassault Falcon 2000	35.5"	CFE company
HTF7000	Cessna Citation Longitude, Gulfstream G280, Embraer Legacy 500/450	34.2"	Honeywell

Two sets of fan blades were created to represent fan blades in the 40 inch diameter business class engines that are (1) thin and (2) thick. These blades were derived from the FBO model[5] and modified with industry input to make their dimensions reasonable with respect to current fan blade thicknesses and geometries for solid titanium blades. These blade thicknesses and geometries were chosen to be reflective of a range of fan blades thicknesses for 40 inch diameter engines so that blade thickness could be one of the parameters studied in this investigation; however, these parametric models are not supposed to represent any specific engines currently in service. Both blades are composed of a titanium alloy (Ti-6Al-4V). The two blade geometries chosen are used to illustrate the effect of the blade thickness on the ingestion event. It is expected that the damage from an ingestion event would fall within the range of damages present between the thin and thick ingestion cases. It is also expected that the thicker blades will be more robust to foreign object damage; however if the thicker blade is released it is more likely to penetrate the fan containment ring. Each set of blades was connected to the fan disk from the FBO model[5].

The fan containment ring is another critical component of the engine model. A modern containment ring composed of a multilayer composite fabric wrapped around a metal ring, which was developed in a previous FAA project[7], is used in the engine model. The thicknesses of the aluminum ring of 0.18 inches and the Kevlar® wraps of 0.968 inches were selected with industry input as reasonable thicknesses for a 40 inch diameter fan. The fan containment ring was constructed around the fans and connected to the upstream and downstream portions of the nacelle from the FBO model[5].

A generic biconic nosecone was also developed for this study to see the effect of a UAV impact on a generic nosecone. The nosecone is made of aluminum and has a thickness of 0.12 inches. The nosecone is connected to a transition section, also with a minimum thickness of 0.12 inches, which is connected to the fan disk.

3.2 CAD MODELING

The fan disk geometry was generated using CAD software and information from the FAA FBO report[5] detailing its geometry. Each set of fan blades was also generated using CAD software. A National Advisory Committee for Aeronautics (NACA) 4410 airfoil for the root and NACA 4403 airfoil for the tip was used for the thin blade. The profiles were connected using a sweep tool where the angles and thicknesses changed linearly from the root to the tip of the blade. The geometry model of the thick blade was created in a similar manner using a NACA 4414 profile for the root and NACA 4405 profile for the tip. Both fans have blades angled at the root and tip, in this case, 17° at the root and 60° at the tip. The thin blades have airfoil cross sections with a maximum root thickness of 0.47 inches and a maximum tip thickness of 0.17 inches. The thick blades have airfoil cross sections with a maximum root thickness of 0.66 inches and a maximum tip thickness of 0.25 inches. An image of the full set of thin fan blades in the engine is shown in Figure 5, while an image of the thick fan blades are shown in Figure 6(a), and an image of the blade tip profiles for both geometries is shown in Figure 6(b). For both fan stages, fillets were used to merge the blades to the disk to avoid stress concentrations that would have resulted from sharp corners.

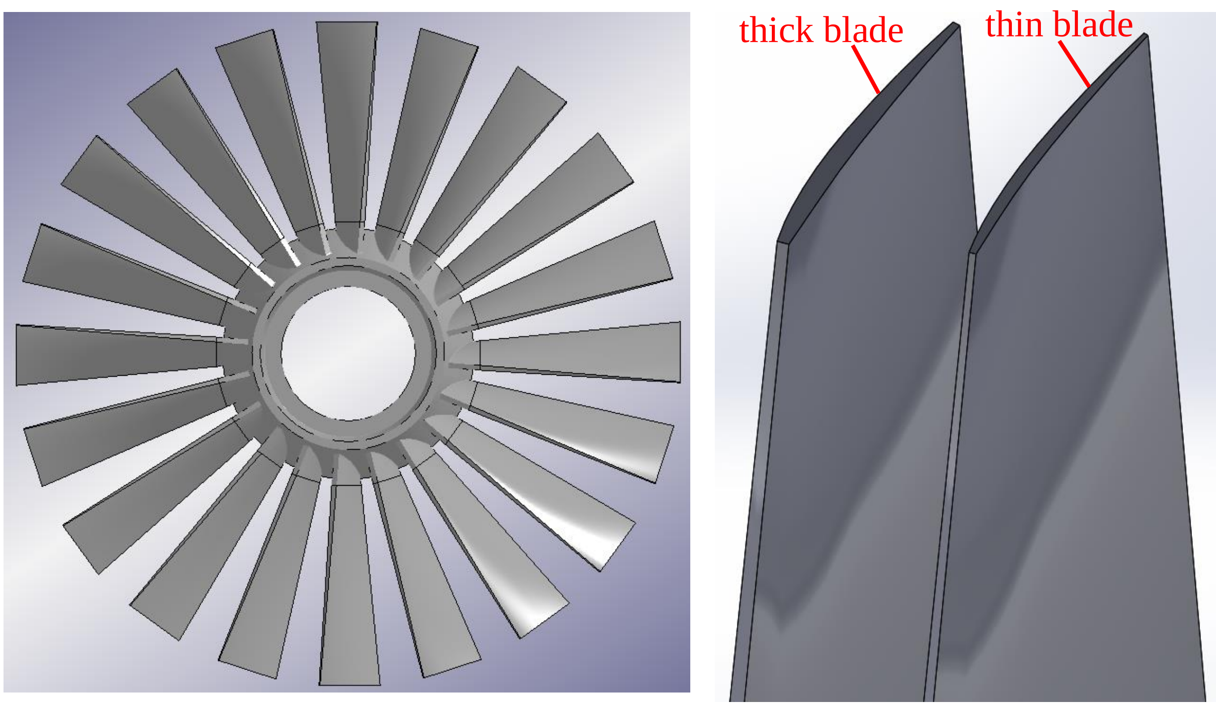

(a) Full fan stage with thick blades (b) Blade tip profiles for each thickness

Figure 6: Fan stage geometries

The fan containment ring was taken from the AWG website[8]. Slight scaling changes were made to the geometry to ensure that the fan stages would fit inside. The containment ring was also connected to the upstream and downstream portions of the nacelle developed in the FAA FBO project[6]. Slight scaling was also applied to the nacelle to match it to the containment ring.

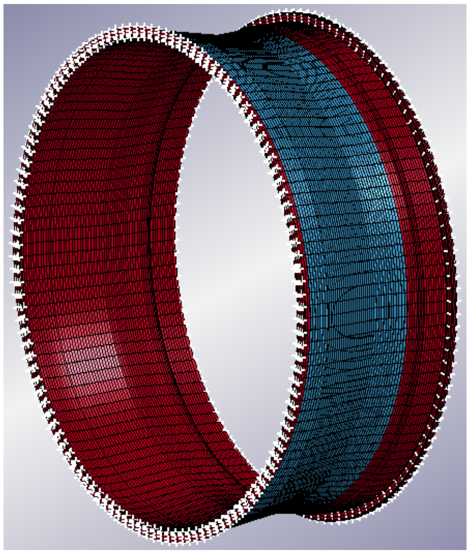

(a) Containment ring alone

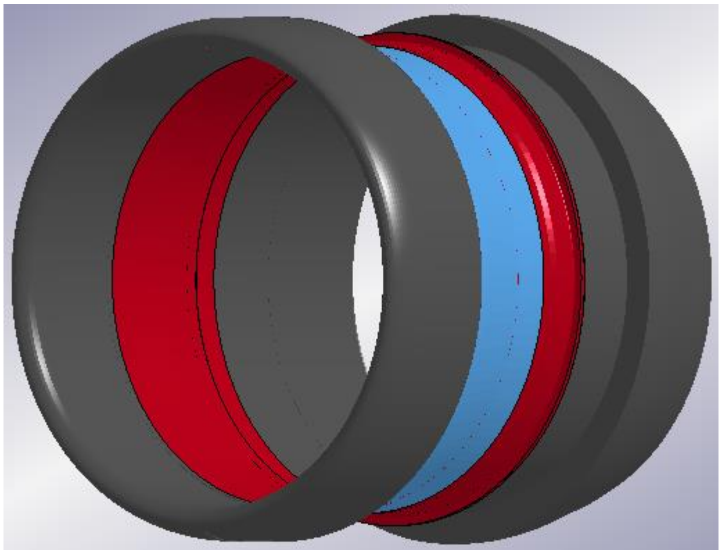

(b) Containment ring connected to nacelle

Figure 7: Nacelle for generic fan stage

The nosecone was designed with a biconic shape with industry input for a reasonable thickness and geometry. Figure 8 shows the assembled nosecone and transition and a cross-sectional view of the nosecone and transition sections. The thickness of the majority of the nosecone and the transition components is 0.12 inches. The bottom of the transition section, which connects to the fan disk, is considerably thicker than the rest of the transition to ensure proper mating with the fan disk.

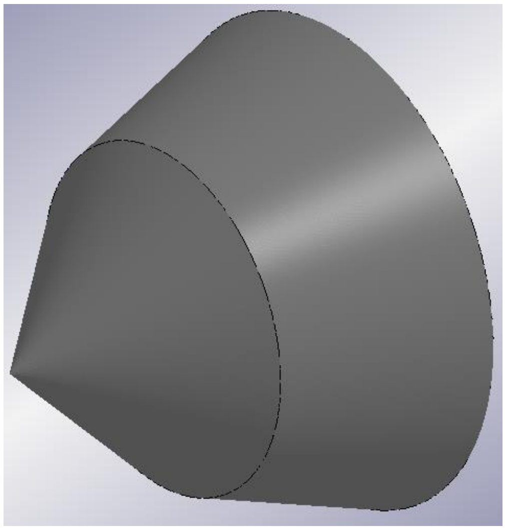

(a) Assembled nosecone and transition

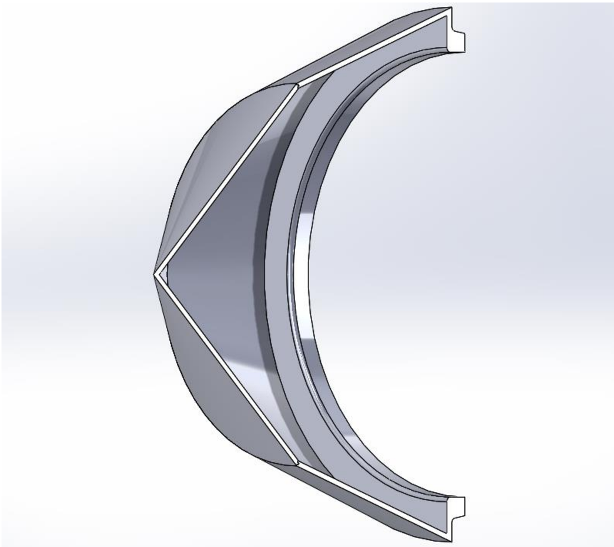

(b) Cross-sectional view of nosecone and transition

Figure 8: Generic biconic nosecone

3.3 FINITE ELEMENT MODELS

Multiple FE models were generated for the fan stages used in the ingestion studies. The different meshes were developed with the location of the impact in mind. The location on the fan where the impact occurs requires a refined mesh to accurately capture the expected failure modes included in the material models. The multiple meshes with refinements in the specified regions are needed to keep the model a reasonable size so that the computational simulations are tractable, while also obtaining accurate results where the impacts take place.

A single FE model of each of the other components was used for all impact studies. The nosecone mesh was created to be very refined so that it could accurately assess damage in the case when the nosecone is impacted. The element size for the nosecone was 0.02 inches and a picture of the nosecone FE model is shown in Figure 9. To save on computational resources, the nosecone was made rigid in cases where it was not impacted. Other components such as the containment ring, nacelles, and shaft were taken from the FBO model[6] and the containment model[8] and the meshes were not altered beyond slight scaling changes.

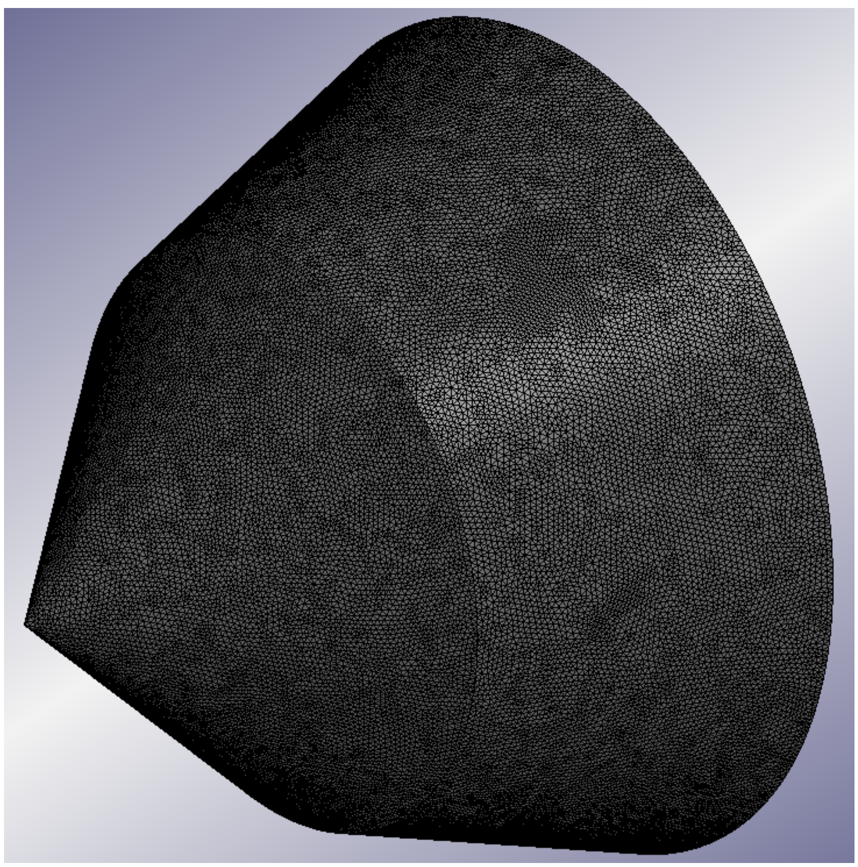

Figure 9: Mesh of the nosecone

Two element types were used in the fan. The elements in the refined portion of the blades are 8 noded hexahedrals (elform=1) under *SECTION_SOLID[9]. The disk and coarse portion of blades are made of solid 4 node tetrahedrons (elform = 10) under *SECTION_SOLID[9]. The inlet and outlet from the FBO model[6] are shells (elform=16) under *SECTION_SHELL and the aluminum containment model[8] is made of shell thickness elements (elform=5) under *SECTION_TSHELL while the Kevlar wrap is made of Belytschko-Tsay shells (elform=2) under *SECTION_SHELL.

In order to connect the refined hexahedron portion of the blade to the coarser tetrahedron portion of a blade or the disk, tied contacts of type *CONTACT_TIED_NODES_TO_SURFACE_CONSTRAINED_OFFSET[9] were used. A node set with the nodes on the bottom surface of the blades were used as slave nodes and the disk was used for the master nodes in the contact with the static and dynamic friction coefficients set to 0.3. As seen in some of the test runs in section 4. , this tied contact did produce some stress concentrations on the blade elements connected to the disk. In some cases these elements experienced plastic deformations, but were not subjected to failure. The simulations with significant amounts of damage resulted in failing elements close to the impact location on the blades, which was away from the tied contacts.

The boundary condition for the containment casing has the lengthwise outermost nodes (shown in white in Figure 7(a)) fully restricted from displacement. The upstream and downstream portion of the nacelle is made into a rigid body via *MAT_RIGID[9], and has all translational and rotational degrees of freedom restricted. Damage to the nacelle was outside the scope of the current project.

With the exception of the nosecone impact cases, the nosecone and drive shaft were made into rigid bodies via *MAT_RIGID[9] with all but their engine rotational axis degrees of freedom restricted. In the nosecone impact cases, a node set of the interfacing nodes on both the fan and the nosecone transition section were made into a single nodal rigid body with *CONSTRAINED_NODAL_RIGID_BODY_SPC[9]. The same was done between the nosecone and nosecone transition.

The innermost nodes along the disk for the fan were used to form a rigid body via *COSTRAINED_NODAL_RIGID_BODY_SPC[9], with all but their engine rotational axis degree of freedom restricted. An initial velocity was assigned to the fan using *INITIAL_VELOCITY_GENERATION[9]. The rotational velocity of the fan decreases slightly as energy is transferred to the UAV during the collision.

3.3.1 Material Definition

The engine model was composed of three materials: aluminum 2024, a titanium alloy (Ti-6Al-4V) and Kevlar® 49. The nosecone is composed of aluminum 2024. The fan blades and disk are composed of the titanium alloy, and the containment ring is composed of 0.18 inches of aluminum wrapped in 0.968 inches of Kevlar®.

The aluminum and titanium were modeled with *MAT_TABULATED_JOHNSON_COOK (*MAT_224)[9, 10]. MAT_224 is an isotropic constitutive material model designed to capture plastic damage and failure within metals. Here we summarize a few points of *MAT_224 which are discussed in the AWG *MAT_224 user guide[10]. *MAT_224 includes strain rate and temperature dependence in calculating the plastic failure strain for elements in the FE model:

$$\varepsilon_{pf} = f(\tau, \theta_L) g(\dot{\varepsilon}_p) h(T) i(l_c)$$

Where ε_{pf} is the plastic failure strain for an element, $\tau,$ is the triaxiality, θ_L is the Lode parameter, $\dot{\varepsilon}_p$ is the plastic strain rate, T is the temperature, and l_c is the element size[10]. A *MAT_224 material model is made by measuring the strain of a material under the different loading conditions. To build the material model, experiments are conducted to find the relation between strain and stress, strain rate, temperature, and element size (i.e., find the functions f, g, h, i, above). Within the model, elements fail when their failure criterion F is greater or equal to one, where the failure criterion, F is defined as:

$$F = \int \frac{\dot{\varepsilon}_p}{\varepsilon_{pf}} dt$$

Thus, by summing the ratio of strain rate to plastic strain over each time step, element failure is calculated. The advantage with this definition of the failure criterion is that it captures accumulated damage over time and elements are not required to reach some instantaneous failure strain value. Undamaged elements have an F value of 0.0 whereas elements that have plastic deformation and are about to fail would have an F value just below 1.0. Any F value above 0.0 indicates some plastic deformation.

Including strain rate and temperature dependencies in the material model is important because of the high velocities involved in aerospace impact events[11]. These high velocity impacts are sensitive to strain rate because the plastic work occurring in such a short time interval creates large temperature increases resulting in local material softening.

Following previous FAA work[12-14]., the Kevlar® containment wrap outside of the casing is modeled in LS-DYNA using *MAT_DRY_FABRIC (*MAT_214). This material model was designed to model high strength woven fabrics such as Kevlar®, which are used to absorb large amounts of energy. *MAT_DRY_FABRIC uses an equivalent continuum formulation to avoid modeling the fibers within the material. Elements of the containment wrap fail by reaching a predetermined strain value in either the transverse or longitudinal material directions. The model of the Kevlar® wrap used here has a single layer of shell elements. In the event of debris penetrating beyond the aluminum casing, failure in the Kevlar® shell elements represents the debris breaking through the Kevlar® wrap. Intermediate cases where the debris break through some but not all of the layers of Kevlar® in a containment wrap would be seen in this model as non-failure of the single layer in the FE model. Predicting the number of failed layers of Kevlar® in the containment wrap requires multiple layers of shell elements and was beyond the scope of the current project.

The LS-DYNA material models were developed in previous FAA projects for the titanium alloy[15, 16], aluminum[17, 18] and Kevlar® wraps[12-14]. The materials were each chosen for their respective components with industrial input to develop the generic engine model; however, other similar materials are often used in real engines. Future UAV ingestion studies may consider alternative materials such as composite fan blades. This will be discussed in future work in section 5.3 .

3.3.2 Discretization

A variety of meshes were made for the fan stage with thin blades for the different ingestion simulations to compromise between computational performance and mesh accuracy. The different collisions are discussed in section 4.1 in Table 3.

The failure criterion used in the material model for the fan, *MAT_224, has a dependence on element size, $i(l_c)$. The element size for *MAT_224 is defined to be the volume divided by the maximum surface area of the element[10]. LS-DYNA will interpolate between points on the regularization plot to find the mesh regularization scale factor for a given element. LS-DYNA extrapolates regularization curves for elements outside those the model was developed from. This is not generally an issue as long as the mesh is relatively well refined since the extrapolation will be small and the curve is smooth with only a weak dependence on element size. Due to the preference for a highly refined mesh in any region where contact occurs, several meshes were created for the thin blades for the various different cases to optimize computational performance and mesh accuracy.

Figure 10 shows a mesh where the tips of four blades were refined with an element size of 0.03 inches. This mesh was used for all of the component level impacts with the tips of the blades except for the quadcopter battery component test.

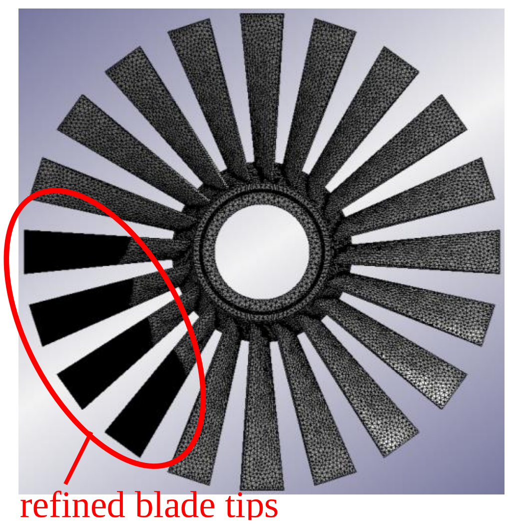

(a) Full stage

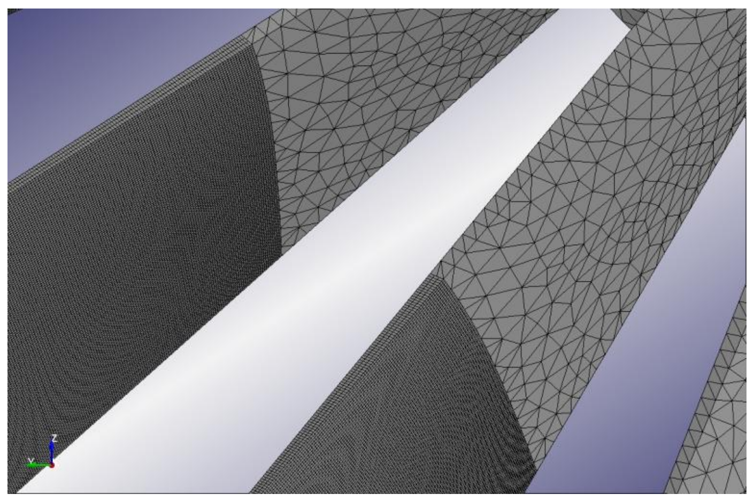

(b) Close-up of mesh interface

Figure 10: Four thin blades refined at the tip

Figure 11 shows a mesh where most of 10 blades were refined with an element size of 0.035 inches and the remaining 10 blades had an element size of 0.08 inches. This mesh was used for the quad-copter tip impacts at all speeds and orientations, the quadcopter battery impact, and the fixed wing approach and orientation cases.

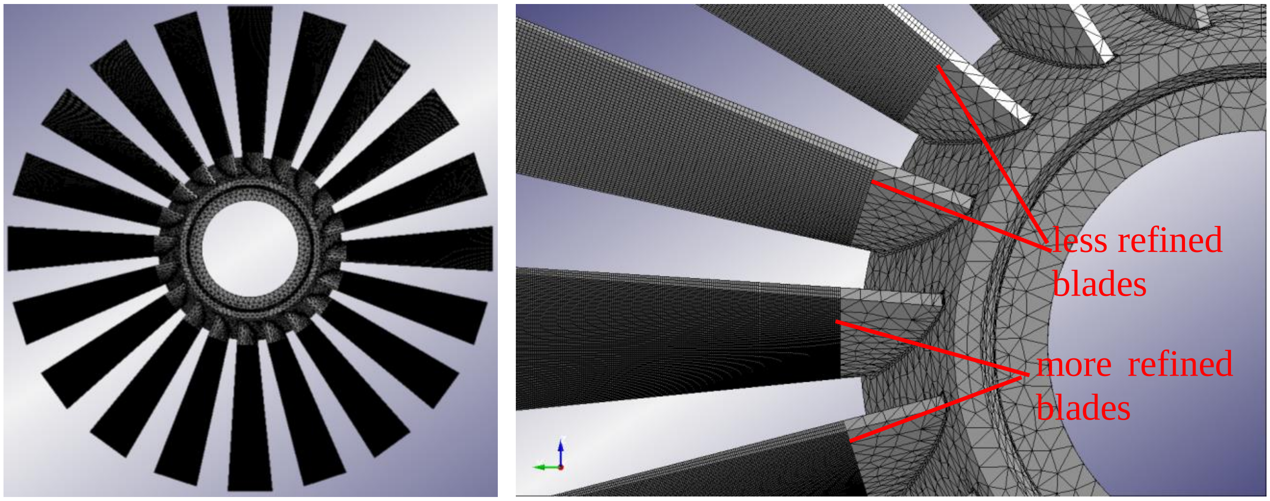

(a) Full stage (b) Close-up of mesh interface

Figure 11: Ten thin blades fully refined

Figure 12 shows a mesh where the tips of all 20 blades had an element size of 0.04 inches. This mesh was used for the fixed wing for the baseline takeoff and flight below 10,000 ft. cases.

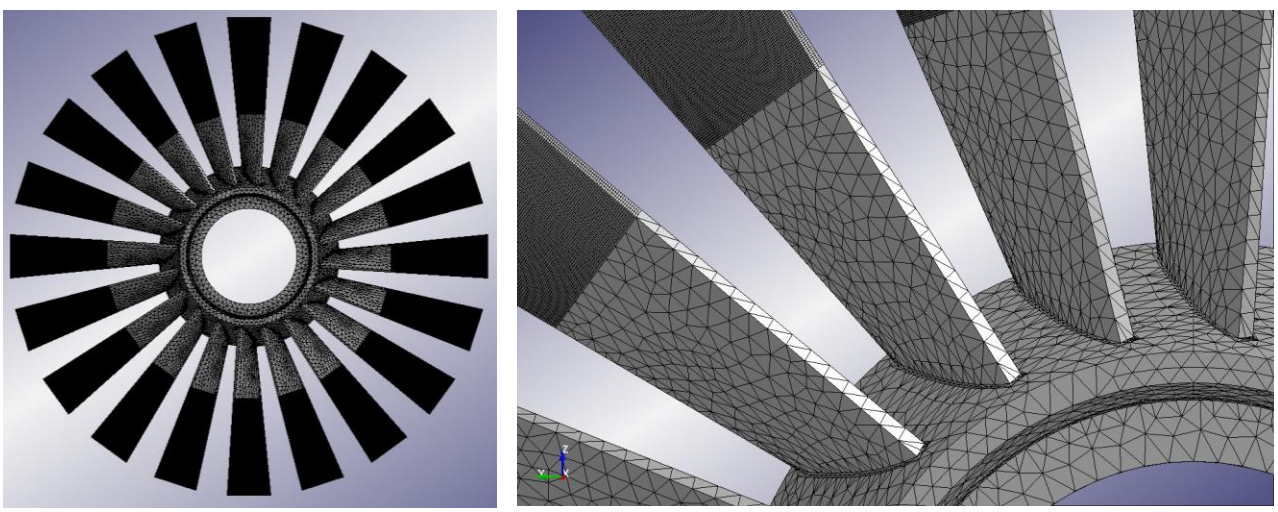

(a) Full stage (b) Close-up of mesh interface

Figure 12: All twenty thin blades refined at the tips

Figure 13 shows a mesh where most of all 20 blades were refined to an element size of 0.06 inches and the disk was also refined. This mesh was used for the inner blade case for the quadcopter.

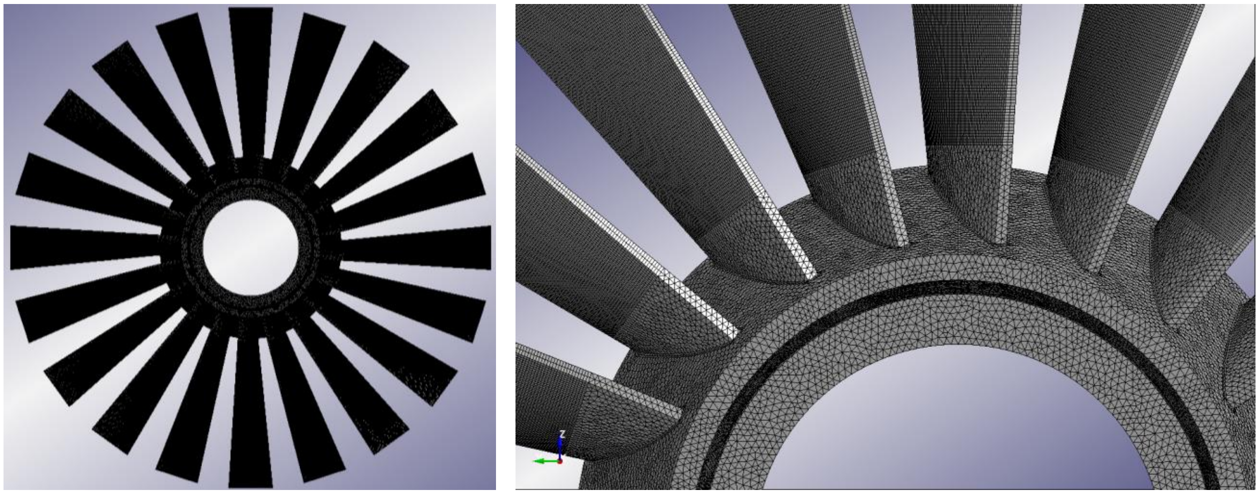

(a) Full stage (b) Close-up of mesh interface

Figure 13: All twenty thin blades and disk refined

Figure 14 shows a mesh where most of all 20 blades were refined to an element size of 0.06 inches but the disk was not refined. This mesh was used for the inner blade case for the fixed wing.

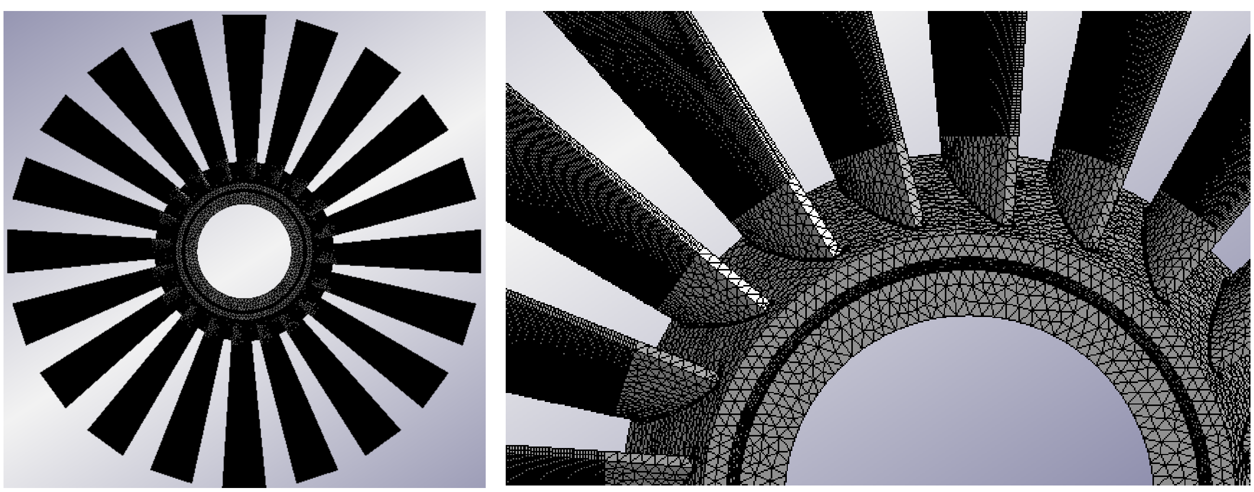

(a) Full stage (b) Close-up of mesh interface

Figure 14: All twenty thin blades refined

Figure 15 shows a mesh of the fan stage with the thick blades. The majority of all the blades were refined with an element size of 0.06 inches.

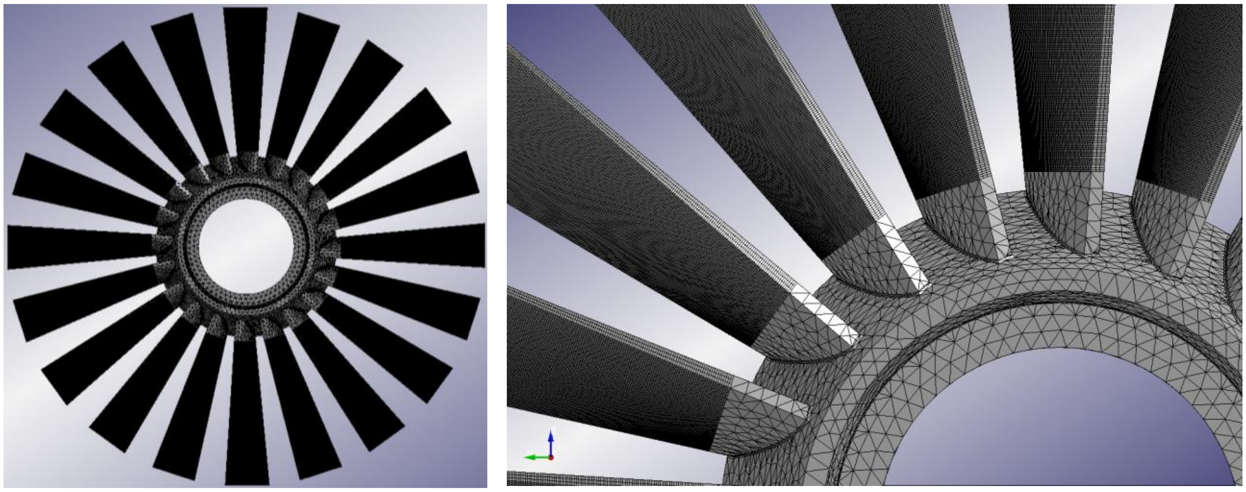

(a) Full stage (b) Close-up of mesh interface

Figure 15: Mesh for thick fan stage with all blades refined

4. UAS-FAN COLLISION SIMULATIONS

This chapter discusses the various impact simulations conducted in this initial computational study. First, a justification of the impact conditions selected for the baseline scenarios is presented. Next, a classification of the damage levels is discussed. After that, a description of the initial set-up for the ingestion is provided. Then, the results of each ingestion case for the quadcopter are discussed and the results are summarized. Finally, the results of each ingestion case for the fixed wing are discussed and the results are summarized.

4.1 SELECTION OF INGESTION CONDITIONS

The ingestion conditions were chosen to capture three different flight conditions that capture the most probable high velocity impact scenarios with a UAV: takeoff, approach and flight below 10,000 ft. The operating conditions of the engine were chosen using the FAA General Operating and Flight Rules (14 CFR Part 91)[19] and an FAA Report on the UAV ingestion hazard[20]. The maximum flight speeds and maximum fan blade tip speeds are shown in Table 2.

Table 2: Engine operating conditions for three scenarios

Flight Phase	**Maximum Aircraft Speed (knots)**	**Fan Blade Tip Speed (ft./s)**
Takeoff	180	1422
Below 10,000 ft.	250	995
Approach	180	355

The operating conditions for these flight conditions were used to define a test matrix for this initial engine ingestion study to determine the effects of several parameters. These parameters include the phase of the flight, the object that is impacting the engine, the location of the impact on the fan stage, the thickness of the fan blades and the orientation of the impact. Note that in this initial study the maximum speed of the plane is used and the UAV is assumed to be stationary when it is ingested. The relative speed of the impact can be larger, and it depends on the top speed of the particular UAV that is ingested, and if it is moving towards the engine (as opposed to away from it). A summary of the test cases analyzed in this report are given in Table 3. Note that the primary focus of the cases is on the takeoff scenario because it was expected that this would be the flight condition that would lead to the most damage in the engine.

Table 3: Test matrix focused on takeoff flight condition

Test Type	**Plane Speed (knots)**	**Impact Location**	**Fan Speed (RPM)**	**Fan Blade**	**Relative Orientation**	**UAV Model - Component**
Takeoff Baseline 1	***180***	***outer blade***	***8500***	***thin***	***Direct***	***quadcopter***
Takeoff Component 1	180	outer blade	8500	thin	Direct	**motor**
Takeoff Component 2	180	outer blade	8500	thin	Direct	**camera**
Takeoff Component 3	180	outer blade	8500	thin	Direct	**battery**
Takeoff Location 1	180	**inner blade**	8500	thin	Direct	quadcopter
Takeoff Location 2	180	**nosecone**	8500	thin	Direct	**motor**
Takeoff Location 3	180	**nosecone**	8500	thin	Direct	**camera**
Takeoff Location 4	180	**nosecone**	8500	thin	Direct	**battery**
Takeoff geometry	180	outer blade	8500	**thick**	Direct	quadcopter
Takeoff Orientation	180	outer blade	8500	thin	**90° pitch**	quadcopter
Approach 1	180	outer blade	**2000**	thin	Direct	quadcopter
Below 10,000 ft. 1	**250**	outer blade	**6000**	thin	Direct	quadcopter
Takeoff Baseline 2	***180***	***outer blade***	***8500***	***thin***	***Direct***	***fixed wing***
Takeoff Component 1	180	outer blade	8500	thin	Direct	**motor**
Takeoff Component 2	180	outer blade	8500	thin	Direct	**camera**
Takeoff Component 3	180	outer blade	8500	thin	Direct	**battery**
Takeoff Location 1	180	**inner blade**	8500	thin	Direct	fixed wing
Takeoff Location 2	180	**nosecone**	8500	thin	Direct	**motor**
Takeoff Location 3	180	**nosecone**	8500	thin	Direct	**camera**
Takeoff Location 4	180	**nosecone**	8500	thin	Direct	**battery**
Takeoff geometry	180	outer blade	8500	**thick**	Direct	fixed wing
Takeoff Orientation	180	outer blade	8500	thin	**180° yaw**	fixed wing
Approach 2	180	outer blade	**2000**	thin	Direct	fixed wing
Below 10,000 ft. 2	**250**	outer blade	**6000**	thin	Direct	fixed wing

Images of the quadcopter with respect to the fan in the direct, and 90° pitch orientation are shown in Figure 16, and images of the fixed wing in the direct and 180° yaw orientation are shown in Figure 17.

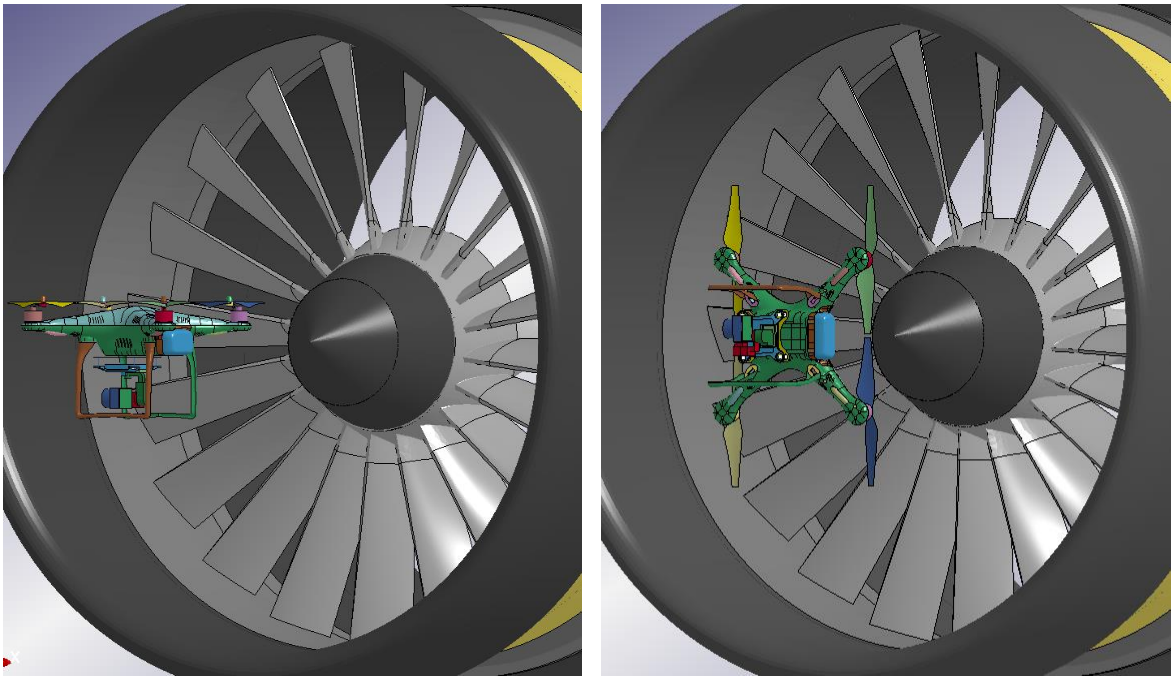

(a) Direct (b) 90° pitch

Figure 16: Orientations of the quadcopter

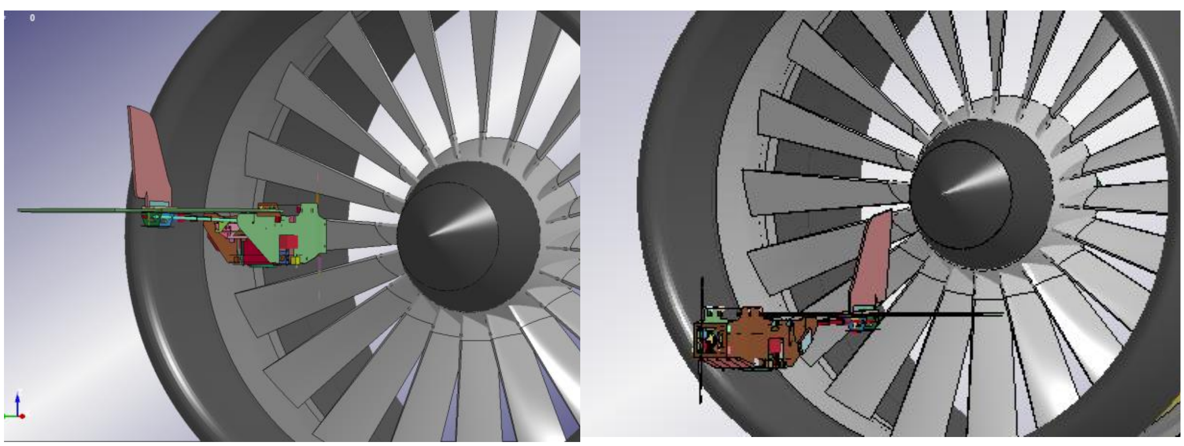

(a) Direct (b) 180° yaw

Figure 17: Orientations of the fixed wing

4.2 SETTING UP THE INGESTION SIMULATIONS

4.2.1 High Velocity Impact Setup

The work presented in this report is focused on three flight phases for the different ingestion scenarios: takeoff, approach and flight below 10,000 ft. The takeoff scenario was chosen as the baseline scenario since it is likely the most dangerous ingestion scenario. In the takeoff scenario the 40 inch fan was set to rotate at 8500 rpm, at this speed blade tip velocities are transonic. The impact of the UAV near the tip of the blades results in a violent collision, where many of the default LS-DYNA settings are insufficient. The time step scale factor under *CONTROL_TIMESTEP[9] was reduced from the default value of 0.9 to as low as 0.55 for some of the simulations to properly capture the high speed impact.

The contact used between both UAVs and the engine is *CONTACT_ERODING_SURFACE_TO_SURFACE[9, 11], with a part set containing the entire UAV as the slave and a part set with the engine as the master. The *CONTACT_ERODING setting updates the contact algorithm as elements fail and removes these elements from the calculation. The contact parameter SOFT=2 was chosen to improve contact stability with materials having several order of magnitudes difference in bulk modulus (e.g., contact of the titanium fan blades and the crushable foams in the UAVs). The contact parameter BSORT=10 was chosen to require frequent searching of slave-master pairs in the contact algorithms. This overcame the issue experienced in preliminary simulations with parts of the UAVs passing through some of the fan blades due to the slave-master pairs being identified too infrequently.

4.2.2 Setting Up the Fan Rotation

The fan stage was set to spin at 2000, 6000 and 8500 RPM for the simulations carried out in this report. These rotational speeds create large centripetal accelerations for the elements on the fan. If this initial rotating velocity was applied to a fan when it is at its at-rest position and stiffness, the fan elements would have large oscillations from suddenly rotating from 0 RPM to its operational speed. To avoid this problem, and obtain the loaded nodal positions and initially stressed fan, an implicit dynamic relaxation[9] was run. To accomplish this, a force was applied radially from the symmetry axis at the center of the fan. Using *INTERFACE_SPRINGBACK_LSDYNA the nodal locations and initial stresses of the converged preloaded rotating fan were written to a dynain file[9] that was subsequently imported with the rest of the model when starting the explicit impact calculations.

The innermost nodes of the disk were constrained to form a nodal rigid body with *CONSTRAINED_NODAL_RIGID_BODY_SPC, with all but the engine rotational axis degree of freedom of the nodal rigid body fixed. This holds the fan in position as it is rotating on the drive shaft. The fan is given its initial rotational velocity through *INITIAL_VELOCITY_GENERATION.

The first principal stresses in the thin fan and thick fan are shown in Figure 18 and Figure 19, respectively, for the 8500 RPM speed. Also, the deflection contours for the thin fan and thick fan are shown in Figure 20 and Figure 21, respectively, for the same speed.

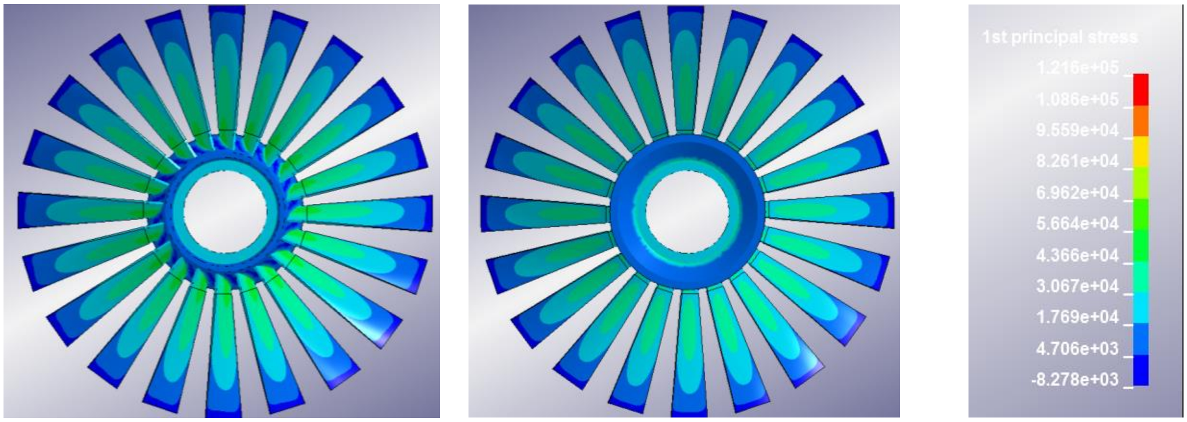

(a) Front (b) Back (c) Scale

Figure 18: The first principal stress from preloading the thin fan with units lbf/in^2

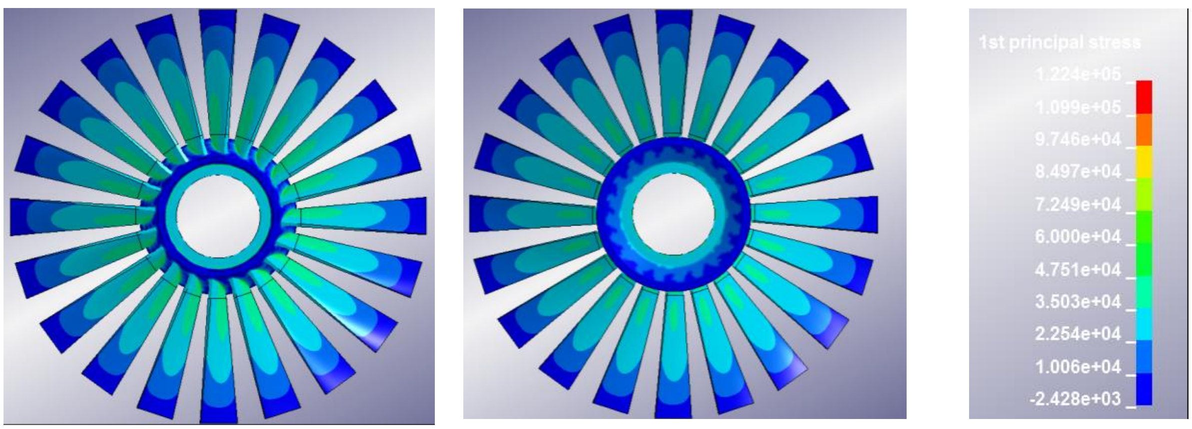

(a) Front (b) Back (c) Scale

Figure 19: The first principal stress from preloading the thick fan with units lbf/in^2

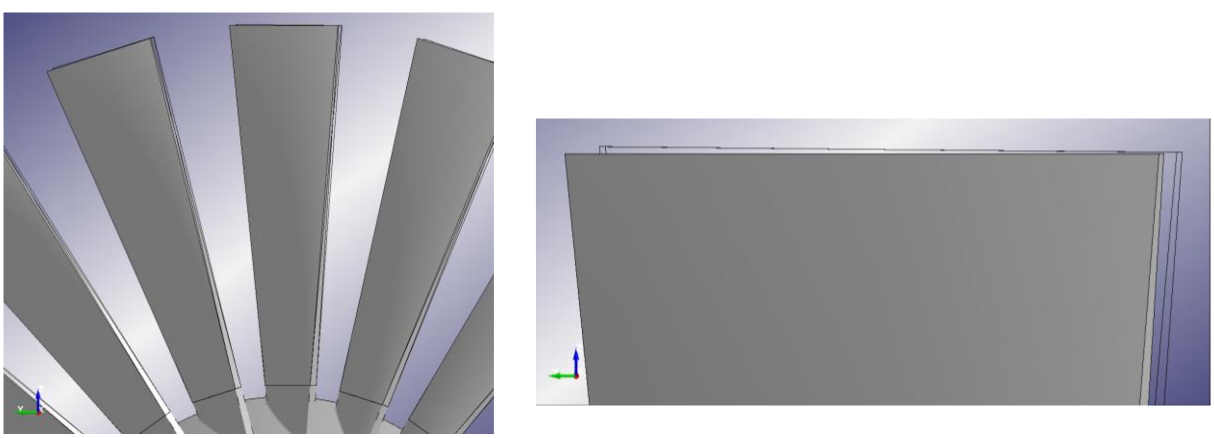

(a) Deflected blades (b) Close up of deflected blade tip

Figure 20: View of thin fan without preloading (solid gray) and with preloading (outline of bladed disk) with radial deflection approximately 0.03 inches at mid-chord

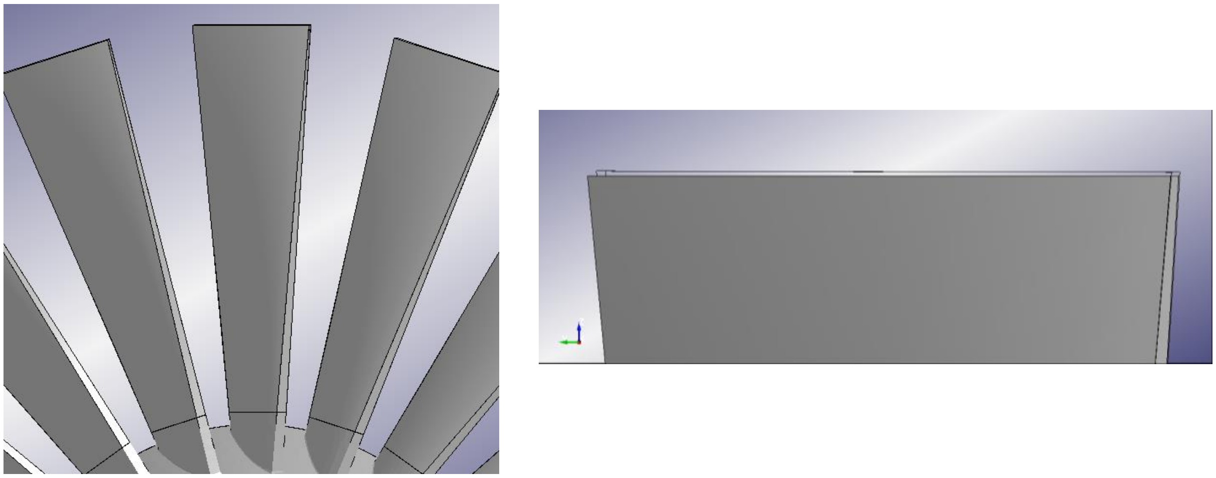

(a) Deflected blades (b) Close up of deflected blade tip

Figure 21: View of thick fan without preloading (solid gray) and with preloading (outline of bladed disk) with radial deflection approximately 0.03 inches at mid-chord

4.3 DAMAGE CATEGORY DEFINITION

The simulations conducted in this study are focused on understanding the effect of the UAV collision with an aircraft engine as it relates to damage in the fan blades, fan containment system, and nosecone. For each of the simulations, the damage to the fan, nosecone, and fan containment system are classified by a set of criteria shown in Table 4.

The lowest damage category, Level 1, generally corresponds to some deformation in the nosecone or the fan blades and possibly some minor material loss in the fan blades with no containment failure. The next category, Level 2, corresponds to a significant material loss from one or multiple blades with the loss of up to one blade, or a crack in the nosecone, but no containment failure. The third category, Level 3, corresponds to the loss of multiple fan blades, or a penetration of the nosecone by the UAV, but no containment failure. Finally, Level 4 corresponds to damage that includes all the other levels and leads to a containment failure in the model.

Table 4: Damage level categories for nosecone, fan, and containment system

Severity	Description	Example
Level 1	• Deformation of fan blades. • Minor material loss from fan blades. • Dent in nosecone. • No containment failure.	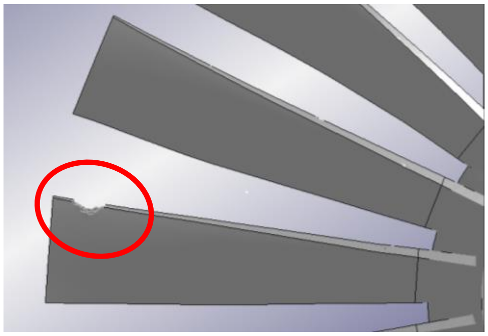
Level 2	• Significant material loss from one or multiple blades. • Loss of up to one full fan blade. • Crack in nosecone. • No containment failure.	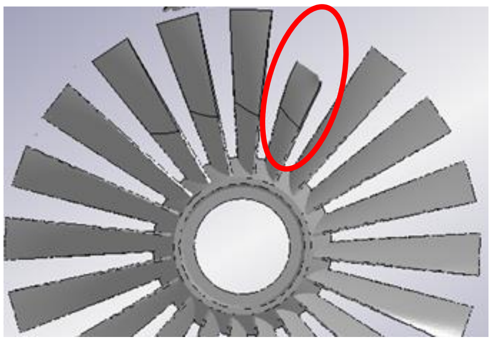
Level 3	• Loss of multiple fan blades. • UAV penetration of the nosecone. • No containment failure.	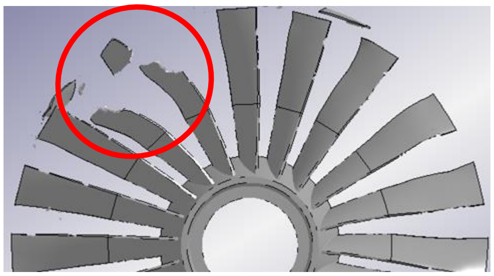
Level 4	• Containment failure due to UAV ingestion.	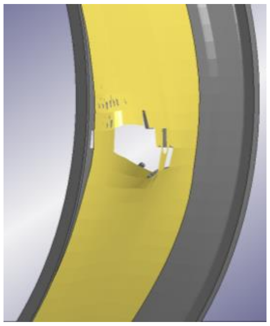

4.4 QUADCOPTER INGESTION STUDIES

This section details the results of the quadcopter (and its components) being ingested into the engine model for the cases listed in the text matrix given in section 4.1 . For these high speed impacts, the simulation times ranged from 3 ms to 6 ms for the various cases. Anywhere from one blade (in a component level test) to fifteen blades were impacted during the ingestion cases.

4.4.1 Takeoff Baseline

As mentioned in section 4.1 the takeoff scenario is expected to incur the most damage to the engine due to the high rotational speed of the fan in this case. The baseline case consists of the full quadcopter hitting the fan in the direct orientation shown in Figure 16. The baseline case also consists of hitting the outer part of the fan, where the fan geometry is the thin blade geometry developed for the generic 40 inch engine model. The relative speed of the quadcopter to the engine is 180 knots and the fan is rotating at 8500 RPM. Figure 22 depicts the kinematics of the ingestion. Figure 23 shows the damage caused to the blades.

The quadcopter ingestion for the baseline takeoff case results in the loss of multiple blade tips as well as damage to multiple other blades, but there was no damage to the fan containment case. Since the impact resulted in the loss of multiple blade tips, but there was no damage to the containment case the severity was classified as Level 3.

Figure 22: Kinematics of the quadcopter ingestion for the takeoff baseline case

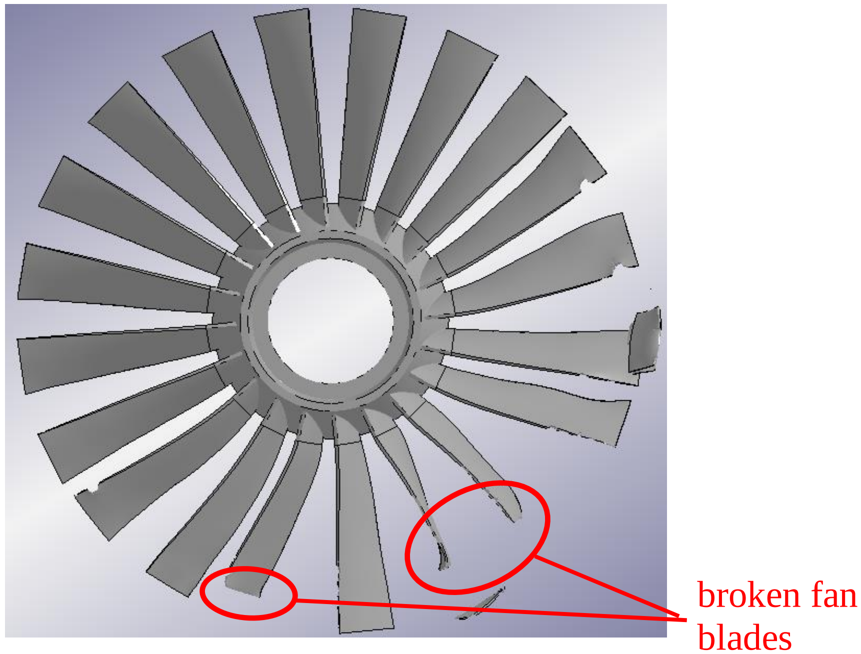

Figure 23: Damage to blades from the quadcopter for the takeoff baseline case

4.4.2 Takeoff Component 1: Motor

The takeoff component 1 case has the same setup as the baseline case, but instead of the full quad-copter just the motor is ingested into the engine. This case consists of hitting the outer part of the fan, where the fan geometry is the thin blade geometry developed for the generic 40 inch engine model. The relative speed of the motor to the engine is 180 knots and the fan is rotating at 8500 RPM. Figure 24 depicts the kinematics of the ingestion. Figure 25 shows the plastic work in the blades due to ingestion.

The quadcopter motor ingestion results in some plastic deformation in the blade that impacts the motor. Since this case involved minor damage to a single blade the severity was classified as Level 1.

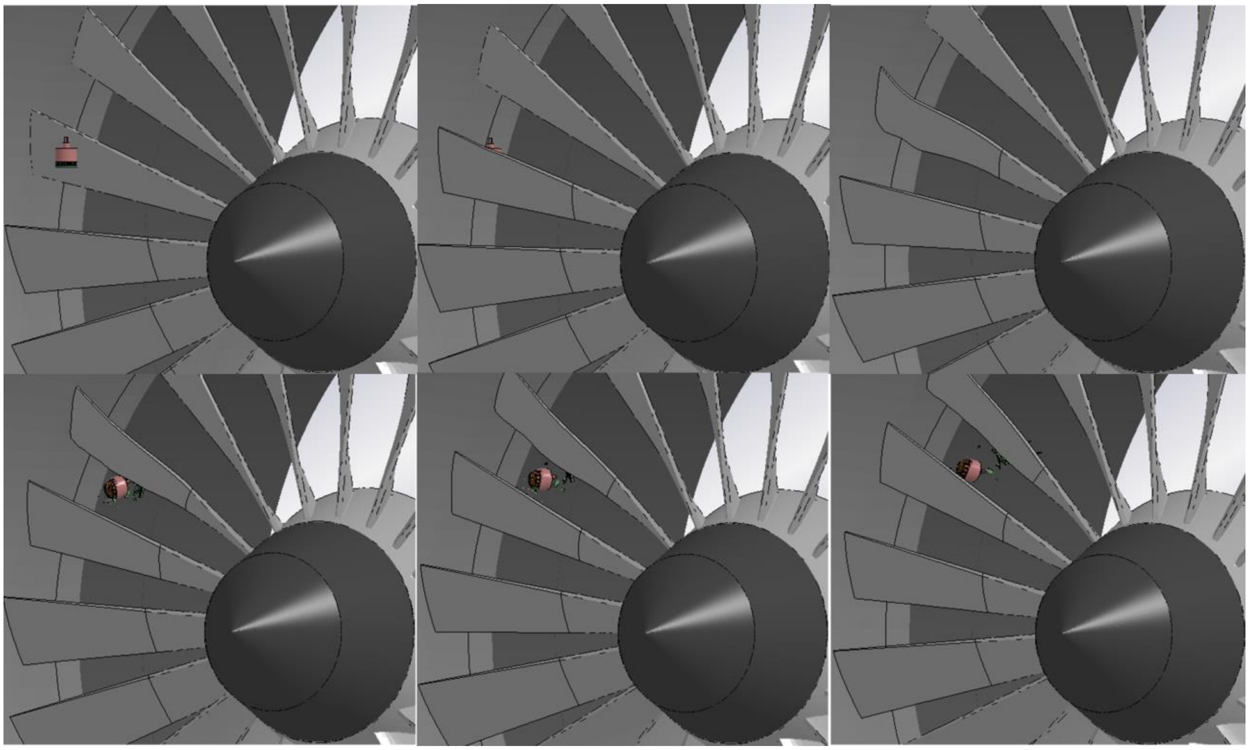

Figure 24: Kinematics of the quadcopter motor ingestion for the takeoff component 1 case

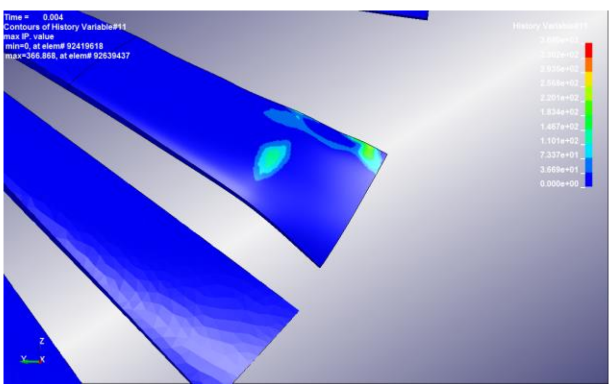

(a) Plastic work (front view)

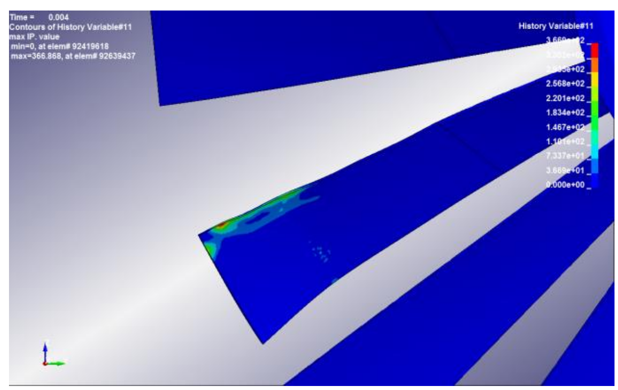

(b) Plastic work (back view)

Figure 25: Plastic work in blades from the quadcopter motor for the takeoff component 1 case

4.4.3 Takeoff Component 2: Camera

The takeoff component 2 case has the same setup as the baseline case, but instead of the full quadcopter just the camera is ingested into the engine. This case consists of hitting the outer part of the fan, where the fan geometry is the thin blade geometry developed for the generic 40 inch engine model. The relative speed of the camera to the engine is 180 knots and the fan is rotating at 8500 RPM. Figure 26 depicts the kinematics of the ingestion. Figure 27 shows the plastic work in the blades due to the ingestion.

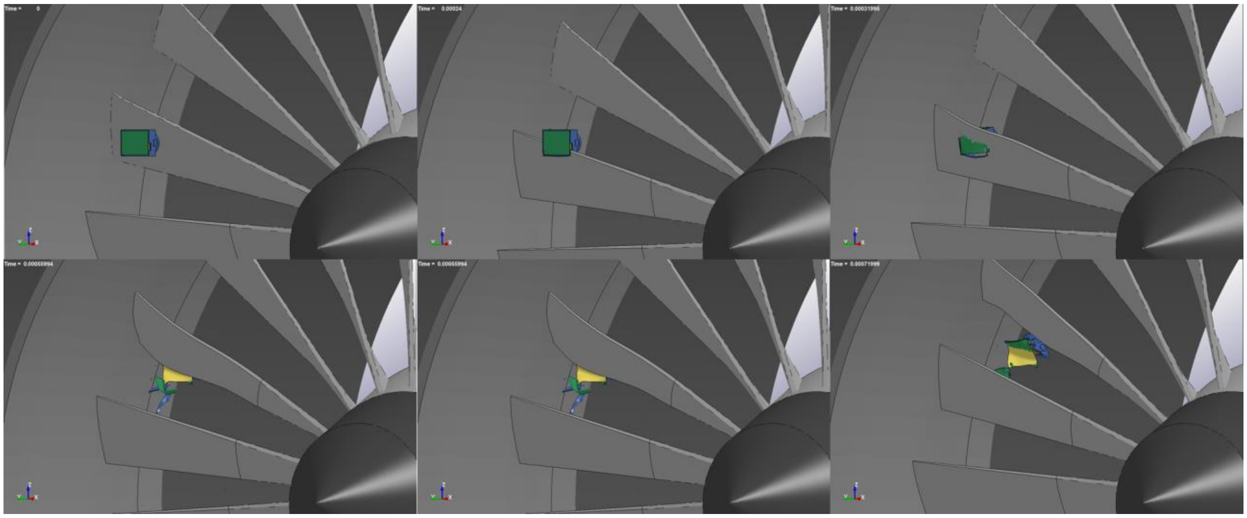

Figure 26: Kinematics of the quadcopter camera ingestion for the takeoff component 2 case

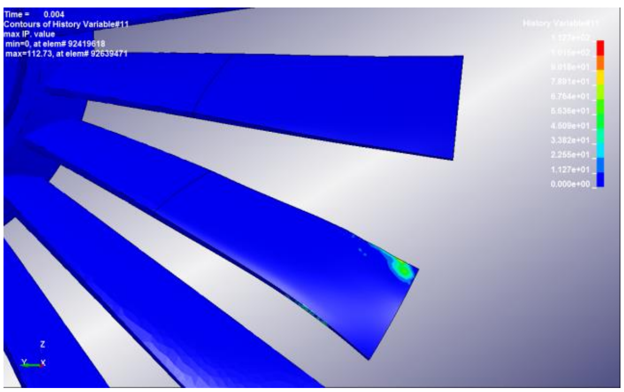

(a) Plastic work (front view)

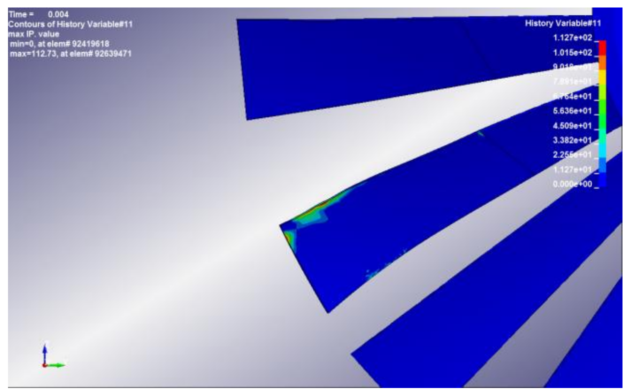

(b) Plastic work (back view)

Figure 27: Plastic work in the blades for the takeoff component 2 case

The quadcopter camera ingestion results in some plastic deformation in the blade that impacts the camera. Since this case involved minor damage to a single blade the severity was classified as Level 1.

4.4.4 Takeoff Component 3: Battery

The takeoff component 3 case has the same setup as the baseline case, but instead of the full quadcopter just the battery is ingested into the engine. This case consists of hitting the outer part of the fan, where the fan geometry is the thin blade geometry developed for the generic 40 inch engine model. The relative speed of the battery to the engine is 180 knots and the fan is rotating at 8500 RPM. Figure 28 depicts the kinematics of the ingestion. Figure 29 shows the plastic work in the blades due to the ingestion.

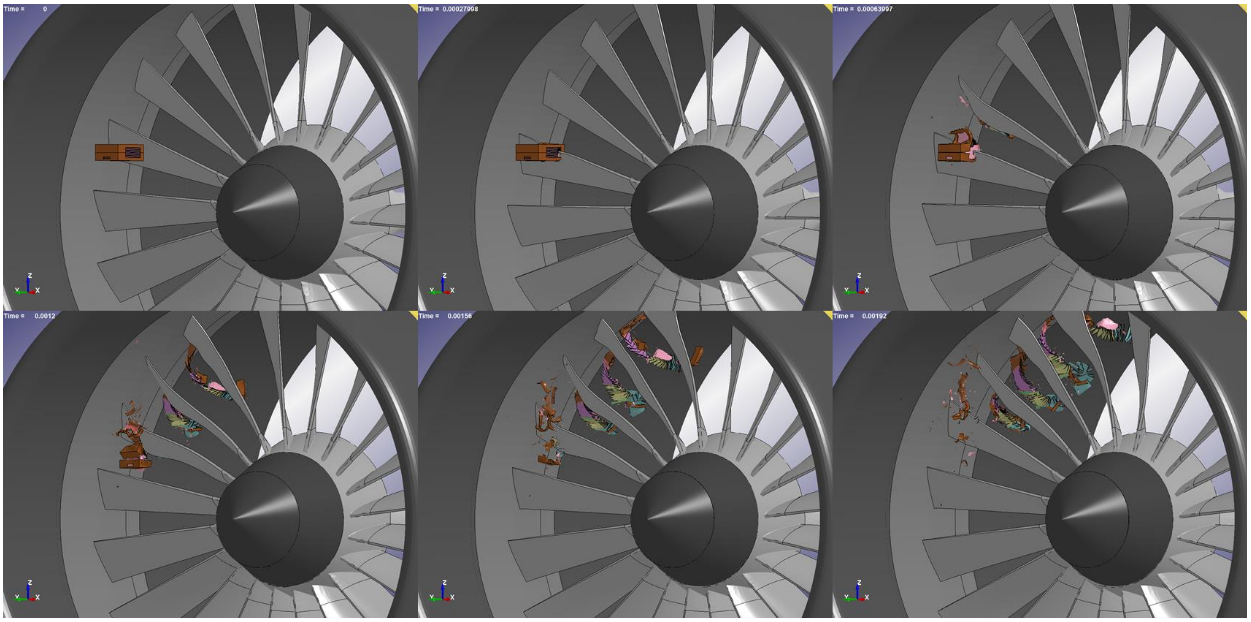

Figure 28: Kinematics of the quadcopter battery ingestion for the takeoff component 3 case

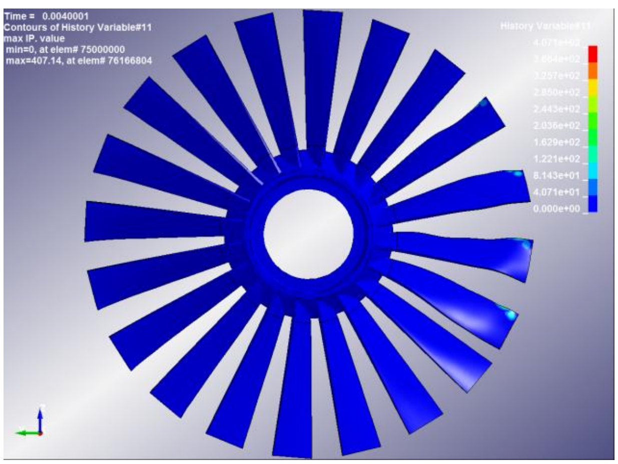

(a) Plastic work (front view)

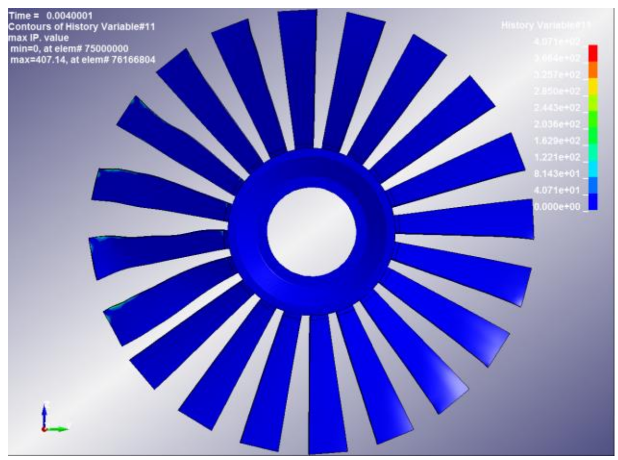

(b) Plastic work (back view)

Figure 29: Plastic work in the blades for the takeoff component 3 case

The quadcopter battery ingestion results in some plastic deformation in the blade that impacts the battery, while also causing a blade tip rub against the casing. Since this case did not involve the loss of a blade or a containment failure the severity was classified as Level 1. Also, in this type of ingestion when the battery is fully destroyed the risk of fire from the battery is low. This was demonstrated during the component level tests for the quadcopter and discussed in the companion report[2].

4.4.5 Takeoff Location 1: Inner Blade

The takeoff location 1 case has the same setup as the baseline case, but instead of the quadcopter hitting the outer part of the blade, the quadcopter hits the inner part of the blade and the disk. This case consists of the full quadcopter hitting the fan in the direct orientation shown in Figure 16. The fan geometry is the thin blade geometry developed for the generic 40 inch engine model. The relative speed of the quadcopter to the engine is 180 knots and the fan is rotating at 8500 RPM. Figure 30 depicts the kinematics of the ingestion. Figure 31 shows the damage caused to the blades.

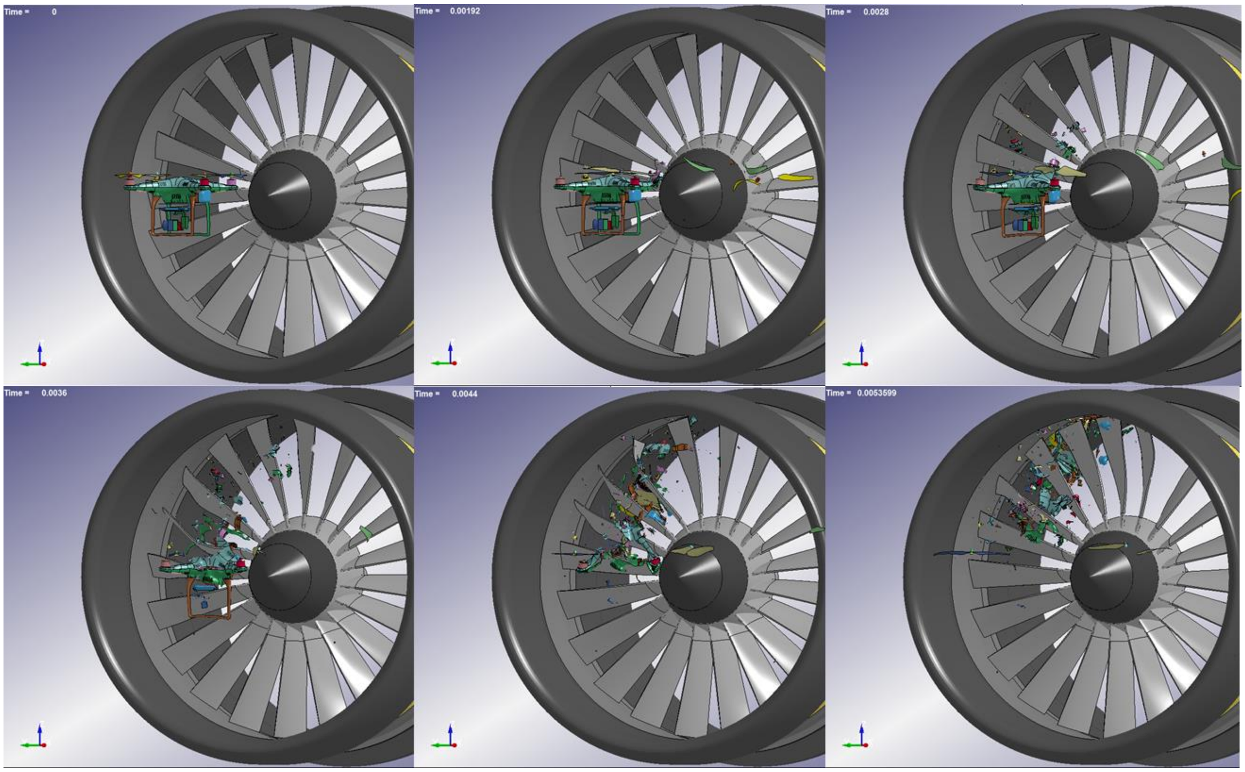

Figure 30: Kinematics of the quadcopter ingestion for the takeoff location 1 case

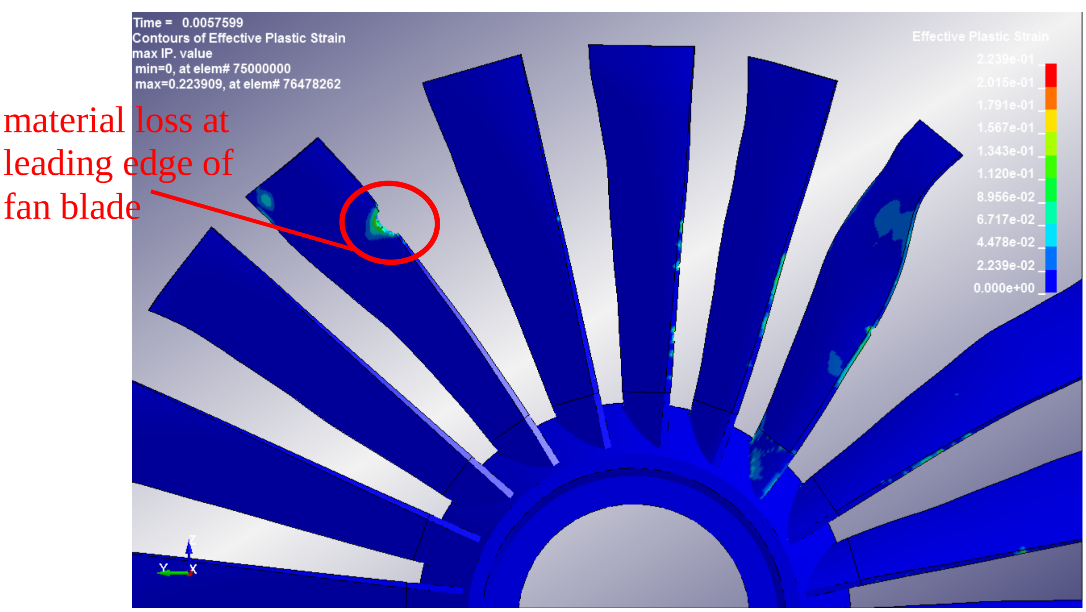

Figure 31: Effective plastic strain in blades for the takeoff location 1 case

The quadcopter ingestion for the inner blade impact results in some plastic deformation in multiple blades, and some material loss in one blade. Since the damage to the blades was relatively minor the severity was classified as Level 1.

4.4.6 Takeoff Location 2: Nosecone - Motor

The takeoff location 2 case has the same setup as the baseline case, but instead of the full quad-copter just the motor is ingested into the engine, and instead of hitting the outer part of the fan it hits the nosecone. The fan geometry is the thin blade geometry developed for the generic 40 inch engine model. The relative speed of the motor to the engine is 180 knots and the fan is rotating at 8500 RPM. Figure 32 depicts the kinematics of the ingestion. Figure 33 shows the plastic work in the nosecone, which results in a small dent and is classified as Level 1 damage.

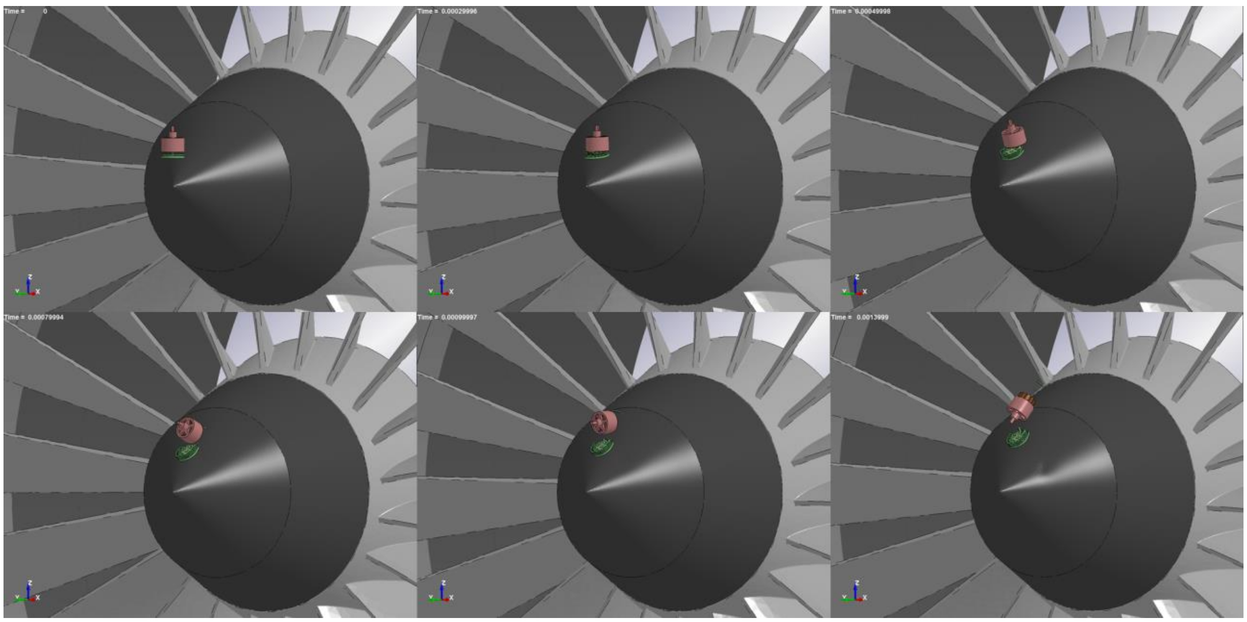

Figure 32: Kinematics of the quadcopter motor ingestion for the takeoff location 2 case

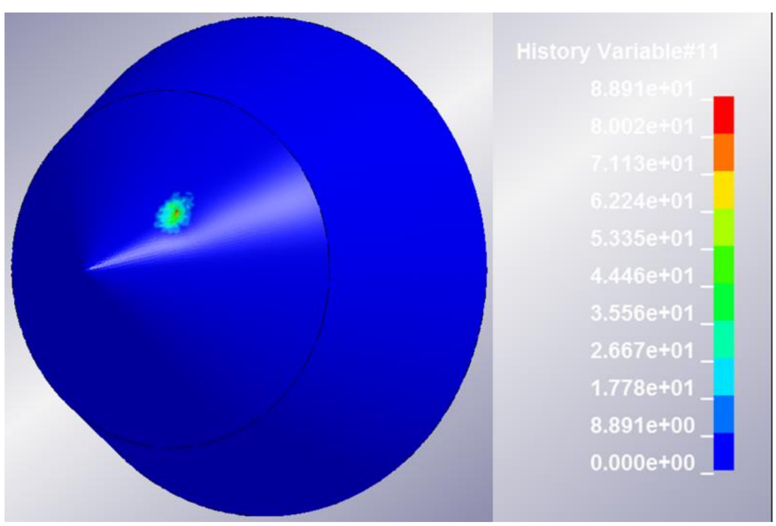

Figure 33: Plastic work in the nosecone for the takeoff location 2 case

4.4.7 Takeoff Location 3: Nosecone - Camera

The takeoff location 3 case has the same setup as the baseline case, but instead of the full quad-copter just the camera is ingested into the engine, and instead of hitting the outer part of the fan it hits the nosecone. The fan geometry is the thin blade geometry developed for the generic 40 inch engine model. The relative speed of the camera to the engine is 180 knots and the fan is rotating at 8500 RPM. Figure 34 depicts the kinematics of the ingestion. Figure 35 shows the plastic work in the nosecone, which is very localized and is classified as Level 1 damage.

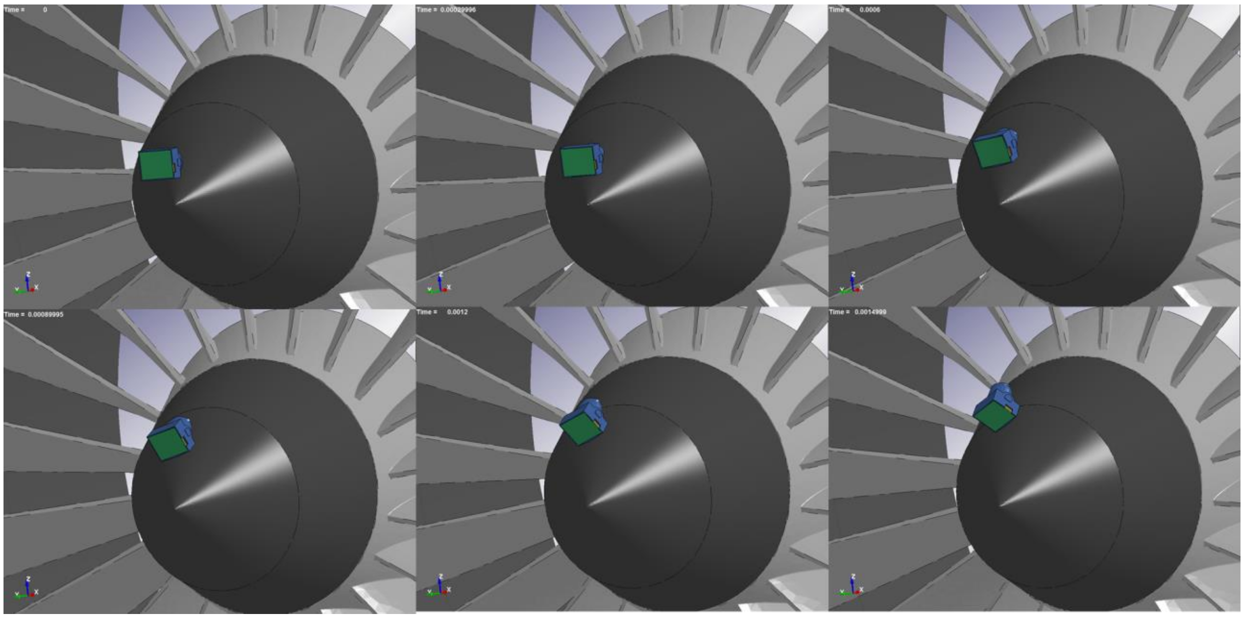

Figure 34: Kinematics of the quadcopter camera ingestion for the takeoff location 3 case

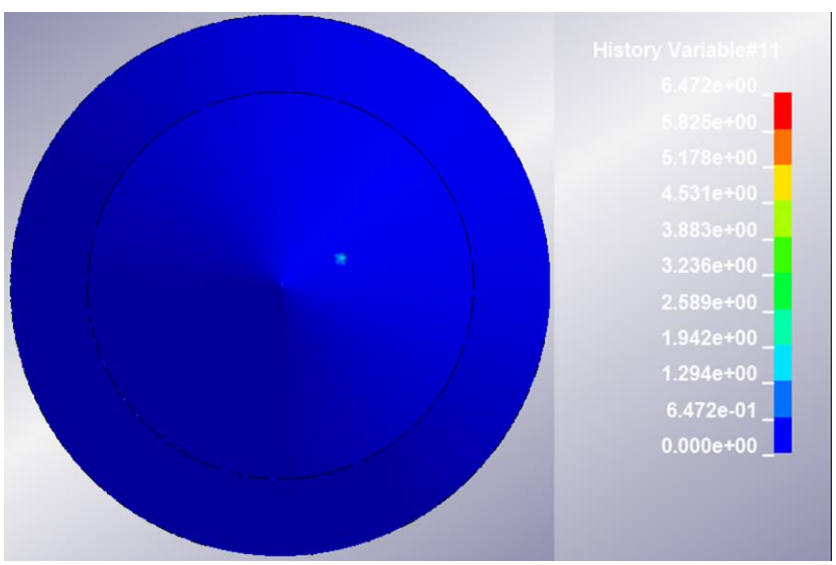

Figure 35: Plastic work in the nosecone for the takeoff location 3 case

4.4.8 Takeoff Location 4: Nosecone - Battery

The takeoff location 4 case has the same setup as the baseline case, but instead of the full quadcopter just the battery is ingested into the engine, and instead of hitting the outer part of the fan it hits the nosecone. The fan geometry is the thin blade geometry developed for the generic 40 inch engine model. The relative speed of the battery to the engine is 180 knots and the fan is rotating at 8500 RPM. Figure 36 depicts the kinematics of the ingestion. Figure 37 shows the plastic work in the nosecone, which results in a small dent and is classified as Level 1 damage.

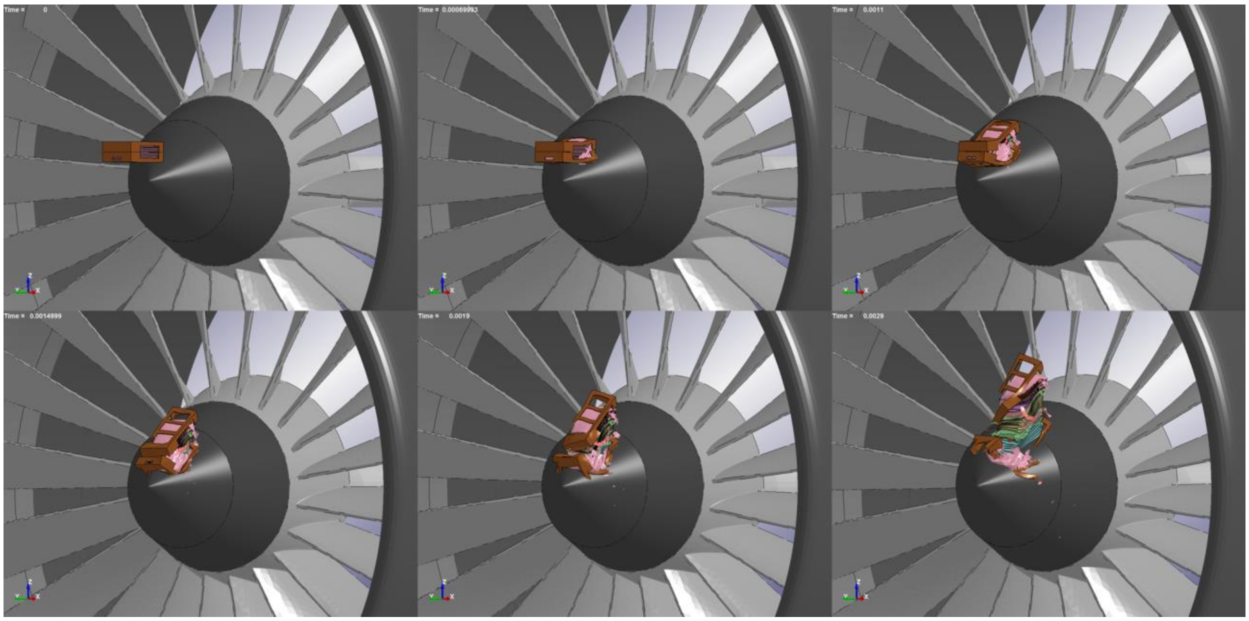

Figure 36: Kinematics of the quadcopter battery ingestion for the takeoff location 4 case

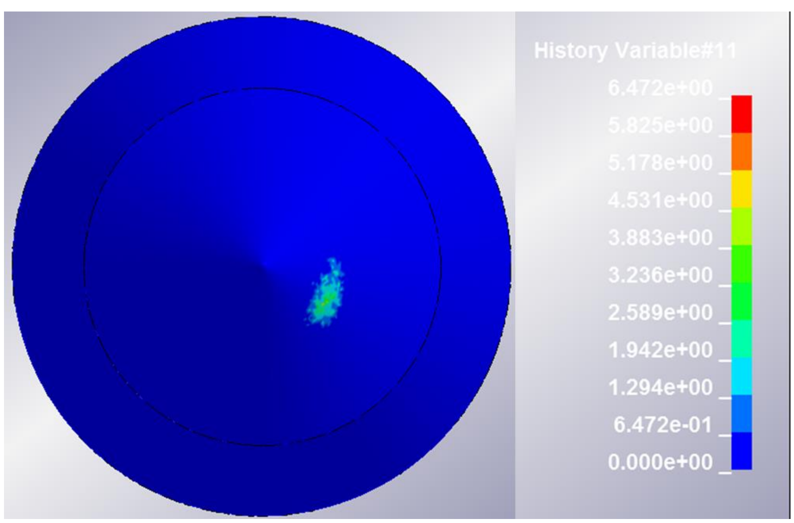

Figure 37: Plastic work in the nosecone for the takeoff location 4 case

4.4.9 Takeoff Geometry

The takeoff geometry case has the same setup as the baseline case, but instead of the thin blade geometry the thick blade geometry for the fan is used. This case consists of the quadcopter hitting the fan in the direct orientation shown in Figure 16 at the outer part of the fan. The fan geometry is the thick blade geometry developed for the generic 40 inch engine model. The relative speed of the quadcopter to the engine is 180 knots and the fan is rotating at 8500 RPM. Figure 38 depicts the kinematics of the ingestion. Figure 39 shows the damage caused to the blades.

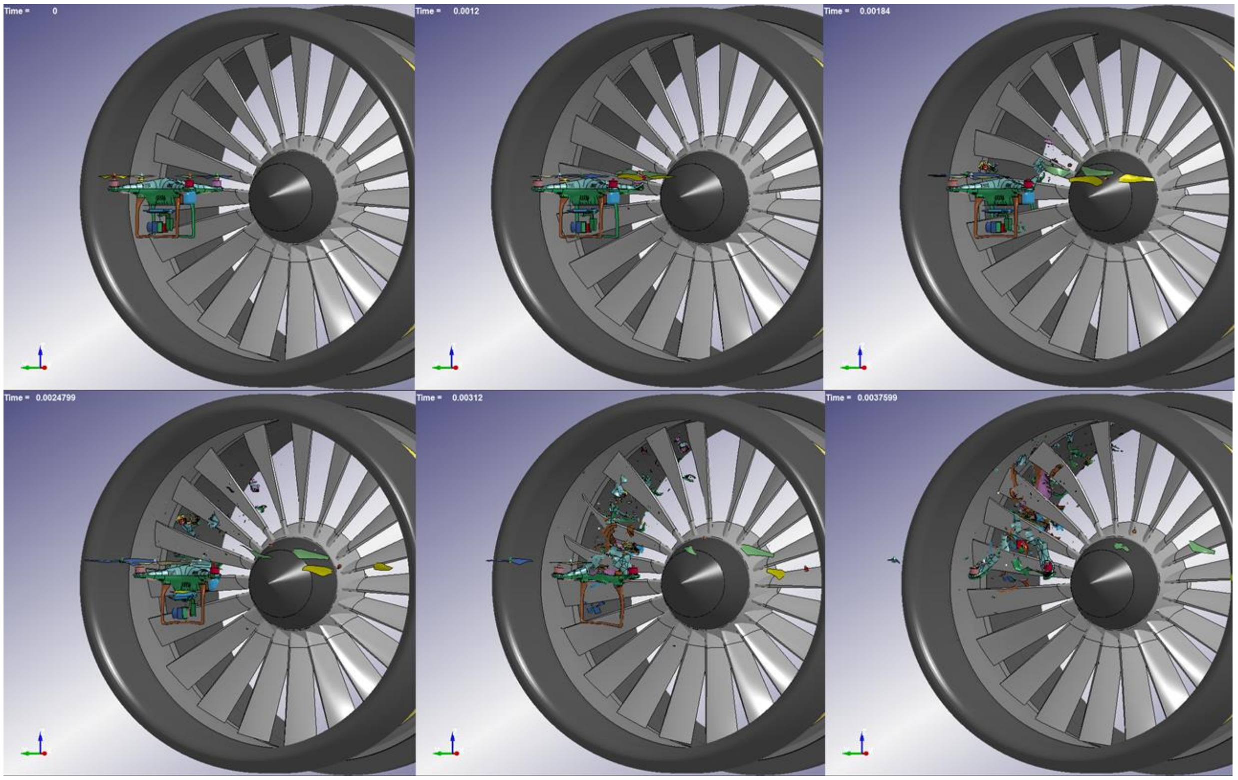

Figure 38: Kinematics of the quadcopter ingestion for the takeoff geometry case

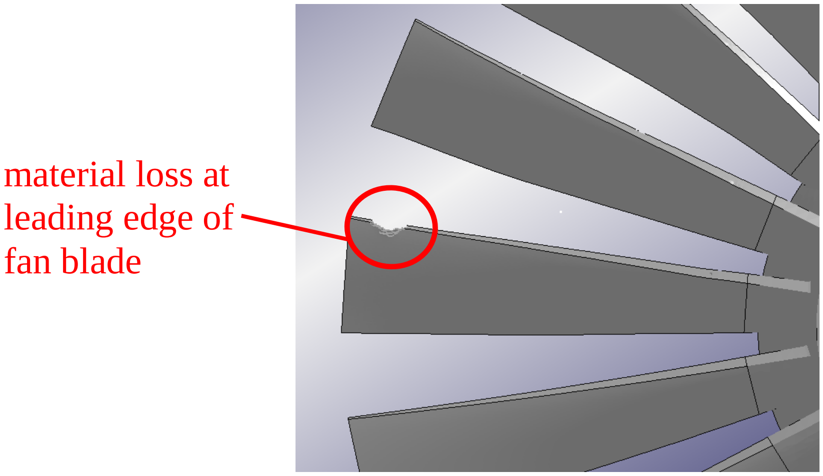

Figure 39: Damage in one blade for the takeoff geometry case

The quadcopter ingestion for the thick fan blades results in some minor plastic deformation in multiple blades, and a little material loss at the leading edge of one blade. Since the overall damage to the blades was minor the severity was classified as Level 1.

4.4.10 Takeoff Orientation

The takeoff orientation case has the same setup as the baseline case except for the orientation of the quadcopter, which has been rotated 90° in its pitch angle (as shown in Figure 16). This case consists of the quadcopter hitting the outer part of the fan, where the fan geometry is the thin blade geometry developed for the generic 40 inch engine model. The relative speed of the quadcopter to the engine is 180 knots and the fan is rotating at 8500 RPM. Figure 40 depicts the kinematics of the ingestion. Figure 41 shows the damage caused to the engine.

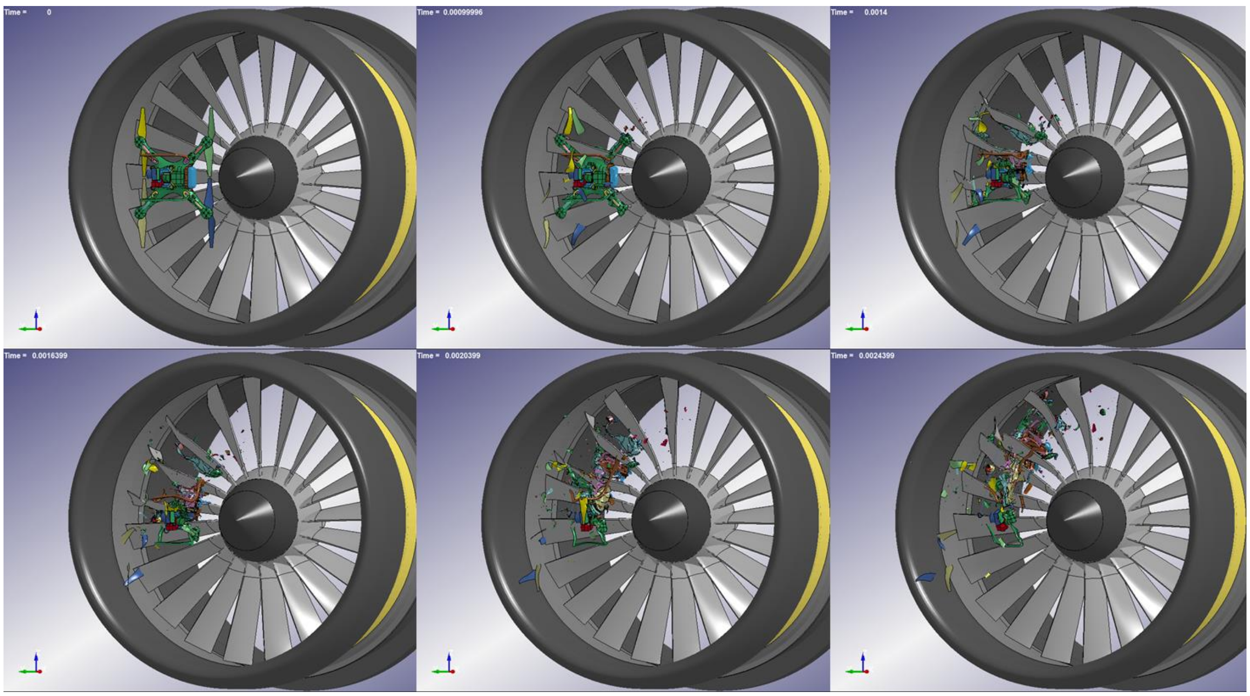

Figure 40: Kinematics of the quadcopter ingestion for the takeoff orientation case

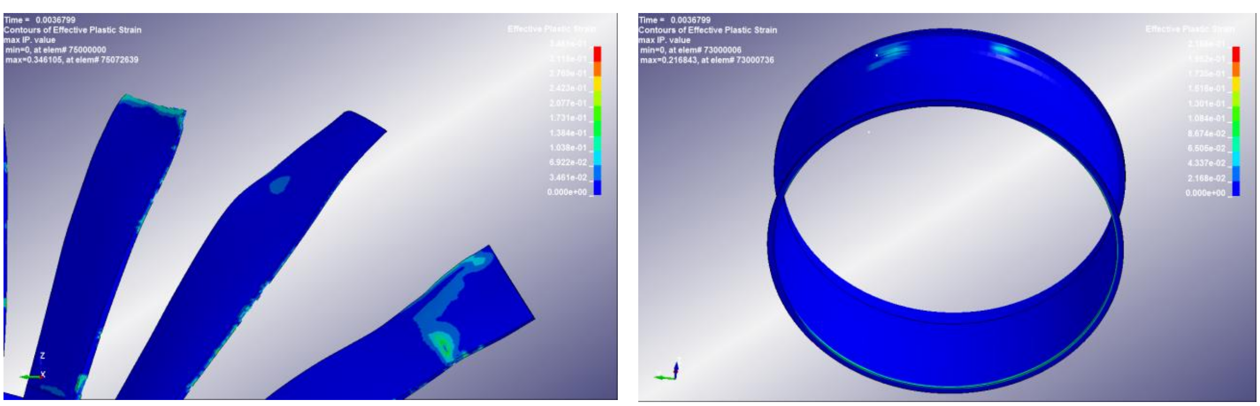

(a) Effective plastic strain in blades (b) Effective plastic strain in containment ring

Figure 41: Damage to engine for the takeoff orientation case

The quadcopter ingestion for when the quadcopter impacts at a 90° pitch orientation results in the loss of a blades tip as well as some plastic deformation in additional blades and some plastic strain in the containment ring. Since the containment ring was not penetrated and only a single blade tip broke the severity was classified as Level 2.

4.4.11 Approach

The approach case has the same setup as the baseline takeoff case, except that the fan is rotating at 2000 RPM instead of 8500 RPM. This case consists of the quadcopter hitting the outer part of the fan, where the fan geometry is the thin blade geometry developed for the generic 40 inch engine model. The relative speed of the quadcopter to the engine is 180 knots and the impact is in the direct orientation shown in Figure 16. Figure 42 depicts the kinematics of the ingestion. Figure 43 shows the damage caused to the blades.

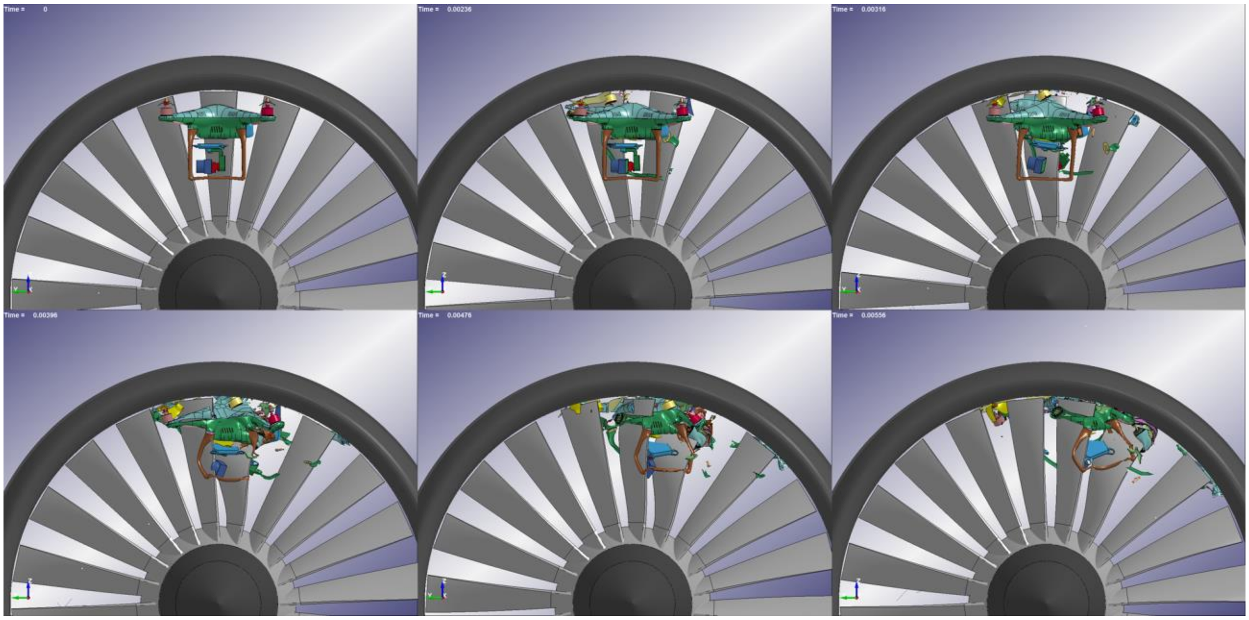

Figure 42: Kinematics of the quadcopter ingestion for the approach case

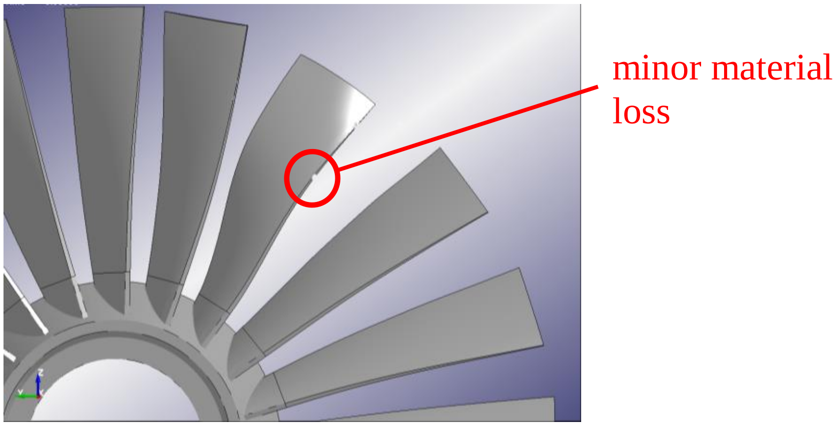

Figure 43: Damage to blades for the approach case

The quadcopter ingestion for the approach case results in some minor plastic deformation in multiple blades, and a little material loss at the leading edge of one blade. Since the overall damage to the blades was minor the severity was classified as Level 1.

4.4.12 Below 10,000 ft.

The flight below 10,000 ft. case has the same setup as the baseline case, except that the fan is rotating at 6000 RPM and the relative velocity of the quadcopter to the engine is 250 knots. This case consists of the quadcopter hitting the outer part of the fan, where the fan geometry is the thin blade geometry developed for the generic 40 inch engine model. The impact is in the direct orientation shown in Figure 16. Figure 44 depicts the kinematics of the ingestion. Figure 45 shows the damage caused to the blades.

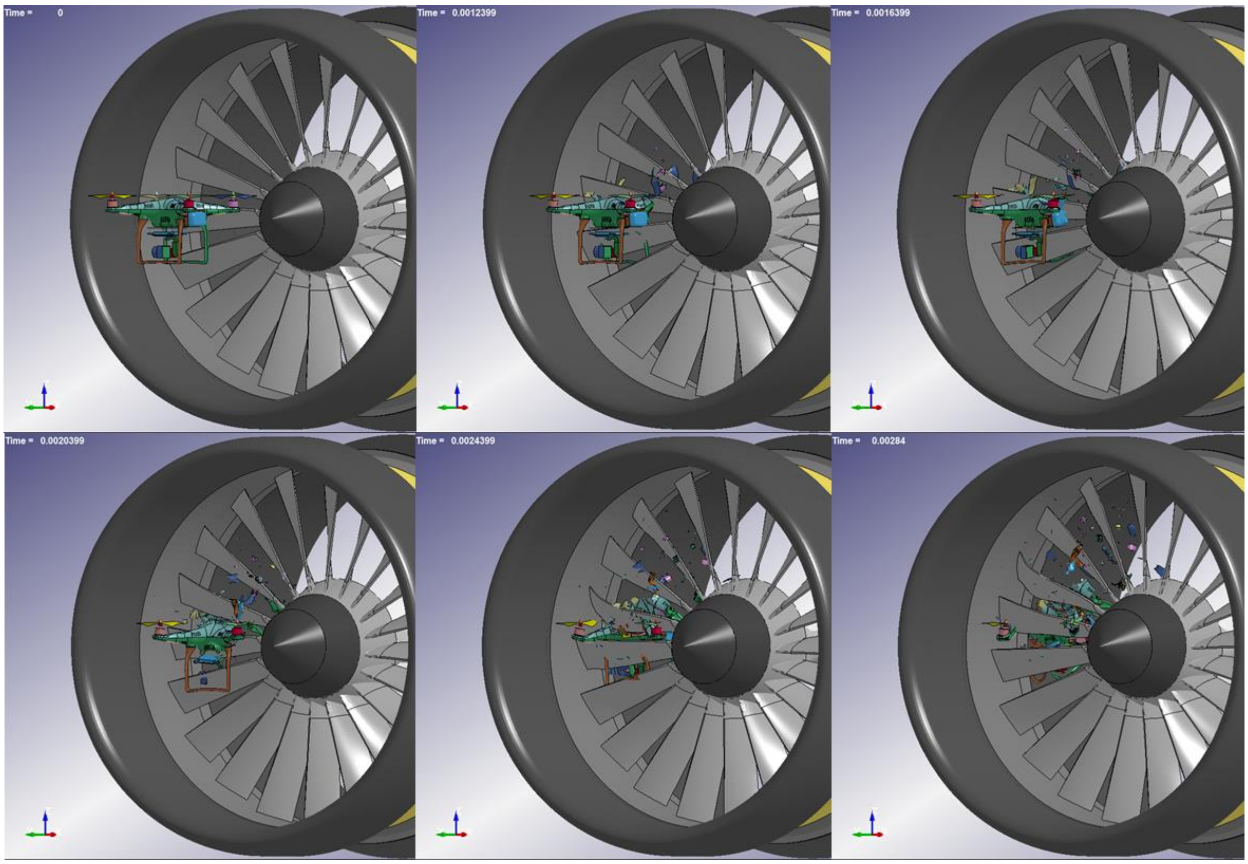

Figure 44: Kinematics of the quadcopter motor ingestion for the below 10,000 ft. case

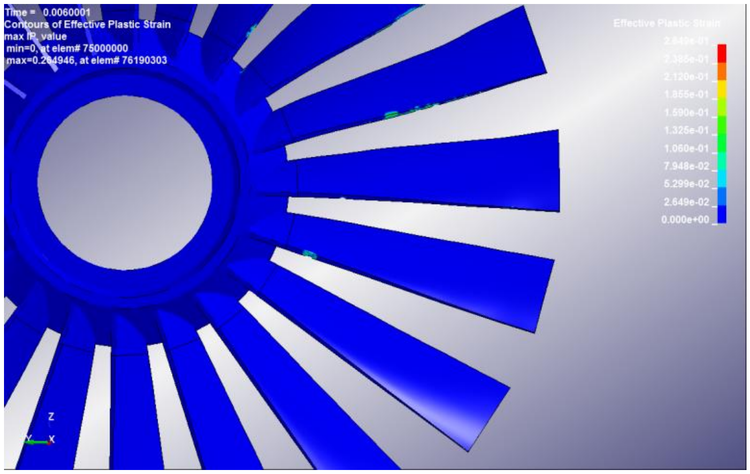

Figure 45: Effective plastic strain in blades for the below 10,000 ft. case

The quadcopter ingestion for the below 10,000 ft. case results in some minor plastic deformation in multiple blades. Since the overall damage to the blades was minor the severity was classified as Level 1.

4.4.13 Summary

A summary of the damages for each quadcopter ingestion scenario is given in Table 5. The damages ranged from Levels 1-3. The component level tests for the three key components (motor, camera and battery) showed that the damage incurred by these hard components depends greatly on the manner in which they impact the fan. In all of the takeoff component tests these components did little damage; however when they were a part of the quadcopter in the takeoff case these key components resulted in the loss of multiple blades. The damage from components outside of the three key components is expected to only result in Level 1 damage in the generic engine model. The damage to the system increases significantly as the ingestion moves from the center (nosecone), to the inner blade and then to the outer blade. This is not unexpected since the relative velocity of the impact increases as the impact moves outward along a radial line. As expected the takeoff scenario is the worst case since the fan has the highest rotational speed for this case.

Table 5: Summary of the damage classifications for the quadcopter ingestions

Test Type	Impact Location	Fan Blade	Relative Orientation	UAV Model - Component	Damage Classification
Takeoff Baseline 1	***outer blade***	***thin***	***direct***	***quadcopter***	**Level 3**
Takeoff Component 1	outer blade	thin	direct	**motor**	**Level 1**
Takeoff Component 2	outer blade	thin	direct	**camera**	**Level 1**
Takeoff Component 3	outer blade	thin	direct	**battery**	**Level 1**
Takeoff Location 1	**inner blade**	thin	direct	quadcopter	**Level 1**
Takeoff Location 2	**nosecone**	thin	direct	**motor**	**Level 1**
Takeoff Location 3	**nosecone**	thin	direct	**camera**	**Level 1**
Takeoff Location 4	**nosecone**	thin	direct	**battery**	**Level 1**
Takeoff geometry	outer blade	**thick**	direct	quadcopter	**Level 1**
Takeoff Orientation	outer blade	thin	**90° pitch**	quadcopter	**Level 2**
Approach 1	outer blade	thin	direct	quadcopter	**Level 1**
Below 10,000 ft. 1	outer blade	thin	direct	quadcopter	**Level 1**

4.5 FIXED WING INGESTION STUDIES

This section details the results of the fixed wing (and its components) being ingested into the engine model for the cases listed in the text matrix given in section 4.1. For these ingestion simulations, the fixed wing without its wings were used. This fixed wing model was used because the width of the fixed wing is larger than the diameter of the engine as shown in Figure 46. The focus of this work was on understanding the effect of certain parameters, such as the point of impact along the fan stage and this required removing the wings. The wing material is lightweight, and although some of the material is stiff, it would do considerably less damage than the core components which include the motor, battery and camera.

For these high speed impacts, the simulation times ranged from 1.2 ms to 14 ms for the various cases. Anywhere from one blade (in a component level test) to all blades were impacted during the ingestion cases.

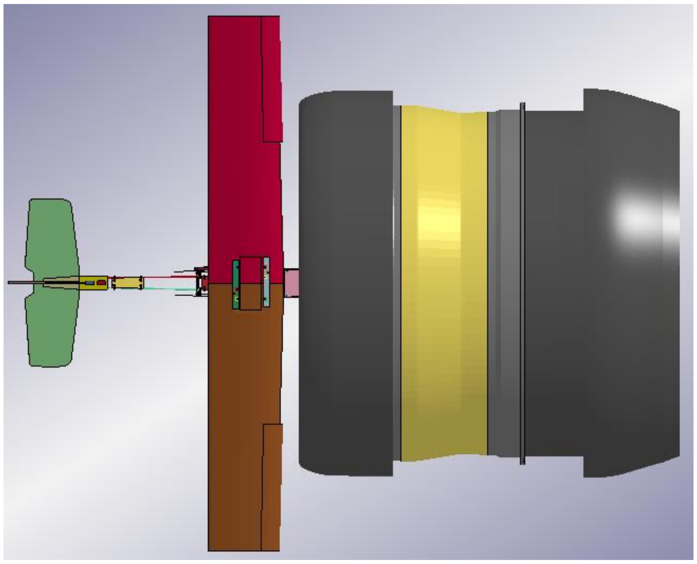

Figure 46: Full fixed wing ingestion into the generic business engine model

4.5.1 Takeoff Baseline

As mentioned in section 4.1 the takeoff scenario is expected to cause the most damage to the engine due to the high rotational speed of the fan in this case. The baseline case consists of the full fixed wing hitting the fan in the direct orientation shown in Figure 17. The baseline case also consists of hitting the outer part of the fan, where the fan geometry is the thin blade geometry developed for the generic 40 inch engine model. The relative speed of the fixed wing to the engine is 180 knots and the fan is rotating at 8500 RPM. Figure 47 depicts the kinematics of the ingestion. Figure 48 shows the damage caused to the blades.

The fixed wing ingestion for the baseline takeoff case results in the loss of multiple blade tips as well as damage to multiple other blades, but there was no significant damage to the fan containment ring. Since the impact resulted in the loss of multiple blade tips, but there was little damage to the containment ring the severity was classified as Level 3.

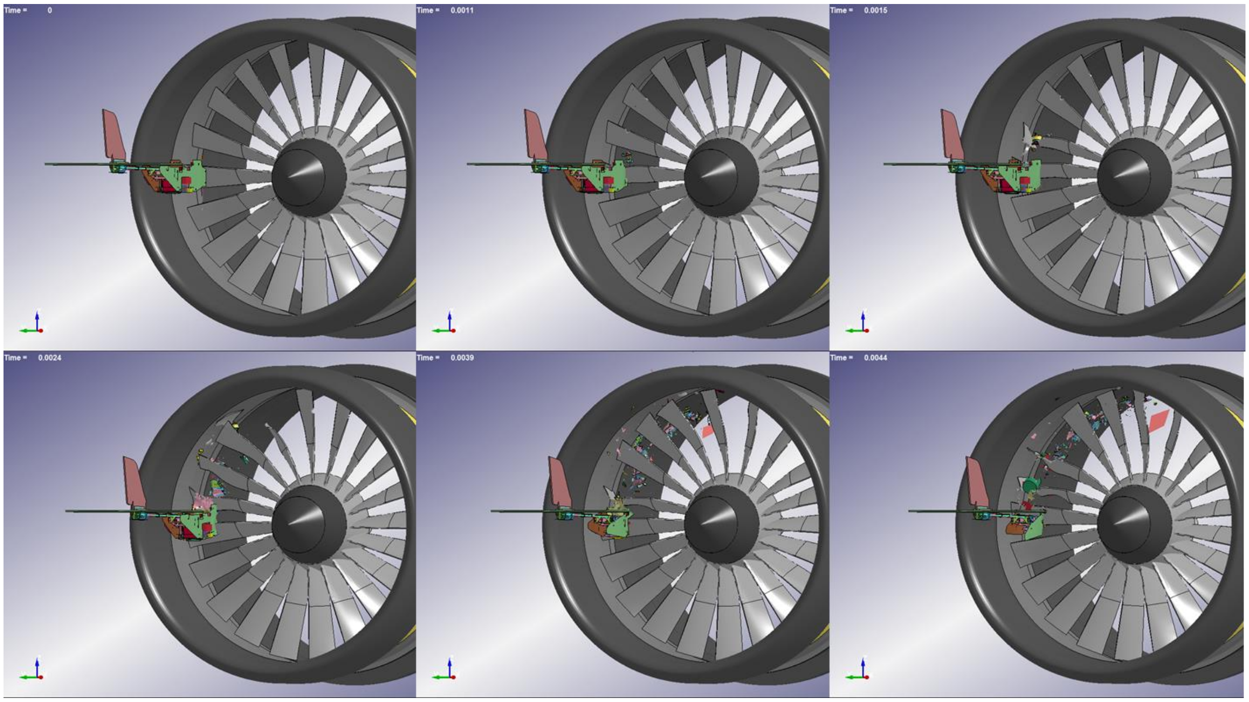

Figure 47: Kinematics of the fixed wing ingestion for the takeoff baseline case

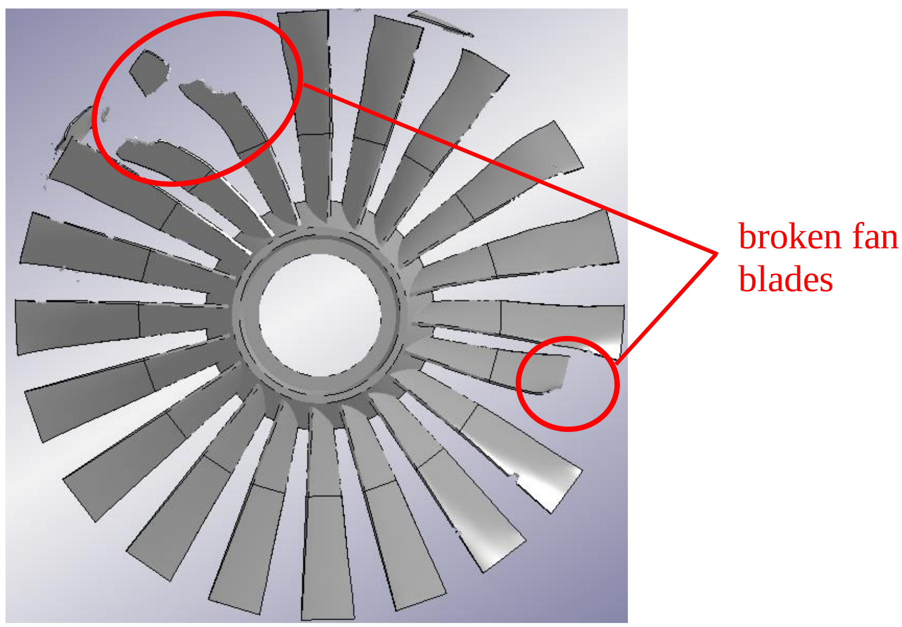

Figure 48: Damage to blades from the fixed wing for the takeoff baseline case

4.5.2 Takeoff Component 1: Motor

The takeoff component 1 case has the same setup as the baseline case, but instead of the full fixed wing just the motor is ingested into the engine. This case consists of hitting the outer part of the fan, where the fan geometry is the thin blade geometry developed for the generic 40 inch engine model. The relative speed of the motor to the engine is 180 knots and the fan is rotating at 8500

RPM. Figure 49 depicts the kinematics of the ingestion with a close-up of the impact as well as a view of the broken blade impacting the containment ring. Figure 50 shows the damage caused to the blades and the containment ring.

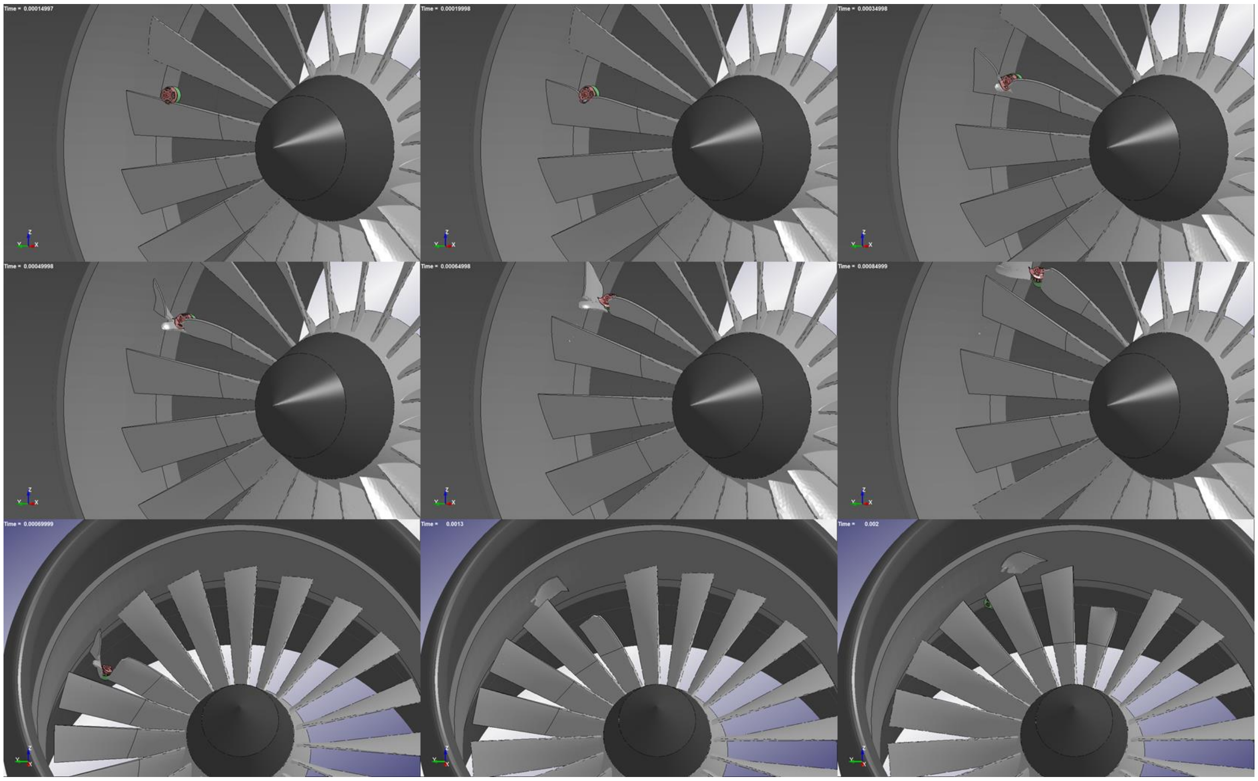

Figure 49: Kinematics of the fixed wing motor ingestion for the takeoff component 1 case

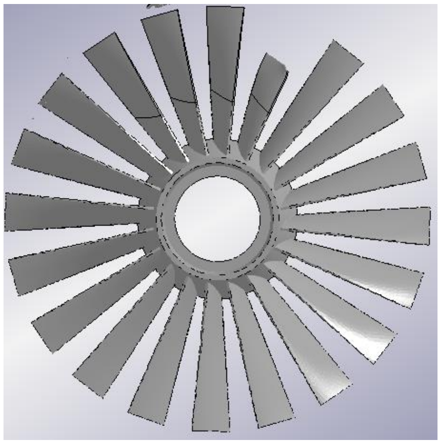

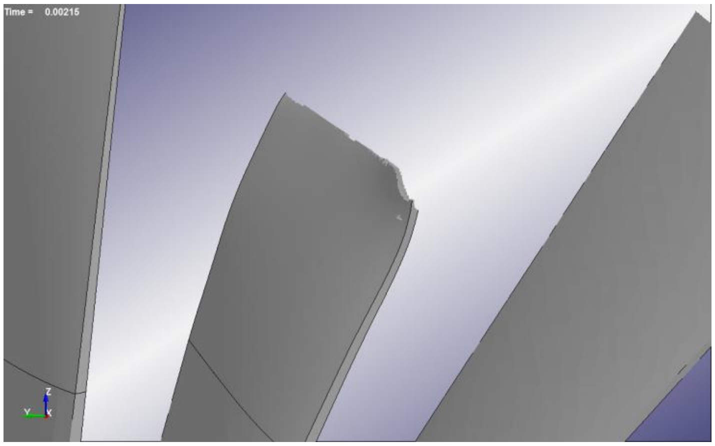

(a) Damage to fan (b) Close-up of tip damage

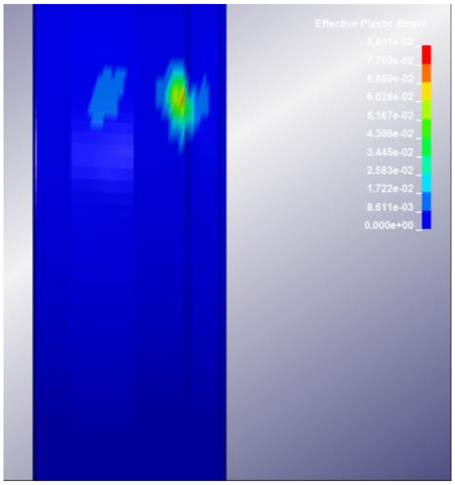

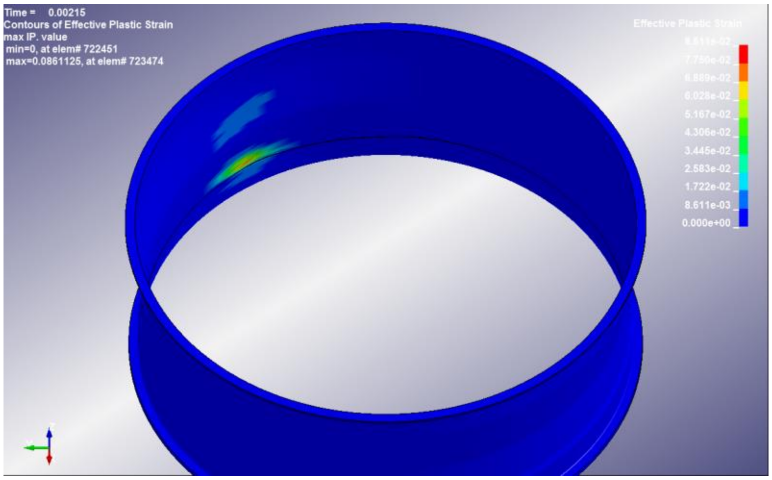

(c) Containment ring plastic strain (d) Interior of containment ring plastic strain

Figure 50: Damage to engine from the fixed wing motor for the takeoff component 1 case

The fixed wing motor ingestion results in the loss of the tip of one blade. There is also some plastic deformation of the containment ring with no penetration. Since this case did not involve the loss of multiple blades or a containment failure the severity was classified as Level 2.

4.5.3 Takeoff Component 2: Camera

The takeoff component 2 case has the same setup as the baseline case, but instead of the full fixed wing just the camera is ingested into the engine. This case consists of hitting the outer part of the fan, where the fan geometry is the thin blade geometry developed for the generic 40 inch engine model. The relative speed of the camera to the engine is 180 knots and the fan is rotating at 8500 RPM. Figure 51 depicts the kinematics of the ingestion. Figure 52 shows the damage caused to the blades.

The fixed wing camera ingestion results in the loss of the tip of one blade and minor damage to a couple of other blades. There is also a little plastic deformation in the containment ring with no penetration. Since this case did not involve the loss of multiple blades or a containment failure the severity was classified as Level 2.

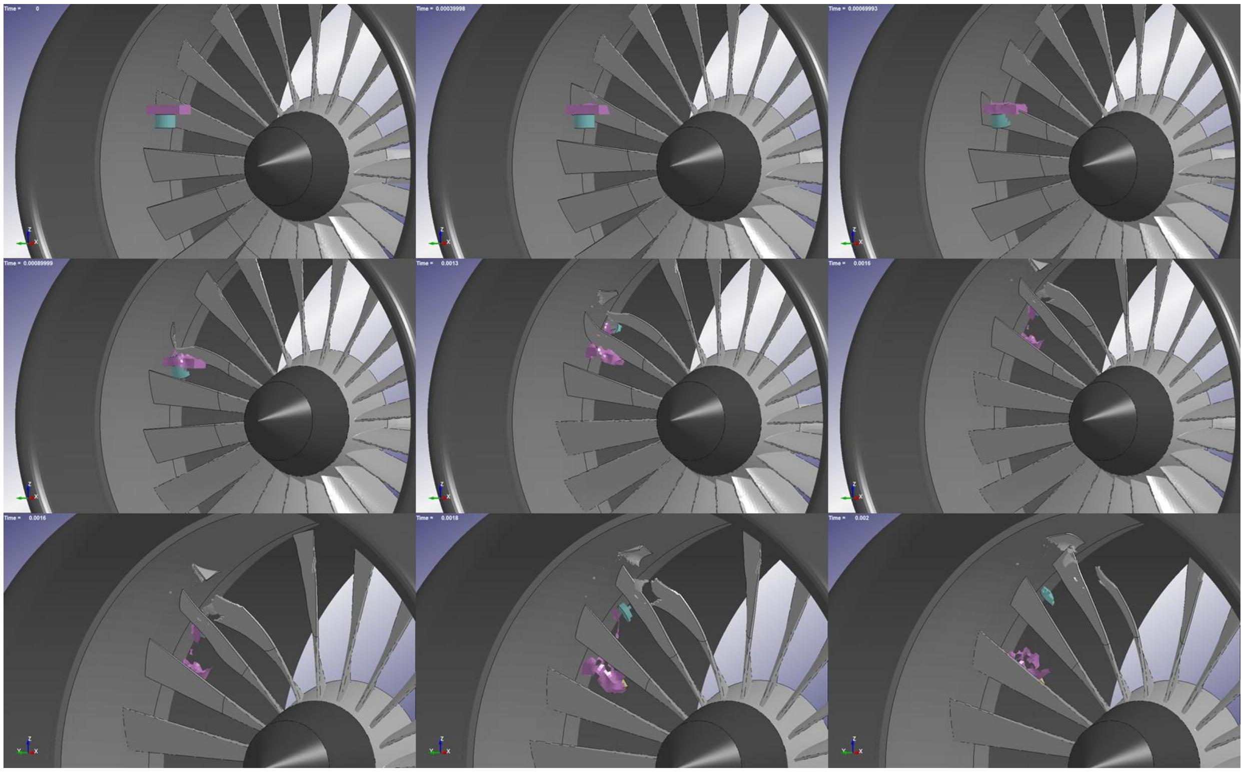

Figure 51: Kinematics of the fixed wing camera ingestion for the takeoff component 2 case

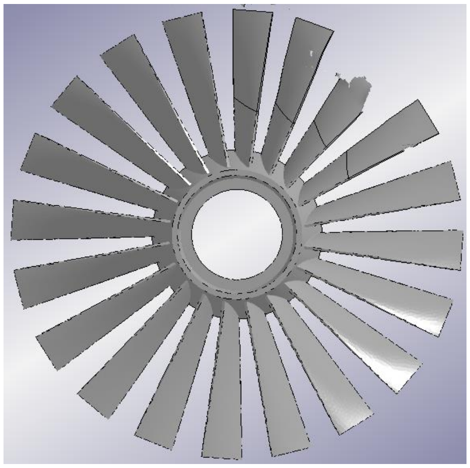

(a) Damage to fan

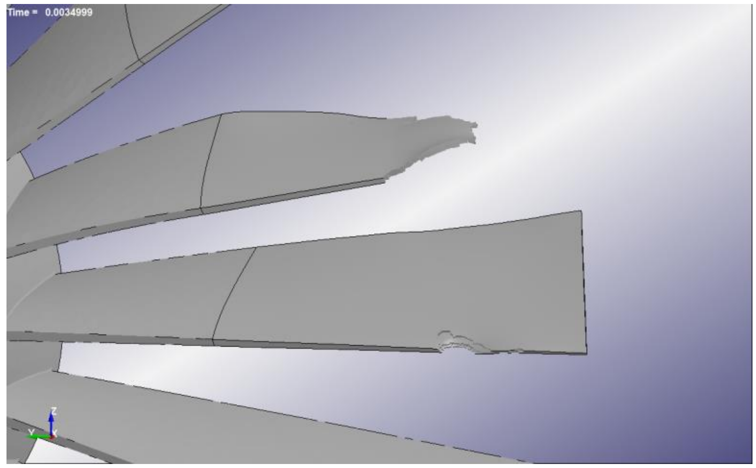

(b) Close-up of tip damage

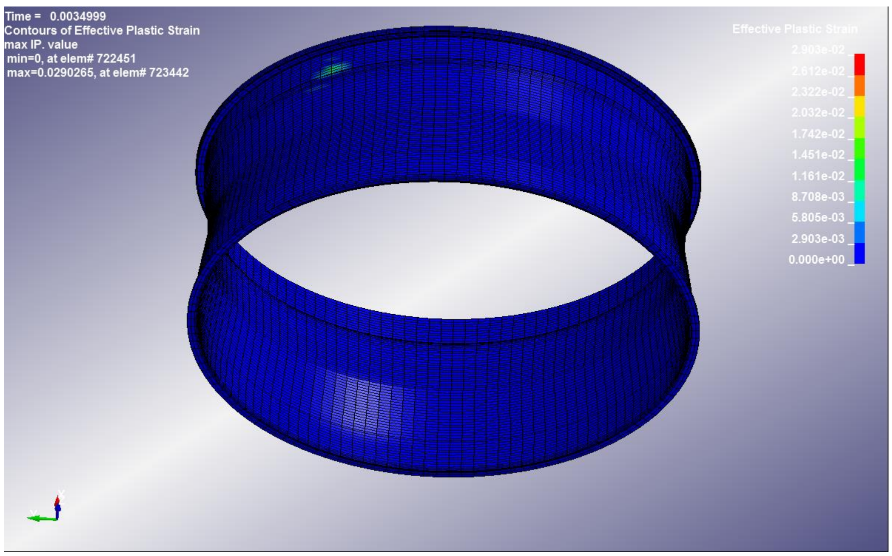

(c) Containment ring plastic strain

Figure 52: Damage to engine for the takeoff component 2 case

4.5.4 Takeoff Component 3: Battery

The takeoff component 3 case has the same setup as the baseline case, but instead of the full fixed wing just the battery is ingested into the engine. This case consists of hitting the outer part of the fan, where the fan geometry is the thin blade geometry developed for the generic 40 inch engine model. The relative speed of the battery to the engine is 180 knots and the fan is rotating at 8500 RPM. Figure 53 depicts the kinematics of the ingestion. Figure 54 shows the damage caused to the blades.

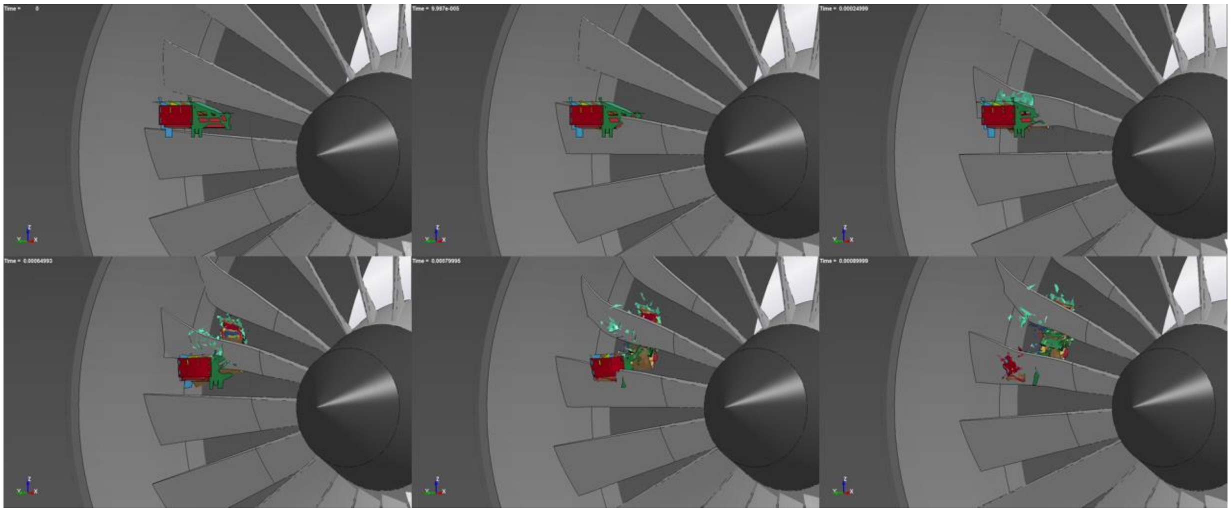

Figure 53: Kinematics of the fixed wing battery ingestion for the takeoff component 3 case

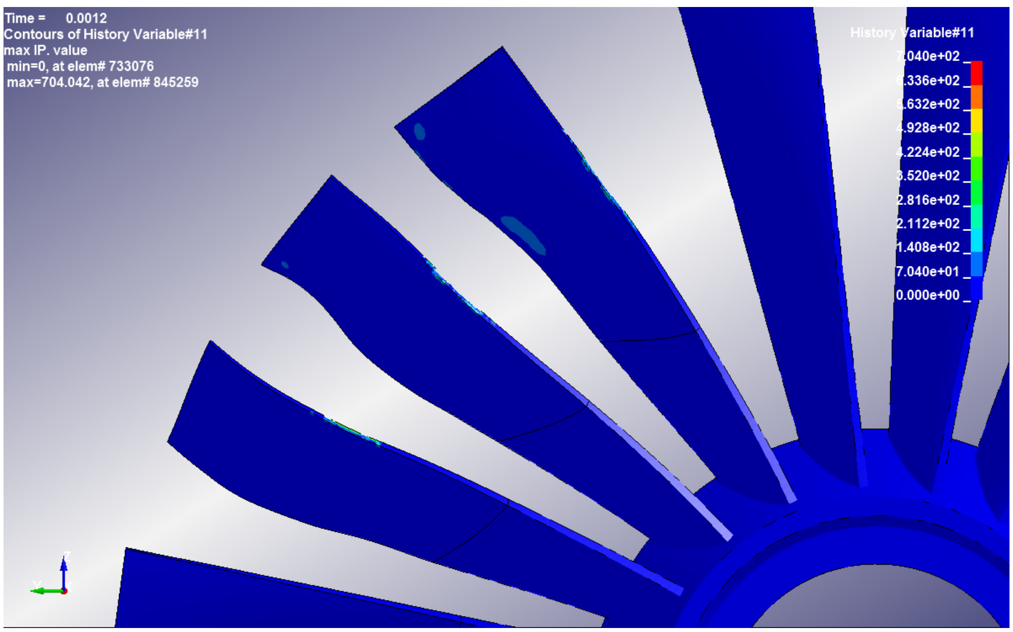

Figure 54: Plastic work in blades for the takeoff component 3 case

The fixed wing battery ingestion results in only plastic deformation in a few blades and no damage to the containment ring. Since this case involved only minor plastic deformation to a few blades it was classified as Level 1.

4.5.5 Takeoff Location 1: Inner Blade

The takeoff location 1 case has the same setup as the baseline case, but instead of the fixed wing hitting the outer part of the blade, the fixed wing hits the inner part of the blade near its root. This case consists of the full fixed wing hitting the fan in the direct orientation shown in Figure 17. The fan geometry is the thin blade geometry developed for the generic 40 inch engine model. The relative speed of the fixed wing to the engine is 180 knots and the fan is rotating at 8500 RPM. Figure 55 depicts the kinematics of the ingestion. Figure 56 shows the damage caused to the blades.

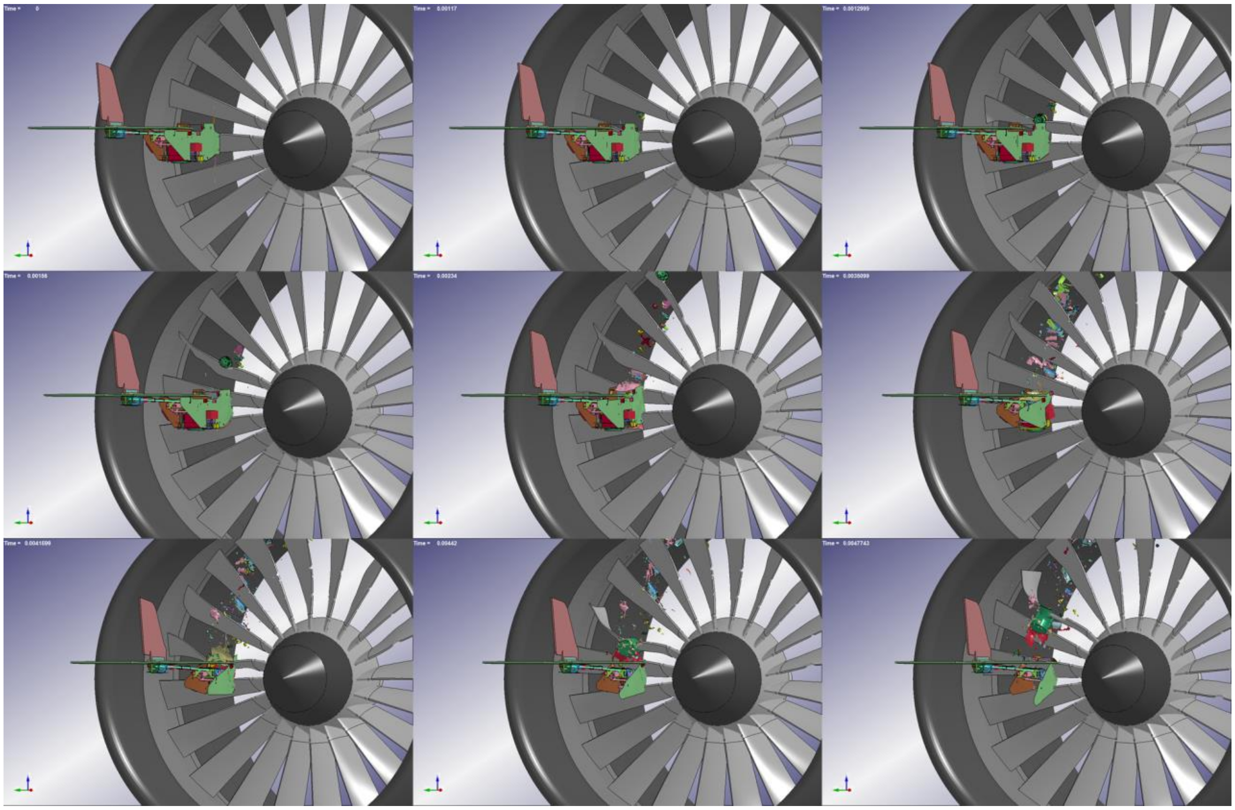

Figure 55: Kinematics of the fixed wing ingestion for the takeoff location 1 case

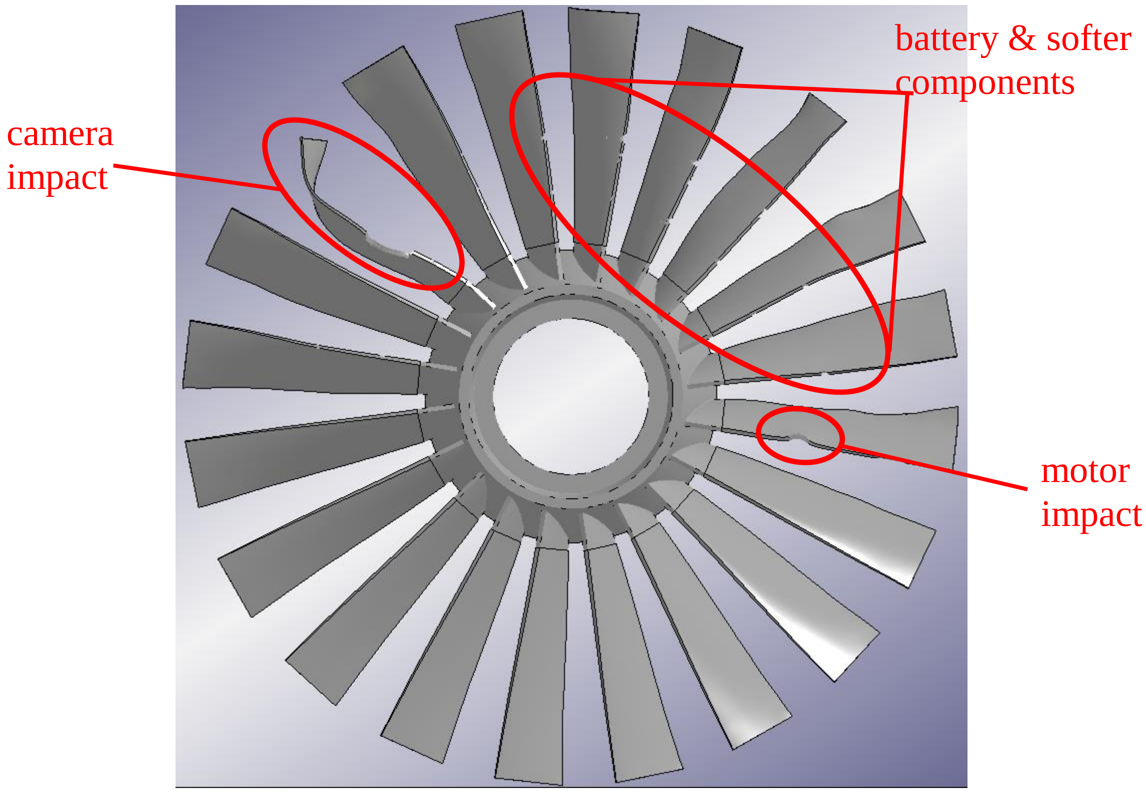

(a) Damage to fan blades

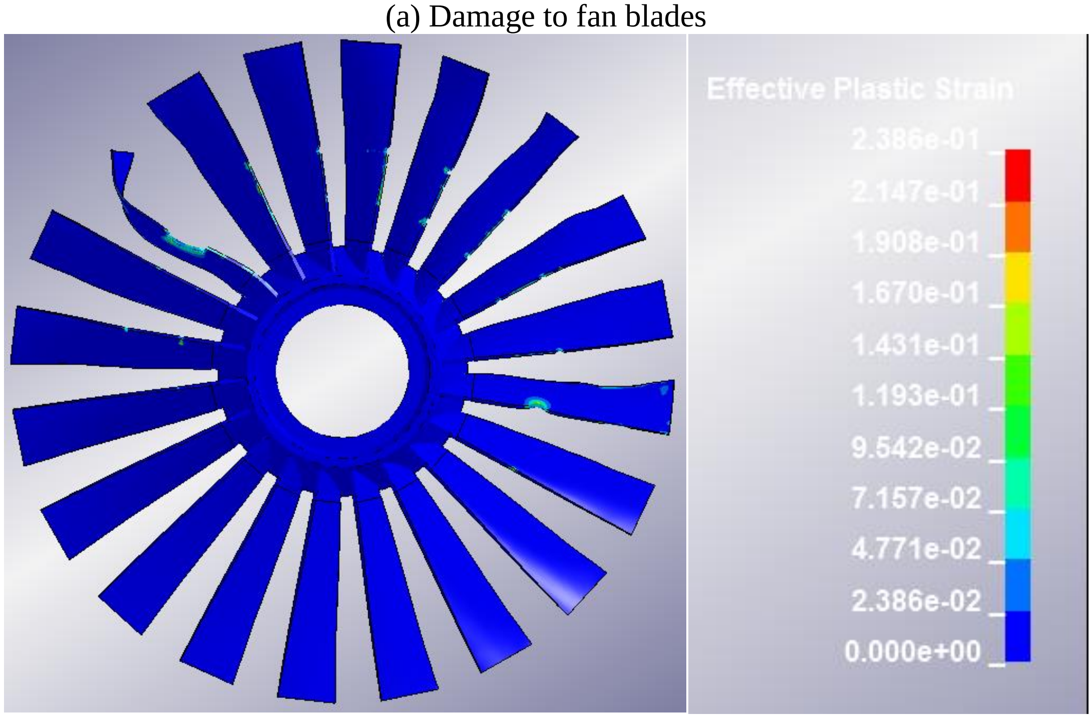

(b) Effective plastic strain in blades

Figure 56: Damage to blades for the takeoff location 1 case

The fixed wing ingestion at the inner part of the blade results in some large plastic deformation in a few blades and significant material loss due to the camera and motor impacts. Since this case involves significant material loss to multiple blades, but no full blade loss, it was classified as Level 2.

4.5.6 Takeoff Location 2: Nosecone - Motor

The takeoff location 2 case has the same setup as the baseline case, but instead of the full fixed wing just the motor is ingested into the engine, and instead of hitting the outer part of the fan it hits the nosecone. The fan geometry is the thin blade geometry developed for the generic 40 inch engine model. The relative speed of the motor to the engine is 180 knots and the fan is rotating at 8500 RPM. Figure 57 depicts the kinematics of the ingestion. Figure 58 shows the plastic strain in the nosecone which results in a small dent, but no penetration and is classified as Level 1 damage.

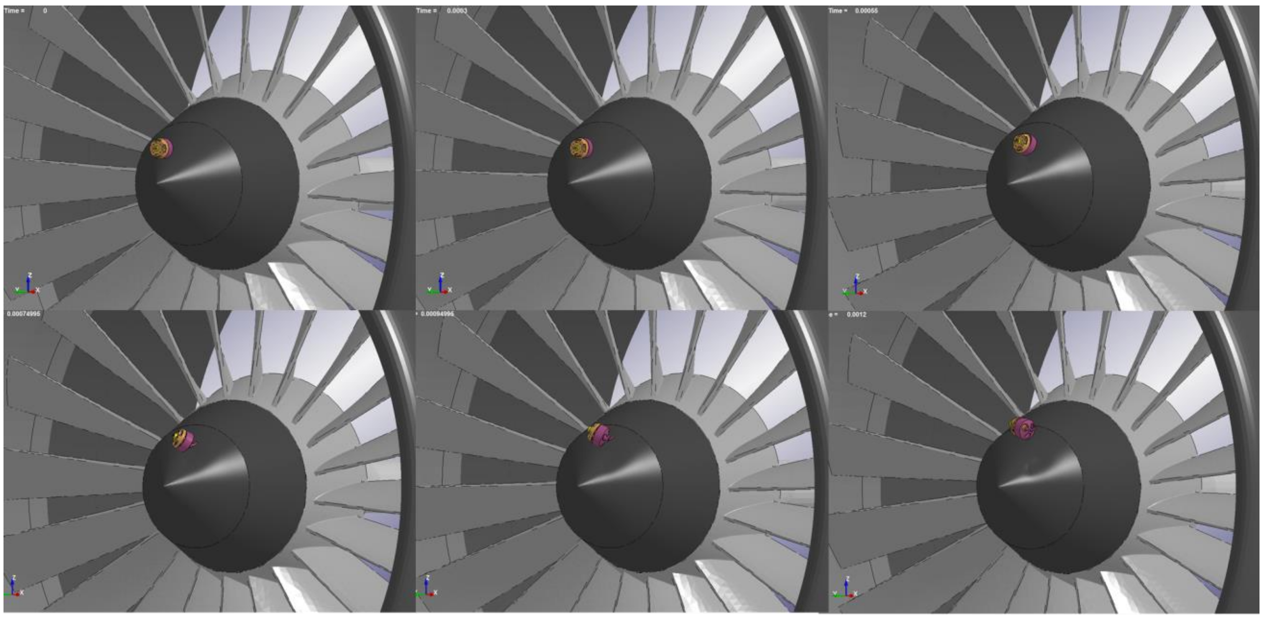

Figure 57: Kinematics of the fixed wing motor ingestion for the takeoff location 2 case

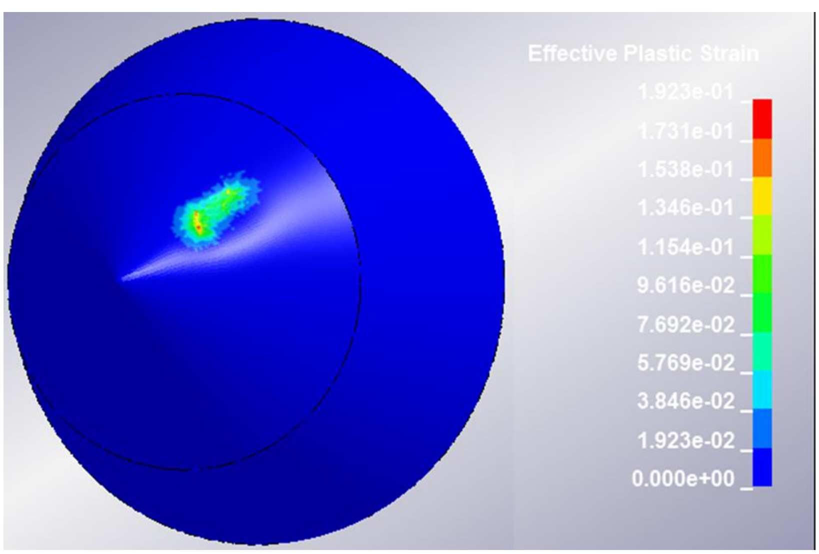

Figure 58: Effective plastic strain in the nosecone for the takeoff location 2 case

4.5.7 Takeoff Location 3: Nosecone - Camera

The takeoff location 3 case has the same setup as the baseline case, but instead of the full fixed wing just the camera is ingested into the engine, and instead of hitting the outer part of the fan it hits the nosecone. The fan geometry is the thin blade geometry developed for the generic 40 inch engine model. The relative speed of the camera to the engine is 180 knots and the fan is rotating at 8500 RPM. Figure 59 depicts the kinematics of the impact. Figure 60 shows the plastic strain in the nosecone which results in a sizeable dent, but no penetration and is classified as Level 1 damage.

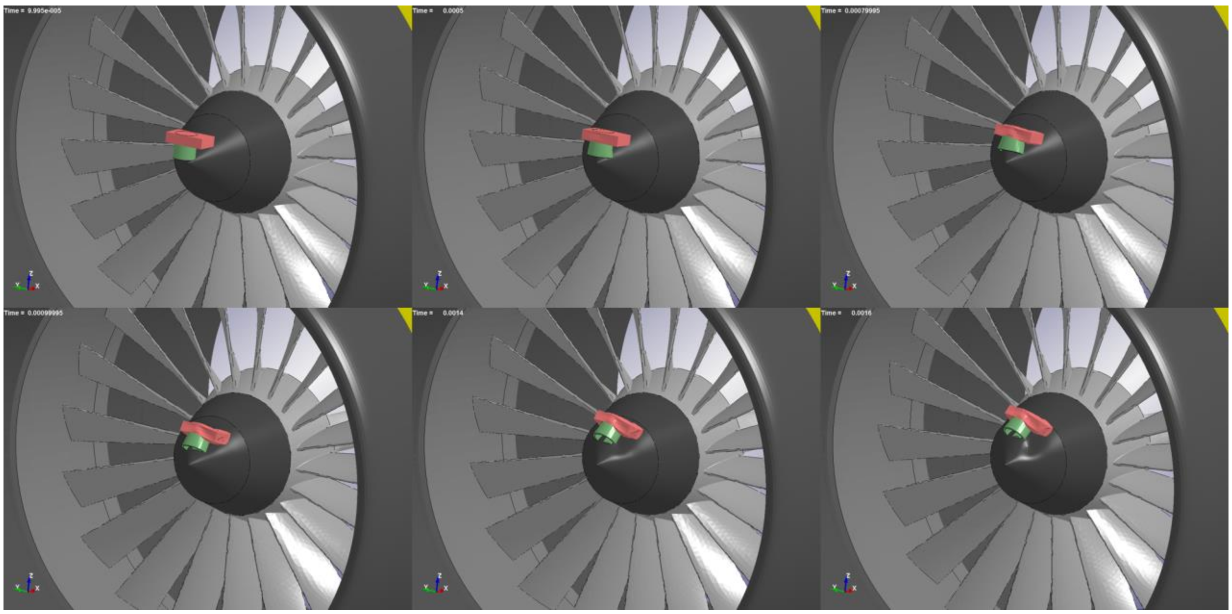

Figure 59: Kinematics of the fixed wing camera ingestion for the takeoff location 3 case

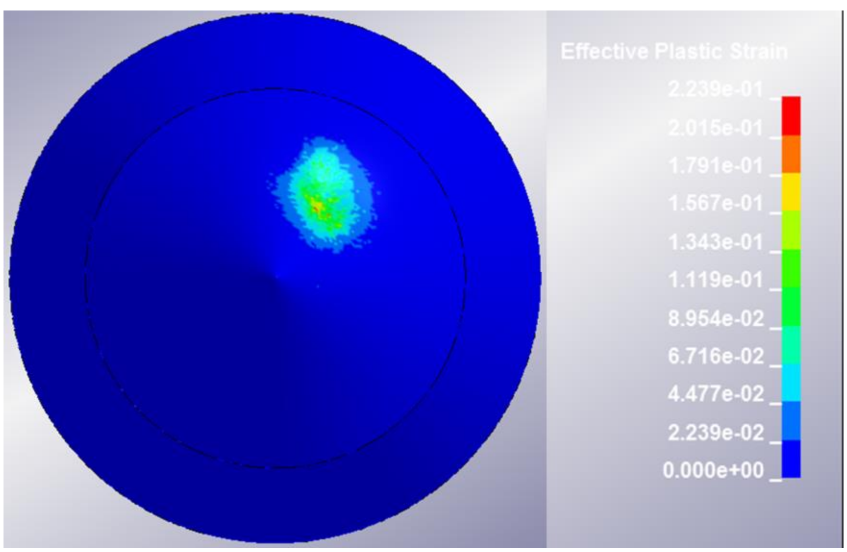

Figure 60: Effective plastic strain in the nosecone for the takeoff location 3 case

4.5.8 Takeoff Location 4: Nosecone - Battery

The takeoff location 4 case has the same setup as the baseline case, but instead of the full fixed wing just the battery is ingested into the engine, and instead of hitting the outer part of the fan it hits the nosecone. The fan geometry is the thin blade geometry developed for the generic 40 inch engine model. The relative speed of the battery to the engine is 180 knots and the fan is rotating at 8500 RPM. Figure 61 depicts the kinematics of the ingestion. Figure 62 shows the damage caused to the nosecone in terms of the plastic work done, note that there is no penetration of the nosecone and the damage is classified as Level 1 damage.

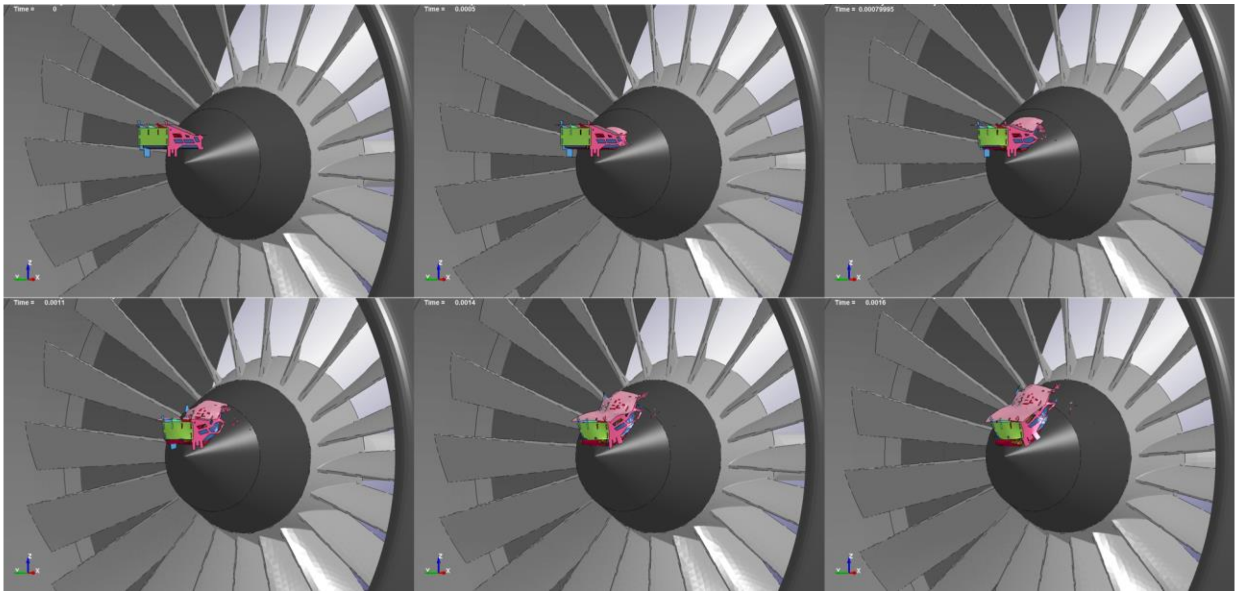

Figure 61: Kinematics of the fixed wing battery ingestion for the takeoff location 4 case

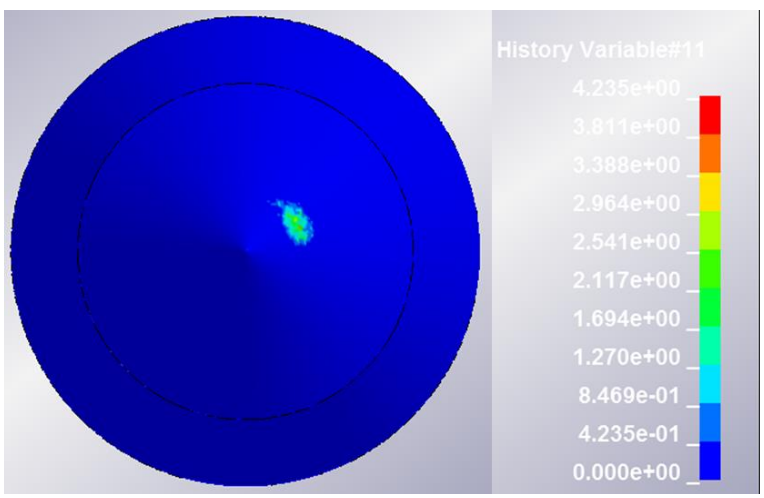

Figure 62: Plastic work in the nosecone for the takeoff location 4 case

4.5.9 Takeoff Geometry

The takeoff geometry case has the same setup as the baseline case, but instead of the thin blade geometry the thick blade geometry for the fan is used. This case consists of the fixed wing hitting the fan in the direct orientation shown in Figure 17 at the outer part of the fan. The fan geometry is the thick blade geometry developed for the generic 40 inch engine model. The relative speed of the fixed wing to the engine is 180 knots and the fan is rotating at 8500 RPM. Figure 63 depicts the kinematics of the ingestion. Figure 64 shows the damage caused to the blades.

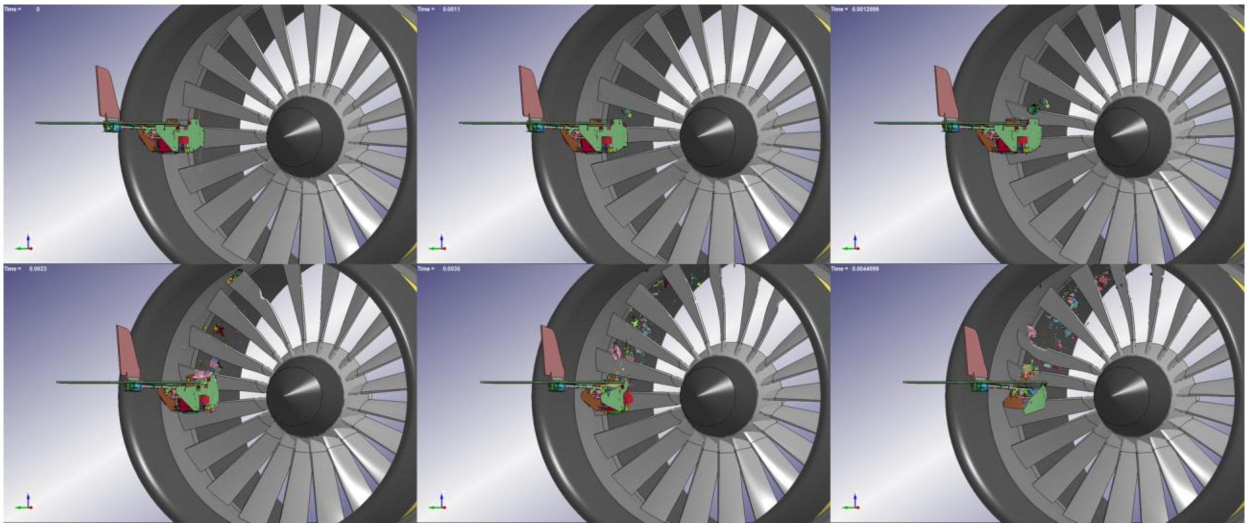

Figure 63: Kinematics of the fixed wing ingestion for the takeoff geometry case

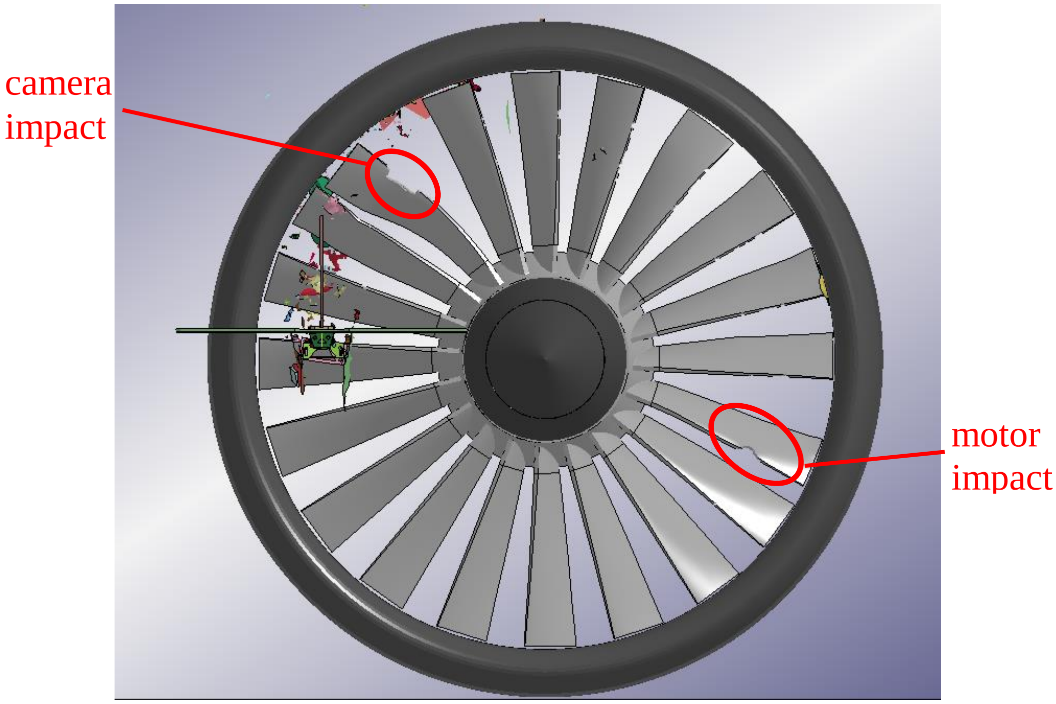

Figure 64: Damage to blades for the takeoff geometry case

The fixed wing causes significant damage to the leading edge of the blades that impact the motor and the camera. There is also minor damage to many other blades due to impacting other softer components of the fixed wing including the battery. Since this case involves significant material loss to multiple blades, but no loss of containment, it was classified as Level 2.

4.5.10 Takeoff Orientation

The takeoff orientation case has the same setup as the baseline case except for the orientation of the fixed wing, which has been rotated 180° in its yaw angle (as shown in Figure 17). This case consists of the fixed wing hitting the outer part of the fan, where the fan geometry is the thin blade geometry developed for the generic 40 inch engine model. The relative speed of the fixed wing to the engine is 180 knots and the fan is rotating at 8500 RPM. Figure 65 depicts the kinematics of the ingestion. Figure 66 shows the damage caused to the blades.

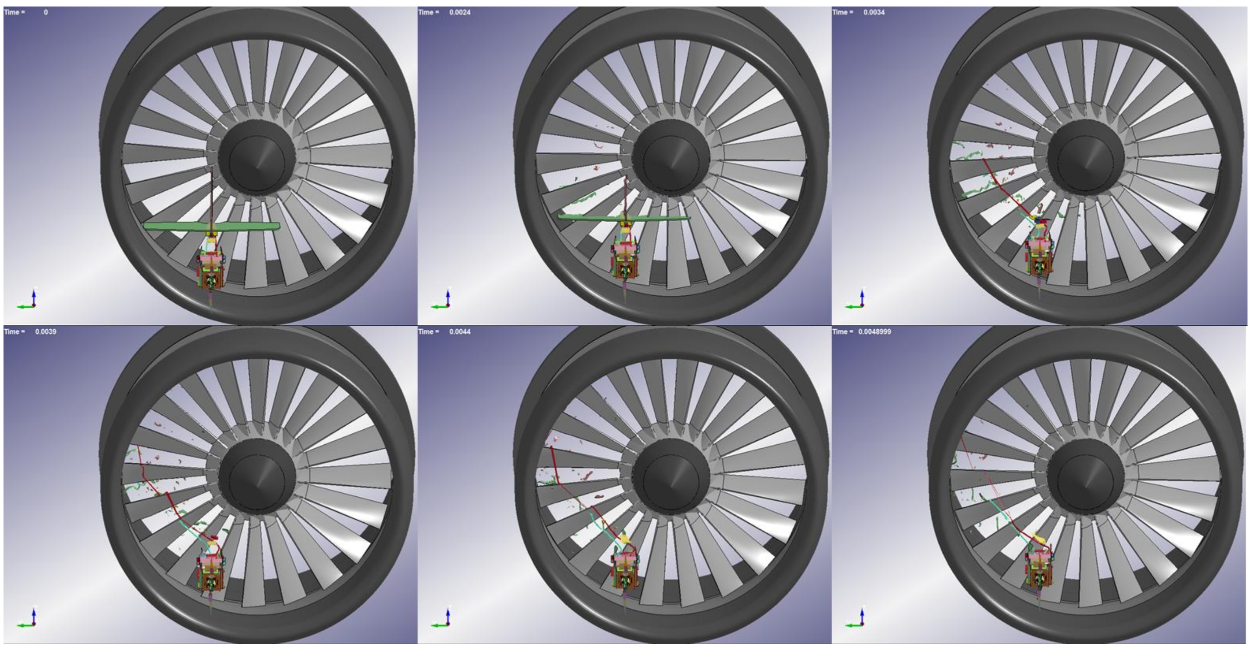

Figure 65: Kinematics of the fixed wing ingestion for the takeoff orientation case

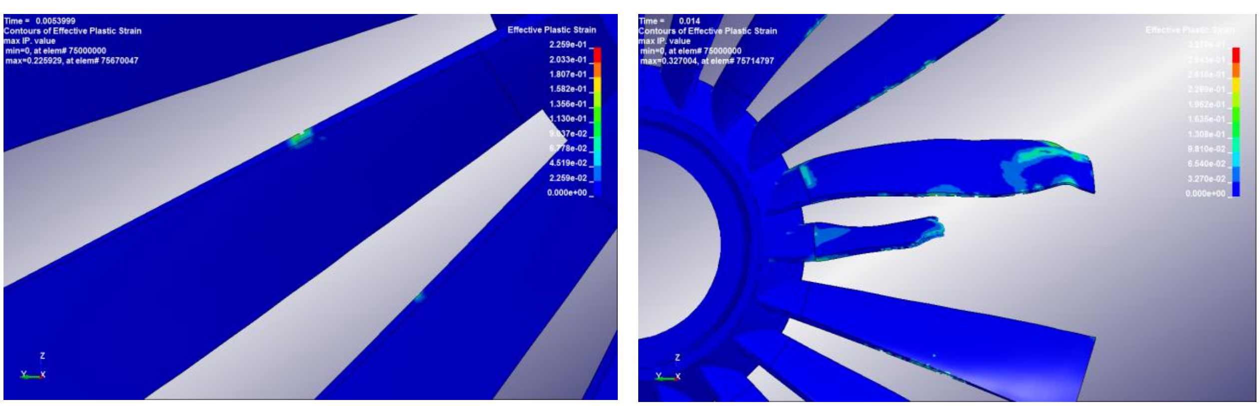

(a) Effective plastic strain from tail impact only (b) Effective plastic strain from camera impact

Figure 66: Effective plastic strain in blades for the takeoff orientation case

The ingestion of the fixed wing at the 180° yaw orientation results in the loss of the tip of one blade and plastic strain in a couple of other blades. Note that the damage caused to the fan from the tail of the fixed wing before the camera or motor impact the fan results in very minor plastic strain in the fan. Since this case did not involve the loss of multiple blades or a containment failure the severity was classified as Level 2.

4.5.11 Approach

The approach case has the same setup as the baseline takeoff case, except that the fan is rotating at 2000 RPM instead of 8500 RPM. This case consists of the fixed wing hitting the outer part of the fan, where the fan geometry is the thin blade geometry developed for the generic 40 inch engine model. The relative speed of the fixed wing to the engine is 180 knots and the impact is in the direct orientation shown in Figure 17. Figure 67 depicts the kinematics of the ingestion. Figure 68 shows the damage caused to the blades.

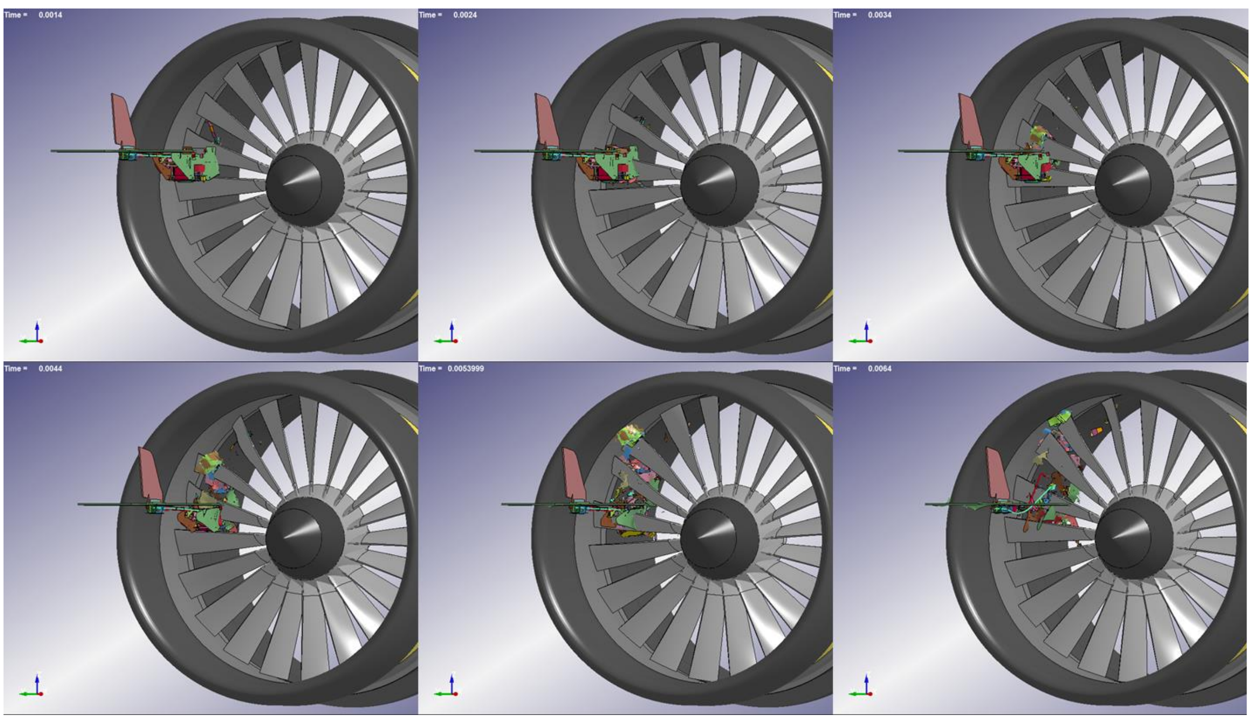

Figure 67: Kinematics of the fixed wing ingestion for the approach case

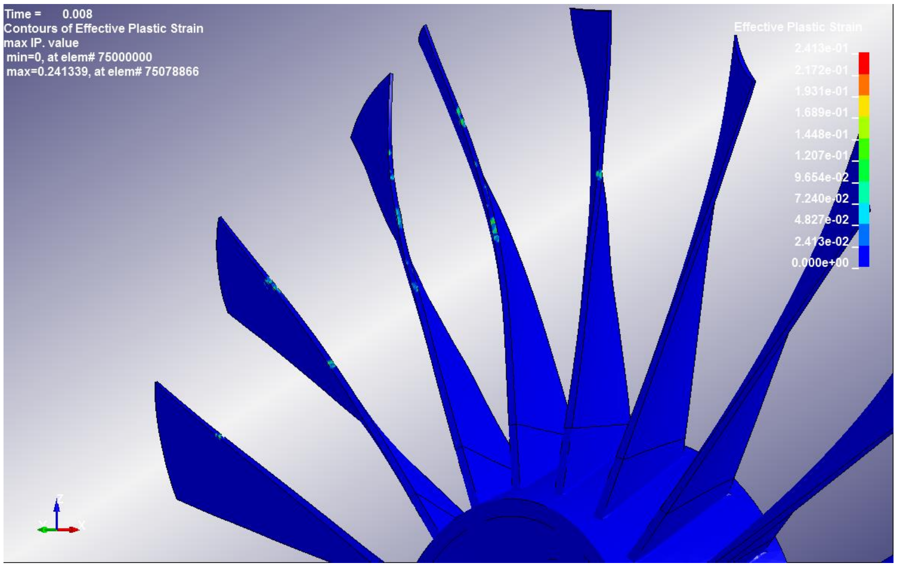

Figure 68: Effective plastic strain in blades for the approach case

The fixed wing approach case results in some minor plastic deformation in multiple blades. Since the overall damage to the blades was minor the severity was classified as Level 1.

4.5.12 Below 10,000 ft.

The flight below 10,000 ft. case has the same setup as the baseline case, except that the fan is rotating at 6000 RPM and the relative velocity of the fixed wing to the engine is 250 knots. This case consists of the fixed wing hitting the outer part of the fan, where the fan geometry is the thin blade geometry developed for the generic 40 inch engine model. The impact is in the direct orientation shown in Figure 17. Figure 69 depicts the kinematics of the ingestion. Figure 70 shows the damage caused to the blades.

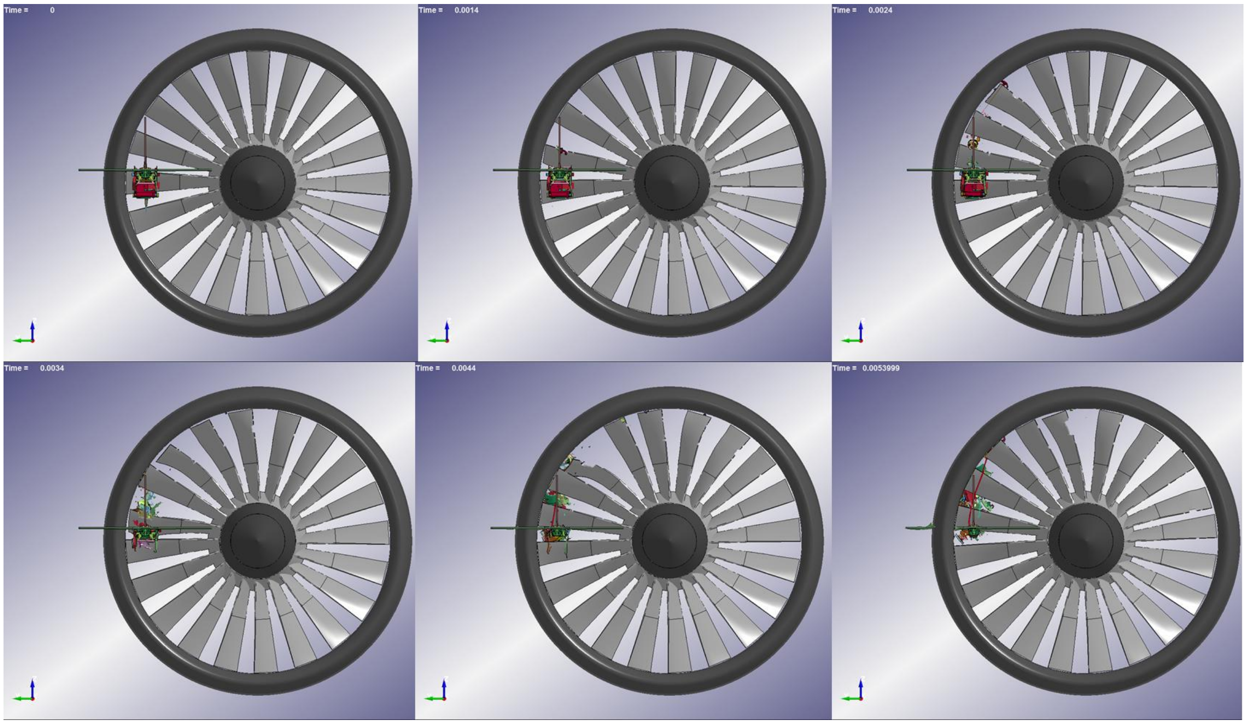

Figure 69: Kinematics of the fixed wing motor ingestion for the below 10,000 ft. case

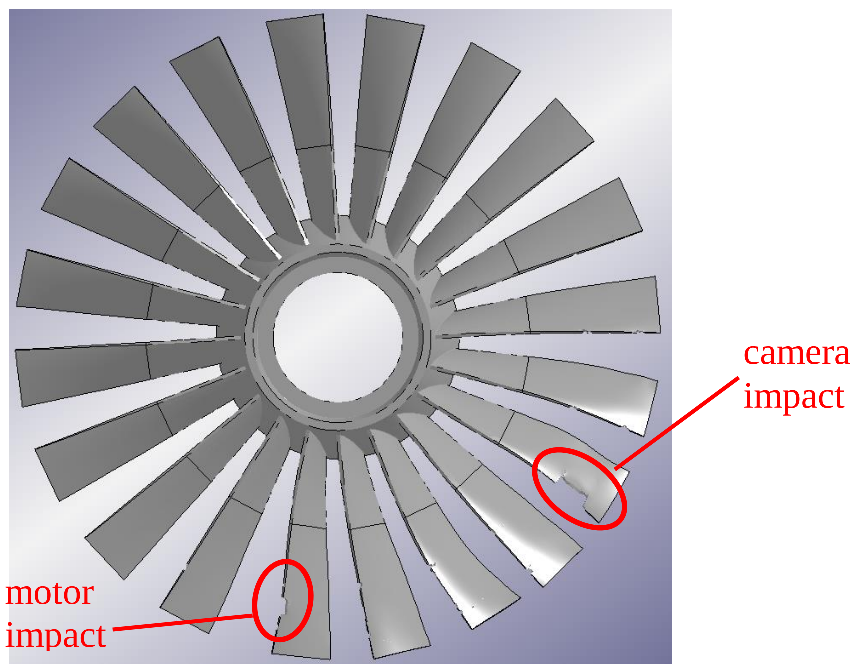

Figure 70: Damage to blades for the below 10,000 ft. case

For the flight below 10,000 ft. case, the fixed wing causes significant damage to the leading edge of the blades that impact the motor and the camera. There is also minor damage to many other blades due to impacting other softer components of the fixed wing including the battery. Since this case involves significant material loss to multiple blades, but no loss of containment, it was classified as Level 2.

4.5.13 Summary

A summary of the damages for each fixed wing ingestion scenario is given in Table 6. The damages ranged from Levels 1-3. The component level tests for the three key components (motor, camera and battery) provided insight into the expected level of damage from these components. The camera is expected to do the most damage followed by the motor and finally the battery. The damage from components outside of the three key components resulted in only Level 1 damage to the generic engine. Note that the wings that were removed from the fixed wing model were made of similar material to the tail of the fixed wing, which did little damage to the fan. The damage to the system increases significantly as the ingestion moves from the center (nosecone), to the inner blade and then to the outer blade. This is not unexpected since the relative velocity of the impact increases as the impact moves out from the center along a radial line. As expected the takeoff scenario is the worst case since the fan has the highest rotational speed for this case.

Table 6: Summary of the damage classifications for the fixed wing ingestions

Test Type	**Impact Location**	**Fan Blade**	**Relative Orientation**	**UAV Model - Component**	**Damage Classification**
Takeoff Baseline 2	***outer blade***	***thin***	***direct***	***fixed wing***	**Level 3**
Takeoff Component 1	outer blade	thin	direct	**motor**	**Level 2**
Takeoff Component 2	outer blade	thin	direct	**camera**	**Level 2**
Takeoff Component 3	outer blade	thin	direct	**battery**	**Level 1**
Takeoff Location 1	**inner blade**	thin	direct	fixed wing	**Level 2**
Takeoff Location 2	**nosecone**	thin	direct	**motor**	**Level 1**
Takeoff Location 3	**nosecone**	thin	direct	**camera**	**Level 1**
Takeoff Location 4	**nosecone**	thin	direct	**battery**	**Level 1**
Takeoff geometry	outer blade	**thick**	direct	fixed wing	**Level 2**
Takeoff Orientation	outer blade	thin	**180° yaw**	fixed wing	**Level 2**
Approach 2	outer blade	thin	direct	fixed wing	**Level 1**
Below 10,000 ft. 2	outer blade	thin	direct	fixed wing	**Level 2**

5. CONCLUSIONS AND FURTHER WORK

5.1 MODELS

This work presents two models of fan stages for generic aircraft engines for mid-size business jets. The fan diameters for each fan is 40 inches and the models are not supposed to represent any current engine in service; rather they were chosen with industrial input as reasonable approximations of solid titanium blades that are on the thick and thin side of blades for 40 inch diameter fans. The fans are within a containment ring[8], which is connected to a nacelle[5] upstream and downstream of the fan. A biconic nosecone was also included in the model. The materials of each critical component are composed of materials commonly used in engines and are discussed in the jet engine definition section.

The UAVs used in the collision studies were developed by collaborating groups. The first model[2] is the DJI Phantom 3 standard edition which is referred to as the quadcopter model in this report. It was chosen since the DJI Phantom family are the most common UAS under 5 lbs. It was developed at Wichita State University – NIAR. The second model[3] is the Precision Hawk Lancaster Hawkeye Mark III, which is a lightweight fixed wing UAV with a maximum takeoff weight of about 4.0 lbs. The Precision Hawk is referred to as the fixed wing model in this report. This model was developed at Mississippi State University and was chosen to learn about some of the differences between fixed wing and quadcopter ingestions.

5.2 COLLISION ANALYSIS

The damage to an engine during an ingestion of a UAV is dependent on many variables, including the type of fan, the rotational speed of the fan, the components of the UAV that impact the fan, the orientation of the impact, the location of the impact along the fan, and the relative speed of the vehicles.

This report focused on an ingestion event when a generic mid-size business jet engine ingests a UAV during takeoff. Several of the parameters that affect the ingestion were studied using deviations from a baseline takeoff scenario where the UAV hit near the tip of the thin fan blades. A classification of the different damage possibilities is shown in Table 7. Each of the ingestion scenarios have been defined in Table 3 and are classified by their damage level in

Table 8.

Table 7: Damage level categories for nosecone, fan, and containment system

Severity	Description	Example
Level 1	• Deformation of fan blades. • Minor material loss from fan blades. • Dent in nosecone. • No containment failure.	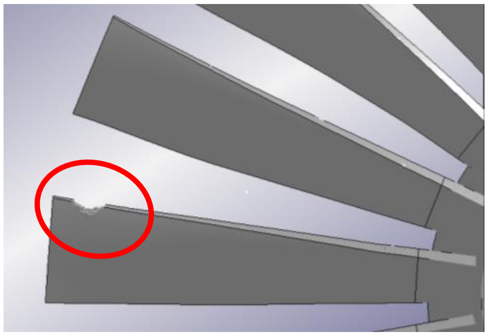
Level 2	• Significant material loss from one or multiple blades. • Loss of up to one full fan blade. • Crack in nosecone. • No containment failure.	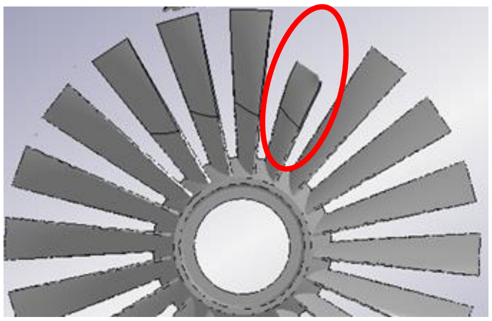
Level 3	• Loss of multiple fan blades. • UAV penetration of the nosecone. • No containment failure.	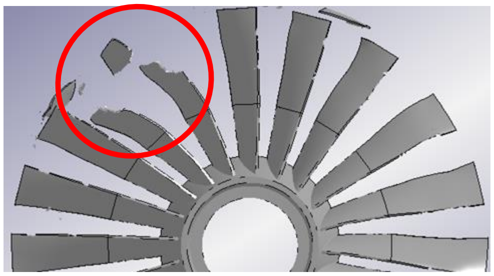
Level 4	• Containment failure due to UAV ingestion.	

Table 8: Damage classification for each ingestion scenario

Test Type	**Impact Location**	**Fan Blade**	**Relative Orientation**	**UAV Model - Component**	**Damage Classification**
Takeoff Baseline 1	***outer blade***	***thin***	***direct***	***quadcopter***	**Level 3**
Takeoff Component 1	outer blade	thin	direct	**motor**	**Level 1**
Takeoff Component 2	outer blade	thin	direct	**camera**	**Level 1**
Takeoff Component 3	outer blade	thin	direct	**battery**	**Level 1**
Takeoff Location 1	**inner blade**	thin	direct	quadcopter	**Level 1**
Takeoff Location 2	**nosecone**	thin	direct	**motor**	**Level 1**
Takeoff Location 3	**nosecone**	thin	direct	**camera**	**Level 1**
Takeoff Location 4	**nosecone**	thin	direct	**battery**	**Level 1**
Takeoff geometry	outer blade	**thick**	direct	quadcopter	**Level 1**
Takeoff Orientation	outer blade	thin	**90° pitch**	quadcopter	**Level 2**
Approach 1	outer blade	thin	direct	quadcopter	**Level 1**
Below 10,000 ft. 1	outer blade	thin	direct	quadcopter	**Level 1**
Takeoff Baseline 2	***outer blade***	***thin***	***direct***	***fixed wing***	**Level 3**
Takeoff Component 1	outer blade	thin	direct	**motor**	**Level 2**
Takeoff Component 2	outer blade	thin	direct	**camera**	**Level 2**
Takeoff Component 3	outer blade	thin	direct	**battery**	**Level 1**
Takeoff Location 1	**inner blade**	thin	direct	fixed wing	**Level 2**
Takeoff Location 2	**nosecone**	thin	direct	**motor**	**Level 1**
Takeoff Location 3	**nosecone**	thin	direct	**camera**	**Level 1**
Takeoff Location 4	**nosecone**	thin	direct	**battery**	**Level 1**
Takeoff geometry	outer blade	**thick**	direct	fixed wing	**Level 2**
Takeoff Orientation	outer blade	thin	**180° yaw**	fixed wing	**Level 2**
Approach 2	outer blade	thin	direct	fixed wing	**Level 1**
Below 10,000 ft. 2	outer blade	thin	direct	fixed wing	**Level 2**

The damages for the quadcopter and fixed wing ingestion scenarios both have a range from Levels 1-3. As expected the damage from the fixed wing tends to be larger than that of the quadcopter due to its heavier and larger core components, particularly the motor and camera. Other trends can be observed from both the quadcopter and the fixed wing. Namely, the damage to the system increases significantly as the ingestion moves from the center (nosecone), to the inner blade and then to the outer blade. This is not unexpected since the relative velocity of the impact increases as the impact moves out from the center along a radial line. Another reason the nosecone impacts tend to be so much less severe is that the nosecone tends to deflect the object instead of chopping through it like when it impacts the fan blades.

As expected, the takeoff scenario is the worst case since the fan has the highest rotational speed for this case. Other factors that have a major impact on the damage level include the thickness of the blade and the orientation of the UAV during the impact. As expected, the thicker blade holds up much better than the thin blade during the ingestion. Only two orientations were studied in this initial study for each UAV and additional orientations should be investigated, since it was found that the level of damage is greatly dependent on the conditions in which the fan impacts the harder components of the UAV.

None of the ingestion simulations from this preliminary work result in a loss of containment. There is some plastic strain in the containment tank due to blade loss, UAV component impacts, and tip rubs due to the ingestion. The containment tank is not damaged significantly in these events since it is designed to withstand a blade-out event where the blade is ejected at the root while the fan is spinning. In none of the cases considered was the damage severe enough at the disk to break the disk or lose multiple blades at their roots, which could result in a loss of containment.

The ingestion simulations studied in this work focus on damage to the nosecone and fan as well as how well the fan is contained. It does not model components of the engine past the fan such as the compressor, combustor, and turbine. As was discussed in an FAA UAV ingestion safety report[20] a very small hard body fragment as little as 0.66 pounds poses the potential for severe engine damage. So even for the case where there is only minor damage to the fan, the engine might not survive the UAV ingestion.

The energy for the entire system was monitored for all of the simulations via the glstat files from LS-DYNA. In general, it is recommended that the hourglass energy should stay less than 10% of the total energy of the system, and the total energy should stay within a couple percent of its initial value during the calculation provided no external work is performed. The hourglass energy is the work done by forces within LS-DYNA to resist hourglass deformations, which are unphysical deformations of the elements and should be minimized. The parameter ENMASS under *CONTROL_CONTACT was set to 2 which prevents the nodes from failed elements being deleted during the calculations. In these simulations the mass of the elements is lumped into the nodes. Thus when ENMASS=2 and an element fails the nodes and their kinetic energy are not eroded. However, the internal energy of the element is lost and plotted as eroded internal energy in Figure 71 and Figure 72.

The simulations in this work fell into two categories. An example of a case in the first category is shown in Figure 71, which shows the energy for the quadcopter inner blade impact. Cases in this category have excellent values for hourglass and the total energy stays almost constant during the entire calculation. The majority of the total energy is made up of kinetic energy, which comes from the rotating fan and the moving UAV. Additional energy terms that are plotted in Figure 71 include the internal energy, which is due to deformations in the parts being modeled. Sliding (or contact) energy corresponds to the energy dissipated from friction in the contacts between parts, and eroded energy corresponds to the energy lost in the elements that are deleted due to material failure in the crash scenarios. All of the component and about half of the full UAV cases exhibited this type of global energy.

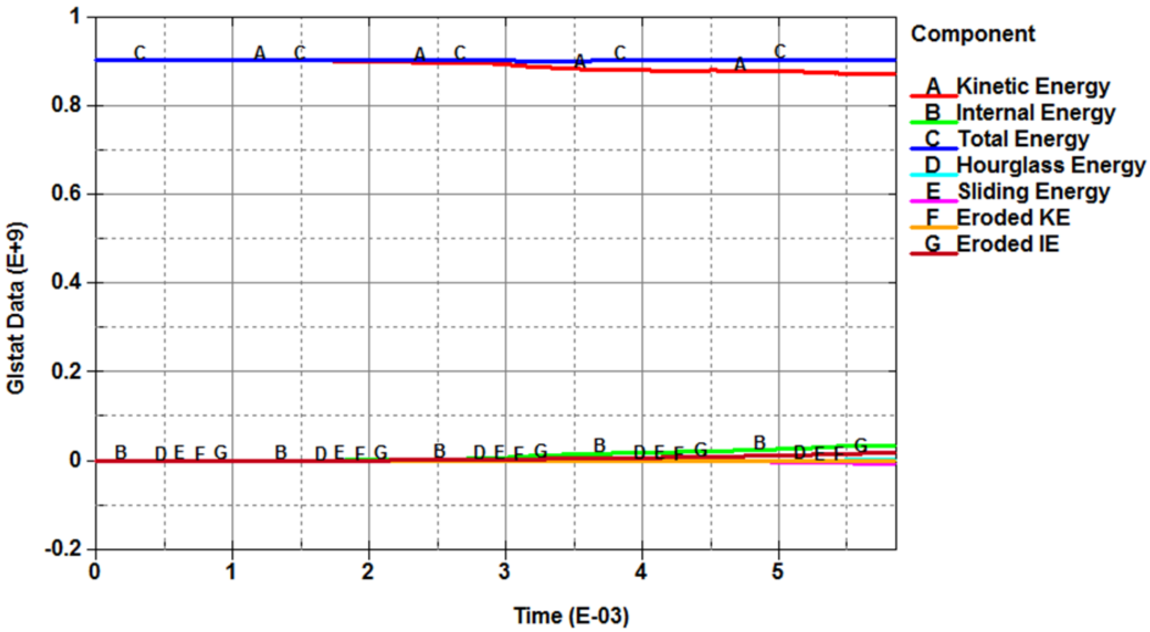

Figure 71: Energy plot for the quadcopter inner blade impact case

An example of the second category of energy behavior is shown in Figure 72, which shows the fixed wing takeoff baseline case. Often long-running explicit FE calculations are prone to instability due to error accumulation. The remaining cases exhibited some numerical instability late in the test runs, after the key components (camera, battery, and motor) had already been impacted by the fan. For these cases, the remaining parts of the UAV did little damage since the majority of the damage to the engine was due to the camera, motor, and battery within the UAVs. In some of the longer running fixed wing cases error accumulated due to the time required for the relatively long UAV to pass through the fan. This error is seen in Figure 72 when the total energy increases at just past 8 ms. This error is small and occurs after the major components have impacted the fan.

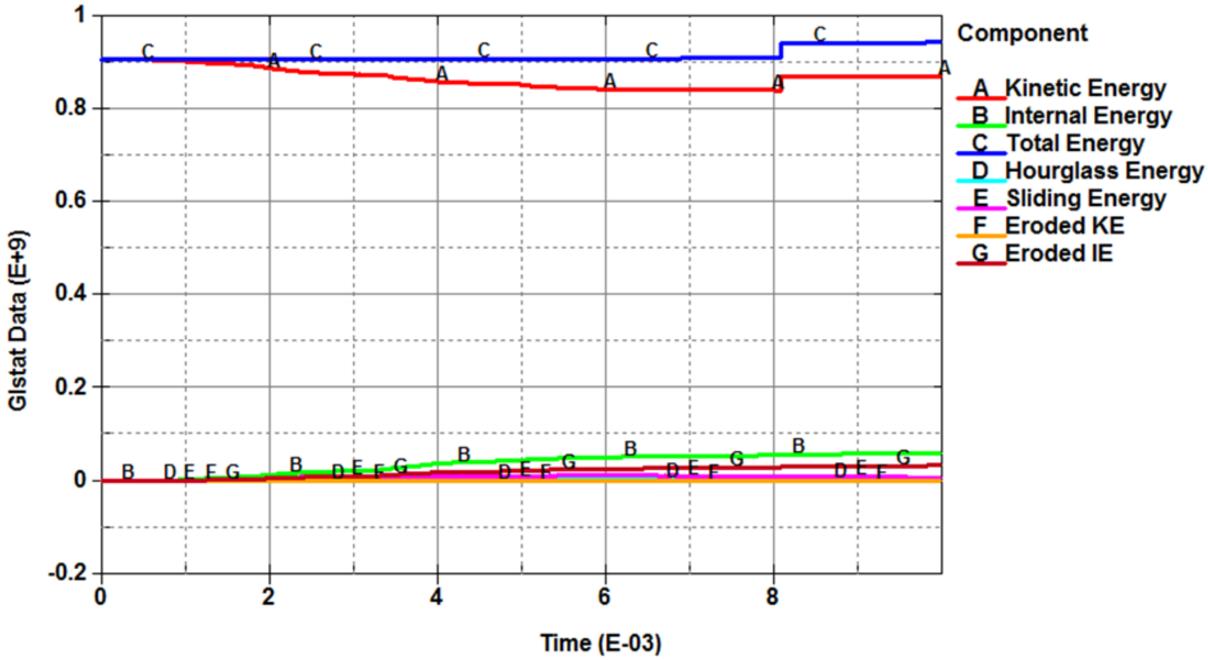

Figure 72: Energy plot for the fixed wing takeoff baseline case

5.3 FUTURE WORK

Further work is needed to understand the potential dangers of a UAV ingestion into an engine. The simulations demonstrated how the damage is dependent on the components being hit, where the harder components (such as the motor, battery and camera) will lead to far more damage than the lighter frame of the UAV. Although the test matrix for this work covered several scenarios there are many additional cases that would provide additional insight into UAV ingestions. In particular, more simulations with different UAV orientations, additional ingestions with the thick fan, and additional nosecone cases where the full UAV impacts the nosecone will provide more insight into the potential damage from a UAV ingestion. Also, the damage-level categories used in this study need to be refined in collaboration with engine industry experts to provide the FAA, engine manufactures, and operators a clear understanding of what the damage could mean to continued operation, engine shutdown and continued flight.

Additional material models for composite fan stages are also needed. Composite fan blades are lightweight and strong, which is why they are used in some commercial fan stages as well as other components in modern aircraft engines. Composites can have significantly different progressive damage and material failure behavior than the titanium alloy (Ti-6Al-4V) studied in this work. There is ongoing research into these composite material models and incorporating them into an engine ingestion simulation is another potential direction of future work.

Additional engine models of commercial jet engines is another area to be investigated. Engines for commercial jets vary greatly in size but are generally larger than the mid-size business jet engine studied in this work. A generic engine model of a commercial engine or a model of an actual commercial jet engine would be a valuable part of future work to understand the effects of the size of the engine on the ingestion event. Furthermore, developing additional models for components downstream of the fan is critical for understanding the full effect of the ingestion event on the engine.

Finally, one of the most critical parts of future work is to conduct full scale ingestion experiments of UAVs into fan stages running at operational speed. These experiments are critical in verifying the computational models that are being developed. Rotating engine experiments (as opposed to stationary engines impacted by UAVs) are particularly critical for several reasons. First, the fan blades will stiffen when rotating at their operational speed due to the centripetal acceleration. Second, in modern fan stages, the actual geometry of the blades will change due to the centripetal acceleration. Finally, the relative velocity of the fan and the UAV comes from both the relative speed between the plane and the UAV and the speed of the rotating fan blades. If the UAV hits the blade close to its tip, the relative velocity can be transonic, which is much greater than the actual speed of the plane in landing and take-off conditions. Once the models are verified experimentally they can then be used confidently for a variety of different ingestion scenarios.

6. REFERENCES

[1] http://osc.edu/ark:/19495/f5s1ph73. Ohio Supercomputer Center. Columbus, OH: Ohio Supercomputer Center; 1987.

[2] Olivares G, Monteros J, Baldridge R, Zinzuwadia C, Gomez L. Volume II – UAS Airborne Collision Severity Evaluation – Quadcopter. FAA Report; 2016.

[3] Olivares G, Lacy T, Monteros J, Kota K, Baldridge R, Zinzuwadia C, Jayakody N, Gomez L. Volume III – UAS Airborne Collision Severity Evaluation – Fixed Wing. FAA Report; 2016.

[4] Cairns D, Johnson G, Edens M, Arnold F. Volume I – UAS Airborne Collision Severity Evaluation – Projectile and Target Definition. FAA Report; 2016.

[5] Sengoz K, Kan S, Eskandarian A. Development of a Generic Gas Turbine Engine Fan Blade-out Full Fan Rig Model. FAA Report DOT/FAA/TC-14/43; 2015.

[6] http://awg.lstc.com/tiki/tiki-index.php?page=QA+Test+Example+2.1. Awg Erif Test Case 2.1: Fan Blade-Off Rig Test, Generic Fan Rig Model. LS-Dyna Aerospace Working Group.

[7] Vintilescu IV. Explicit Finite Element Modeling of Multilayer Composite Fabric for Gas Turbine Engine Containment Systems, Phase II - Part 4: Model Simulation for Ballistic Tests, Engine Fan Blade-out, and Generic Engine. FAA Report DOT/FAA/AR-08/37,P4; 2009.

[8] http://awg.lstc.com/tiki/tiki-index.php?page=QA+Test+Example+2.2. Awg Erif: Test Case 2.2: Fan Blade-Off Containment Test - Generic Soft Wall Containment. LS-Dyna Aerospace Working Group.

[9] LS-DYNA Keyword User's Manual Vol. 1. Livermore, California; 2016.

[10] http://awg.lstc.com/tiki/tiki-index.php?page=Resources. LS-DYNA Aerospace Working Group *Mat_224 User Guide. 2016.

[11] http://awg.lstc.com/tiki/tiki-index.php?page=MGD. LS-DYNA Aerospace Working Group Modeling Guidelines Document. 2016.

[12] Rajan SD, Mobasher B, Vaidya A, Zhu D, Fein J, Deivanayagam A. Explicit Finite Element Modeling of Multilayer Composite Fabric for Gas Turbine Engine Containment Systems, Phase Iv. FAA Report DOT/FAA/TC-13/37; 2014.

[13] Simons J, Erlich D, Shockey D. Part 3: Material Model Development and Simulation of Experiments. Explicit Finite Element Modeling of Multilayer Composite Fabric for Gas Turbine Engine Containment Systems, Phase II FAA Report DOT/FAA/AR-08/37,P3; 2009.

[14] Rajan SD, Mobasher B, Stahlecker Z, Bansal S, Zhu D, Morea M, Dhandapani K. Part 1: Arizona State University Material Model and Numerical Simulations. Explicit Finite Element Modeling of Multilayer Composite Fabric for Gas Turbine Engine Containment Systems, Phase III FAA Report DOT/FAA/AR-10/23,P1; 2011.

[15] Haight S, Wang, L., Du Bois, P., Carney K., Kan C. D. Development of a Titanium Alloy Ti-6al-4v Material Model Used in LS-DYNA. FAA.

[16] Hammer JT. Plastic Deformation and Ductile Fracture of Ti-6al-4v under Various Loading Conditions. FAA Report DOT/FAA/TC-TT14/2; 2014.

[17] Buyuk M. Part 2: Development of a Tabulated Thermo-Viscoplastic Material Model with Regularized Failure for Dynamic Ductile Failure Prediction of Structures under Impact Loading. Development of a New Metal Material Model in LS-DYNA: FAA Report DOT/FAA/TC-13/25, P2; 2014.

[18] Seidt JD. Part 3: Plastic Deformation and Ductile Fracture of 2024 Aluminum under Various Loading Conditions. Development of a New Metal Material Model in LS-DYNA: FAA Report DOT/FAA/TC-13/25, P3; 2014.

[19] U.S. Code of Federal Regulations, Title 14, Part 91, General Operation and Flight Rules. Washington DC: U.S. Government Publishing Office; 2016.
[20] Cordasco D, Emmerling W. Turbofan Engine System Safety of a UAV Ingestion Hazard. 2015.